

ACTA GEO TECHNICA SLOVENICA

2006/1

H. brandl et al.

GROUND-SOURCED ENERGY WELLS FOR
HEATING AND COOLING OF BUILDINGS

N. zannete & D. battelino

MEAN GRAIN SIZE AS FUNCTION OF
SPECTRAL AMPLITUDE: A NEW REGRESSION
LAW FOR MARINE SEDIMENT CORES

B. pulko & B. majes

ANALYTICAL METHOD FOR THE ANALYSIS OF STONE-
COLUMNS ACCORDING TO THE ROWE DILATANCY THEORY

S. škrabl

INTERACTIONAL APPROACH OF
CANTILEVER PILE WALLS ANALYSIS



**ACTA
GEOTECHNICA
SLOVENICA**

ISSN: 1854-0171

ustanovitelji

founders

Univerza v Mariboru, Fakulteta za gradbeništvo
University of Maribor, Faculty of Civil Engineering



Univerza v Ljubljani, Fakulteta za gradbeništvo in geodezijo
University of Ljubljana, Faculty of Civil
and Geodetic Engineering



Univerza v Ljubljani, Naravoslovnotehniška fakulteta
University of Ljubljana, Faculty of Natural
Sciences and Engineering



Slovensko geotehniško društvo
Slovenian Geotechnical Society



Društvo za podzemne in geotehniške konstrukcije
Society for Underground and Geotechnical
Constructions



izdajatelj

publisher

Univerza v Mariboru, Fakulteta za gradbeništvo
University of Maribor, Faculty of Civil Engineering

odgovorni urednik

editor-in-chief

Ludvik Trauner
Univerza v Mariboru

urednika

co-editors

Stanislav Škrabl
Univerza v Mariboru
Bojan Žlender
Univerza v Mariboru

tehnična urednika

desk editors

Bojana Dolinar
Univerza v Mariboru
Borut Macuh
Univerza v Mariboru

lektorica

proof-reader

Metka Brkan

naklada

circulation

700 izvodov - issues

tisk

print

Tercia tisk d.o.o. Ptuj

Revija redno izhaja dvakrat letno. Članki v reviji so recenzirani s strani priznanih mednarodnih strokovnjakov. Baza podatkov v kateri je revija indeksirana: ICONDA - The international Construction database

uredniški odbor

editorial board

Darinka Battelino
Università degli Studi di Trieste
József Farkas
Budapesti Műszaki és Gazdaságtudományi Egyetem
Theodoros Hatzigogos
Aristotle University of Thessaloniki
Rolf Katzenbach
Technische Universität Darmstadt
Zlatko Langof
Univerzitet u Sarajevu
Jakob Likar
Univerza v Ljubljani
Janko Logar
Univerza v Ljubljani
Bojan Majes
Univerza v Ljubljani
Milan Maksimović
Univerzitet u Beogradu
Borut Petkovšek
Zavod za gradbeništvo Slovenije
Mihael Ribičič
Univerza v Ljubljani
César Sagaseta
Universidad de Cantabria
Stephan Semprich
Technische Universität Graz
Abdul-Hamid Soubra
Université de Nantes
Ivan Vaniček
České vysoké učení technické v Praze
Franjo Verič
Sveučilište u Zagrebu

naslov uredništva

address

ACTA GEOTECHNICA SLOVENICA
Univerza v Mariboru, Fakulteta za gradbeništvo
Smetanova ulica 17
2000 Maribor
Slovenija
Telefon / Telephone: +386 (0)2 22 94 300
Faks / Fax: +386 (0)2 25 24 179
E-pošta / E-mail: ags@uni-mb.s

spletni naslov

web address

<http://www.fg.uni-mb.si/journal-ags>

The journal is published twice a year. Papers are peer reviewed by renowned international experts. Indexation data base of the journal: ICONDA - The International Construction Database

VSEBINA

2 Ludvik Trauner
UVODNIK

4 Heinz Brandl in drugi
ENERGIJSKI VODNJAKI S
TALNIM IZVIROM ZA OGREVANJE
IN OHLAJANJE ZGRADOB

28 Nelly Zannete in Darinka Battelino
GRANULOMETRIJA KOT
FUNKCIJA SPEKTRALNE AMPLITUDE:
NOV REGRESIJSKI ZAKON
ZA MORSKE SEDIMENTE

36 Boštjan Pulko in Bojan Majes
ANALITIČNA METODA ZA ANALIZO
GRUŠČNATIH KOLOV Z UPOŠTEVANJEM
ROWE TEORIJE RAZMIKANJA

46 Stanislav Škrabl
INTERAKCIJSKA ANALIZA KONZOLNO
VPETIH PODPORNH KONSTRUKCIJ

60 NAVODILA AVTORJEM

CONTENTS

Ludvik Trauner 3
EDITORIAL

Heinz Brandl et al. 5
GROUND-SOURCED ENERGY
WELLS FOR HEATING AND
COOLING OF BUILDINGS

Nelly Zannete and Darinka Battelino 29
MEAN GRAIN SIZE AS FUNCTION OF
SPECTRAL AMPLITUDE: A NEW REGRES-
SION LAW FOR MARINE SEDIMENT CORES

Boštjan Pulko and Bojan Majes 37
ANALYTICAL METHOD FOR THE ANALYSIS
OF STONE-COLUMNS ACCORDING TO THE
ROWE DILATANCY THEORY

Stanislav Škrabl 47
INTERACTIONAL APPROACH OF
CANTILEVER PILE WALLS ANALYSIS

INSTRUCTIONS FOR AUTHORS 61

UVODNIK

Mednarodna revija Acta Geotechnica Slovenica izhaja že tretje leto. S svojo vsebino in pestrostjo objavljenih člankov je privabila veliko bralcev in naročnikov. Strokovnjaki so v njej objavili široko paleto znanstvenih in strokovnih prispevkov s področij geotehnike, geologije, okoljevarstva, gradbeništva, rudarstva, potresnega izženirstva, energetike in drugih. Prikazani so bili najnovejši dosežki na osnovi eksperimentalnih, analitičnih in/ali numeričnih analiz.

Za zanimive in kvalitetno objavljene prispevke v Acta Geotechnica Slovenica, ki so pripomogli k velikemu mednarodnemu odzivu revije, gre zahvala vsem avtorjem in uredniškemu odboru ter predvsem dosedanjim recenzentom D. Battelino, H. Brandl, A. Breznikar, R. Ilić, Z. Kapović, R. Katzenbach, D. Korošak, J. Likar, J. Logar, Z. Langof, B. Majes, P. Marinos, P. Pavšič, J. Planinić, C. Sagaseta, W. Schubert, S. Semprich, A.H. Soubra, S. Škrabl, A. Umek, W.F. Van Impe. Slednjim se zato želim ob tej priliki še posebej zahvaliti.

Bralcem pričujoče prve številke tretjega letnika revije Acta Geotechnica Slovenica tokrat predstavljam naslednje zanimive prispevke:

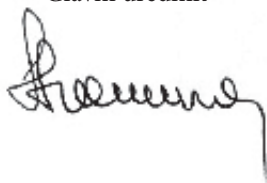
V prvem članku avtor H. Brandl s sodelavci obravnava več načrtovalskih vidikov energijskih vodnjakov, ki se lahko uporabljajo tudi pri načrtovanju globokih energijskih temeljev. Prikazani so različni sistemi energijskih vodnjakov in podani rezultati pilotnega raziskovalnega projekta.

V članku N. Zanette in D. Battelino je prikazana geofizikalna metoda, katera omogoča analizo poroznih, saturiranih morskih sedimentov z uporabo širjenja akustičnega valovanja in primerjava dobljenih rezultatov z rezultati konvencionalnih geomehanskih preiskav.

B. Pulko in B. Majes sta predstavila novo metodo za analizo obnašanja togih temeljev na z gruščnatimi koli izboljšanih tleh. Prikazana je parametrična študija, ki analizira vpliv razmikanja gruščnatega materiala na deformacije in napetosti v temeljnih tleh ter ugoden vpliv na redukcijo posedkov. Rezultati nove metode so primerjani z nekaterimi drugimi analitičnimi metodami in objavljenimi rezultati terenskih testov in opazovanj.

V članku S. Škrabla je podan predlog nove izboljšane metode za geomehanske analize in projektiranje konzolnih podpornih konstrukcij. Metoda temelji na analizi mejnih stanj, vendar so pri razporeditvi aktiviranih vplivov in odporov upoštewane nekatere dodatne interakcijske sovisnosti med podpornimi konstrukcijami in tlemi.

Ludvik Trauner
Glavni urednik



EDITORIAL

The international journal Acta Geotechnica Slovenica is now in its third year of publication. Its versatile contents have attracted many readers and subscribers. Up to now, the journal has published numerous scientific and professional articles from the fields of geotechnics, geology, environment protection, civil engineering, mining, earthquake engineering, power engineering and other. In their contributions, the authors presented the latest achievements in their fields based on experimental, analytical and/or numerical analyses.

The selected topics and their in-depth studies have enhanced the international renown of Acta Geotechnica Slovenica. Merits are due to all the authors, and to the editor's board and peer-reviewers D. Battelino, H. Brandl, A. Breznikar, R. Ilić, Z. Kapović, R. Katzenbach, D. Korošak, J. Likar, J. Logar, Z. Langof, B. Majes, P. Marinos, P. Pavšič, J. Planinić, C. Sagaseta, W. Schubert, S. Semprich, A.H. Soubra, S. Škrabl, A. Umek, W.F. Van Impe. May I use this occasion to thank them all.

Volume 3, issue 1, brings the following topics of interest:

H. Brandl discusses several design criteria of energy wells that can be used in designing deep energy foundations. Different systems of energy wells are presented as well as results of the pilot research project.

N. Zanette and D. Battelino describe an attempt to characterize porous and saturated marine sediments with a non destructive technique, which is the acoustic wave, in order to determine the correlation with geotechnical measurements.

B. Pulko and B. Majes present a new analytical method to analyse the behaviour of rigid foundations stabilized by end bearing stone-columns. The parametric study shows the effect of dilatancy of the granular material on the deformations and stresses in the ground and its beneficial effect on settlement reduction. The results of the new method are compared with some already known analytical methods and some published field test results and observations.

S. Škrabl proposes a new method for the geomechanical analysis and design of cantilever retaining structures. It is based on the limit equilibrium method, but it uses some additional conditions for the interaction between a retaining structure and the ground, when referring to the distribution of the mobilized earth pressures on the structure.

Ludvik Trauner
Editor-in-chief



ENERGIJSKI VODNJAKI S TALNIM IZVIROM ZA OGREVANJE IN OHLAJANJE ZGRADB

HEINZ BRANDL, DIETMAR ADAM IN ROMAN MARKIEWICZ

o avtorjih

Heinz Brandl
Faculty of Civil Engineering,
Vienna University of Technology
Karlsplatz 13, 1040 Dunaj, Avstrija
E-pošta: h.brandl@tuwien.ac.at

Dietmar Adam
Geotechnik Adam ZT GmbH
Wiener Straße 66-72/15/4
2345 Brunn am Gebirge, Avstrija
E-pošta: d.adam@tuwien.ac.at

Roman Markiewicz
Geotechnik Adam ZT GmbH
Wiener Straße 66-72/15/4
2345 Brunn am Gebirge, Austria
E-pošta: markiewicz@geotechnik-adam.at

izvleček

Energijski vodnjaki so termoaktivni elementi za ekonomično črpanje ali shranjevanje energije v tleh - podobni energijskim stebrom in drugim globokotemeljnim elementom, ki se uporabljajo kot toplotni izmenjevalci.

Ogrevanje in hlajenje zgradb zahteva primarni in sekundarni termoaktivni krog, ki sta povezana s toplotno črpalko. V članku obravnavamo več načrtovalskih vidikov energijskih vodnjakov, ki se lahko uporabljajo tudi pri načrtovanju globokih energijskih temeljev. Preskusi termičnega odziva so se pokazali kot primerni za terensko določanje termičnih lastnosti tal, ki so potrebne za optimirano načrtovanje. V članku so obravnavani različni sistemi energijskih vodnjakov in podani rezultati pilotnega raziskovalnega projekta.

ključne besede

energijski vodnjaki, energijski temelji, geotermalna geotehnika, geotermalno ogrevanje/hlajenje, termično-aktivne konstrukcije, termične lastnosti tal, terenski preskusi

GROUND-SOURCED ENERGY WELLS FOR HEATING AND COOLING OF BUILDINGS

HEINZ BRANDL, DIETMAR ADAM and ROMAN MARKIEWICZ

About the authors

Heinz Brandl
Faculty of Civil Engineering,
Vienna University of Technology
Karlsplatz 13, 1040 Wien, Austria
E-mail: h.brandl@tuwien.ac.at

Dietmar Adam
Geotechnik Adam ZT GmbH
Wiener Straße 66-72/15/4
2345 Brunn am Gebirge, Austria
E-mail: d.adam@tuwien.ac.at

Roman Markiewicz
Geotechnik Adam ZT GmbH
Wiener Straße 66-72/15/4
2345 Brunn am Gebirge, Austria
E-mail: markiewicz@geotechnik-adam.at

Abstract

Energy wells are thermo-active elements for an economical extraction or storage of ground energy, similar to energy piles and other deep foundation elements also used as heat exchangers. Heating and/or cooling of buildings requires a primary and secondary thermo-active circuit, commonly connected by a heat pump. The paper gives several design aspects of energy wells which can be also used for the design of deep energy foundations. Thermal response tests have proved suitable for the in-situ determination of thermal ground properties required for an optimised design. Moreover, different systems of energy wells are discussed, and a comprehensive pilot research project is described.

Keywords

energy wells, energy foundations, geothermal geotechnics, geothermal heating/cooling, thermo-active structures, thermal ground properties, field testing

1 INTRODUCTION

The fourth Šuklje Lecture was devoted to geothermal geotechnics as an innovative field of geotechnical engineering (Brandl, 2003). Meanwhile thermo-active ground structures and heat pumps have been used increasingly. In Austria, about 200,000 heat pumps are running presently, and their number increases by more than 5000 per year. Their main purpose was warm water generation first. Since the year 2000 heating (and cooling) of buildings has dominated. It is estimated that these heat pumps save more than 250,000 tons of fuel oil per year.

This corresponds to the Austrian climate strategy of the year 2002 to achieve the Kiyoto targets. The main potential to reduce CO₂ refers to the heating of buildings. Together with other energy consumption (e.g. warm water generation, cooling of buildings), this potential represents about one third of the total sum. Consequently, research has focused on the design of buildings that need minimum energy.

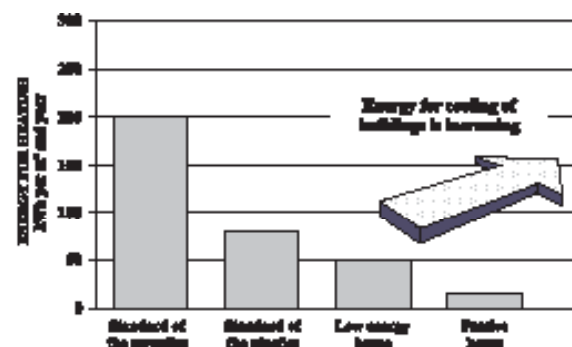


Figure 1. Required energy for the heating of houses in Austria. Improvements since the 1970s.

Fig. 1 illustrates the chronological development of energy saving houses in Europe. The required energy for heating houses has decreased significantly since the nineteen-seventies, but on the other hand the energy for cooling is increasing, mainly due to large glass facades and permanently closed windows of modern

architecture. Ultra Low- to Zero-Energy Houses are also called “Passive Houses”. The term “Passive House” indicates that such buildings need only minimum or no conventional energy as required for “active” heating or cooling. Such an optimal energy balance can be only achieved in exceptional cases. However, thermo-active ground structures or wells may provide sufficient energy for a cheap and clean heating/cooling of buildings.

The temperature felt by persons in a room consists of the air temperature and the radiation temperature (i.e. the temperature of walls and floors), whereby the ratio between air and surface temperature is essential. Compensating too low wall or floor temperature by higher air temperature is felt uncomfortable (e.g. in temporarily uninhabited cold houses which have to be warmed up). Surface temperatures of 20 to 25°C are optimal corresponding to an air temperature between 16° and 21°C. Low temperature heating systems like wall- and floor heating with a large surface radiation fulfil this requirement, whereby the feed temperature of wall heating should not exceed 40°C and the floor temperature 28°C, respectively. This heating system can be coupled in an ideal way with energy foundations, retaining walls, tunnels, and energy wells.

The dominating ground-sourced elements are energy foundations, but energy tunnels, energy wells, retaining structures etc. are also used. Energy foundations may comprise base slabs, piles barrettes, slurry trench systems (single elements or continuous diaphragm walls), concrete columns, and grouted stone columns. Combinations with near-surface earth collectors and

retaining structures are also possible (Fig. 2). Thermo-active ground structures or wells can be used for heating and/or cooling buildings of all sizes, as well as for road pavements, bridge decks, etc.

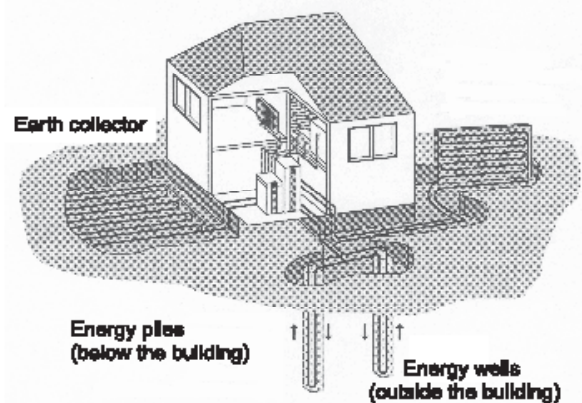


Figure 2. Scheme for heating/cooling a small one-family house with energy foundations and/or energy wells. Also indicated are additional thermo-active ground-source systems.

Energy wells are wells (temporarily) used for groundwater lowering and/or groundwater recharging but simultaneously adapted for energy extraction/storage purposes. The energy systems therefore have a double function, and they work most efficiently if the thermo-active elements are in contact with mobile groundwater in the case of heating or cooling only. However, for seasonal operation (i.e. heating in winter and cooling in summer) rather steady groundwater conditions with a low hydraulic gradient are favourable for seasonal energy extraction and feeding (recharging, storage).

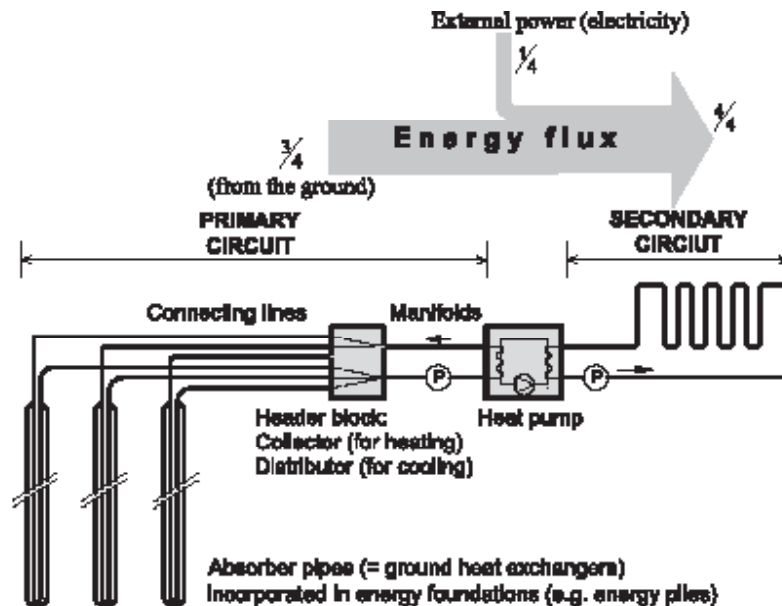


Figure 3. Scheme of a geothermal energy plant with energy piles and an energy flux for COP 4 of the heat pump. COP coefficient of performance defining the heat pump efficiency.

2 THERMO-ACTIVE CIRCUITS FOR ENERGY FOUNDATIONS AND ENERGY WELLS

A thermo-active system consists of the primary circuit below ground and the secondary circuit in the building (Fig. 3).

The primary circuit contains closed pipework in earth-contact concrete elements (piles, barrettes, diaphragm walls, columns, base slabs, and wells) through which a heat carrier fluid is pumped that exchanges energy from the building with the ground. The heat carrier fluid is a heat transfer medium of either water, water with antifreeze (glycol) or a saline solution. Glycol-water mixtures have proved most suitable, containing also additives to prevent corrosion in the header block, valves, the heat pump, etc. Once cast, the pipings within the underground-contact concrete elements are individually joined to a header and manifold block. They are joined by connecting pipes which are normally laid within the blinding beneath the base slab in the case of energy foundations. The secondary circuit is a closed fluid-based building heating or cooling network (secondary pipework) embedded in the floors and walls of the structure or in bridge decks, road structures, platforms etc.

Commonly, primary and secondary circuits are connected via a heat pump that increases the temperature level, typically from 10–15°C to a level between 25°C and 35°C (Fig. 3). All that is required for this process is a low application of electrical energy for raising the originally non-usable heat resources to a higher, usable temperature. The principle of a heat pump is similar to that of a reverse refrigerator (Fig. 10). In the case of the heat pump, however, both the heat absorption in the evaporator and the heat emission in the condenser occur at a higher temperature, whereby the heating and not the cooling effect is utilised.

The coefficient of performance, COP, of a heat pump is a device parameter and is defined by

$$COP = \frac{\text{energy output after heat pump [kW]}}{\text{energy input for operation [kW]}} \quad (1)$$

The value of COP = 4 means that from one portion of electrical energy and three portions of environmental energy from the ground four portions of usable energy are derived (Fig. 3).

The efficiency of a heat pump is strongly influenced by the difference between extracted and actually used temperature. A high user temperature (inflow temperature to the heating system of the secondary circuit) and a low extraction temperature (due to insufficient return-flow temperature) in the heat exchanger (primary circuit) reduce its efficiency. For economic reasons a value of COP ≥ 4 should be achieved. Therefore, the usable temperature in the secondary circuit should not exceed 35–45°C, and the extraction temperature in the absorber pipes should not fall below 0–5°C. Consequently, this technology tends to be limited to low temperature heating (and cooling).

Commonly, electric heat pumps are used, less frequently heat pumps with internal combustion and occasionally absorption heat pumps. For environmental reasons only refrigerants without ozone reduction potential and with a minimum greenhouse potential are allowed for heat pumps. Therefore halogenated fluorinated hydrocarbons should not be used.

The seasonal performance factor (SPF) of a thermo-active system with a heat pump is the ratio of the usable energy output of the system to the energy input required to obtain it. Therefore SPF includes not only the heat pump but also other energy-consuming elements (e.g. circulation pumps). At present, values of SPF = 3.8–4.3 are achieved with standard electric heat pumps. Special devices with direct vaporisation increase SPF by 10–15%.

$$SPF = \frac{\text{useable energy output of the energy system [kWh]}}{\text{energy input of the energy system [kWh]}} \quad (2)$$

Experience has shown that these geothermal cooling/heating systems from energy foundations and other thermo-active ground structures may save up to two-thirds of conventional heating costs. Moreover, they represent an effective contribution to environmental protection by providing clean and self-renewable energy.

If only heating or only cooling is performed, high-permeability ground and groundwater with a high hydraulic gradient are of advantage. However, most economical and environmentally friendly is a seasonal operation with an energy balance throughout the year, hence heating in winter (i.e. heat extraction from the ground) and cooling in summer (i.e. heat sinking/recharging into the ground). In this case low-permeability ground and groundwater with only low hydraulic gradients are favourable.

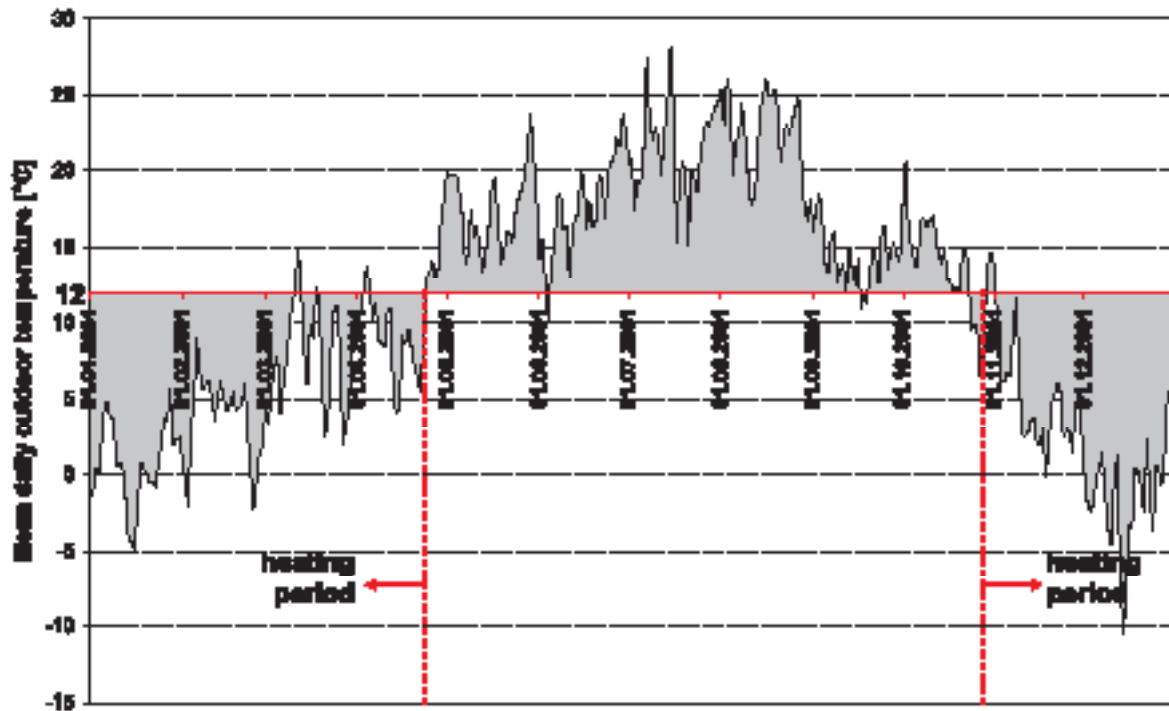


Figure 4. Mean daily outdoor temperatures in Vienna, 2001. If temperature drops below 12°C, room heating is usually necessary.

There is no limitation to the depth of piles or wells as far as the installation of energy absorber systems is concerned. The energy potential increases with depth: hence deeper ground-sourced energy systems are advantageous. The economically minimum length of piles, barrettes or diaphragm wall panels is about 6 m. Energy wells should reach deeper, because they have a lower heat transfer capacity than concrete elements.

The production of electric current from energy foundations and other thermo-active ground structures or wells is theoretically possible but not effective. This is similar to biomasses as base materials: they exhibit a high efficiency for heating (85%) but an extremely low efficiency for producing electric current (25%).

3 DESIGN ASPECTS OF ENERGY WELLS AND FOUNDATIONS

Early ecological energy planning for building can often prevent costly refurbishment and renovation in the future. High-quality energy design involves not only heating and cooling (rooms, water) but also lighting, and it requires a multi-objective optimisation.

An optimised energetic-thermal design should also consider the seasonal heat loss from (un-)insulated slab-on-grade floors or basement walls. Far more energy

and costs are expended in running an inefficiently laid out building than in constructing an efficient one. A proper design should consider the efficiency of the overall building process, including the sustainability of all elements.

The heat that can be extracted from or fed into/stored in the ground depends on the maximum possible heat flux density in the absorber pipe system. There, the heat transport occurs by forced convection of the fluid (usually an antifreeze – water mixture). In order to optimise the absorber pipe system the following parameters have to be considered:

- Diameter and length of pipes;
- Properties of pipe wall (roughness);
- Heat conductivity, specific heat capacity, density and viscosity of fluid circulating in absorber pipes;
- Flow velocity and flow conditions (laminar-turbulent) within absorber pipes.

Complex ground properties and pile or well groups require numerical modelling of the geothermal heating/cooling system.

Fig. 4 shows the daily mean temperatures in Vienna for the year 2001. Such data are needed to design a heating-cooling system whereby it is assumed that heating typically starts at external temperatures lower than 12°C. This provides the heating period for the unsteady numerical models. Fig. 5 illustrates the simulation of the

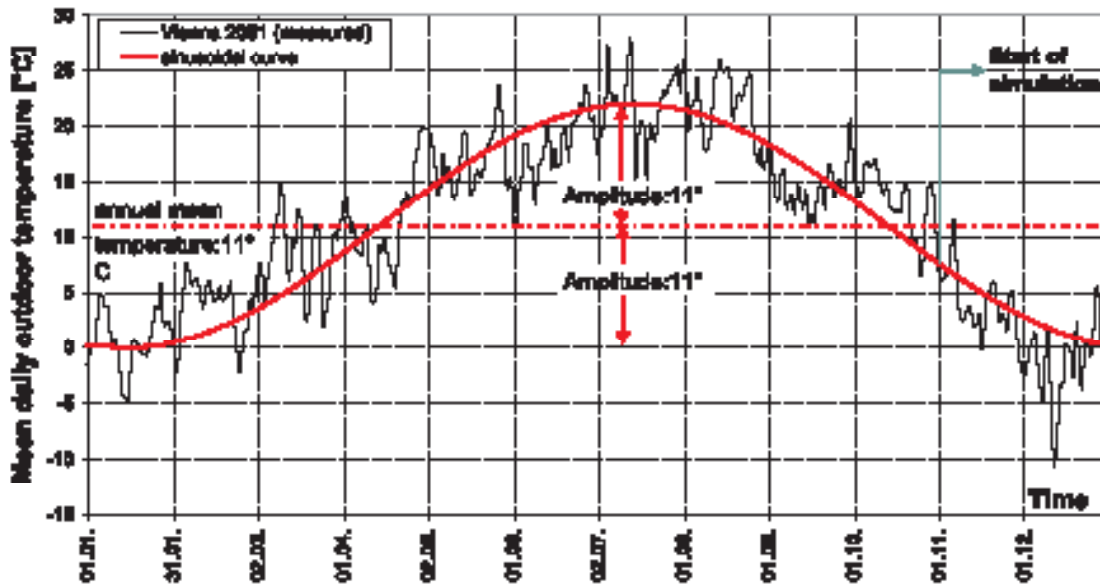


Figure 5. Mean daily outdoor temperatures in Vienna, 2001, with idealised sinusoidal curve for numerical calculations

seasonal course of the air temperature by a sinusoidal curve according to the following equation

$$T_{GS} = T_{m,air} + \Delta T_{air} \cos\left[\frac{2\pi}{P}(t - \epsilon_t)\right] \quad (3)$$

where $T_{GS}(t)$ is the ground surface temperature, t is time, $T_{m,air}$ is the average yearly temperature, ΔT_{out} is the

temperature amplitude, P is the duration period, and ϵ_t is the phase displacement.

In the end, the monthly heating and cooling demands have to be compared with the available output, as indicated in Fig. 6. Moreover, the seasonal course of the absorber fluid temperature (heat carrier fluid temperature) should be predicted.

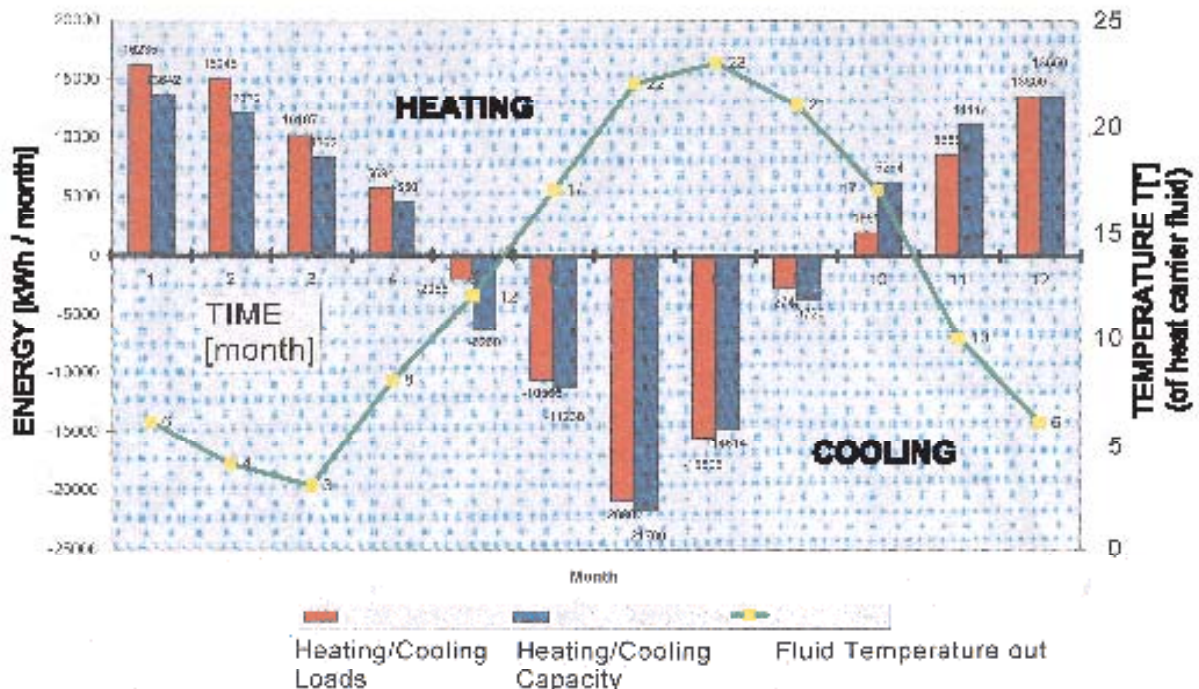


Figure 6. Example of energy demand and output for heating and cooling (annual distribution) of a building founded on energy piles. Temperature of heat carrier fluid is also shown.

Usually, a numerical simulation of the geothermal system is recommended for buildings with a heating and cooling demand of more than 50 kW. This rough value decreases to about 20 kW for buildings where rooms have to be cooled throughout the year. Geometric simplification may lead to significant errors in heat calculation. Therefore three-dimensional analyses should be conducted. The simulation should comprise the expected inflow and outflow temperatures at the energy foundations and the temperature distribution in the ground. Numerical models and computer programs should be reliably calibrated, that is on the basis of long-term measurements and experience from other sites, and on physical plausibility. Otherwise wrong results may be gained, even from well-known suppliers. Experience has shown that the results are very sensitive to even small changes in the finite element mesh. Consequently, the importance of numerical simulations lies rather in parametric studies (to investigate the influence of specific parameters) than in gaining 'exact' quantitative results.

Calculation of the temperature distribution in the ground due to energy foundations or energy wells is increasingly being demanded by local authorities for environmental risk assessment. This refers mainly to possible influences on adjacent ground properties and

on the groundwater by the long-term operation of thermo-active deep foundations.

Monitoring of thermo-active ground-sourced systems is essential for an optimized long-term operation, and to enable sophisticated design of future projects. Fig. 7, for example, shows the temperatures along an energy pile (out of a group) that has been used for heating since 1996. The depicted period between 2002 and 2005 illustrates that a reliable interpretation of date and heat exchanger behaviour requires the daily outdoor mean values. Single outdoor temperature measurements parallel to pile (or well) temperature measurements would not be sufficient.

Proper geothermal energy utilisation requires an interdisciplinary design, especially in the case of houses. Geotechnical engineer, architect, building equipment (sanitation) designer and installer, heating engineer and specialised plumber should cooperate as early as possible to create the most economical energy system. However, the tender for construction should clearly specify individual performances on the site. It has proved suitable to entrust the geothermally experienced plumber with all details of the primary and secondary circuits, beginning with the mounting of the absorber pipe systems in the foundation elements.

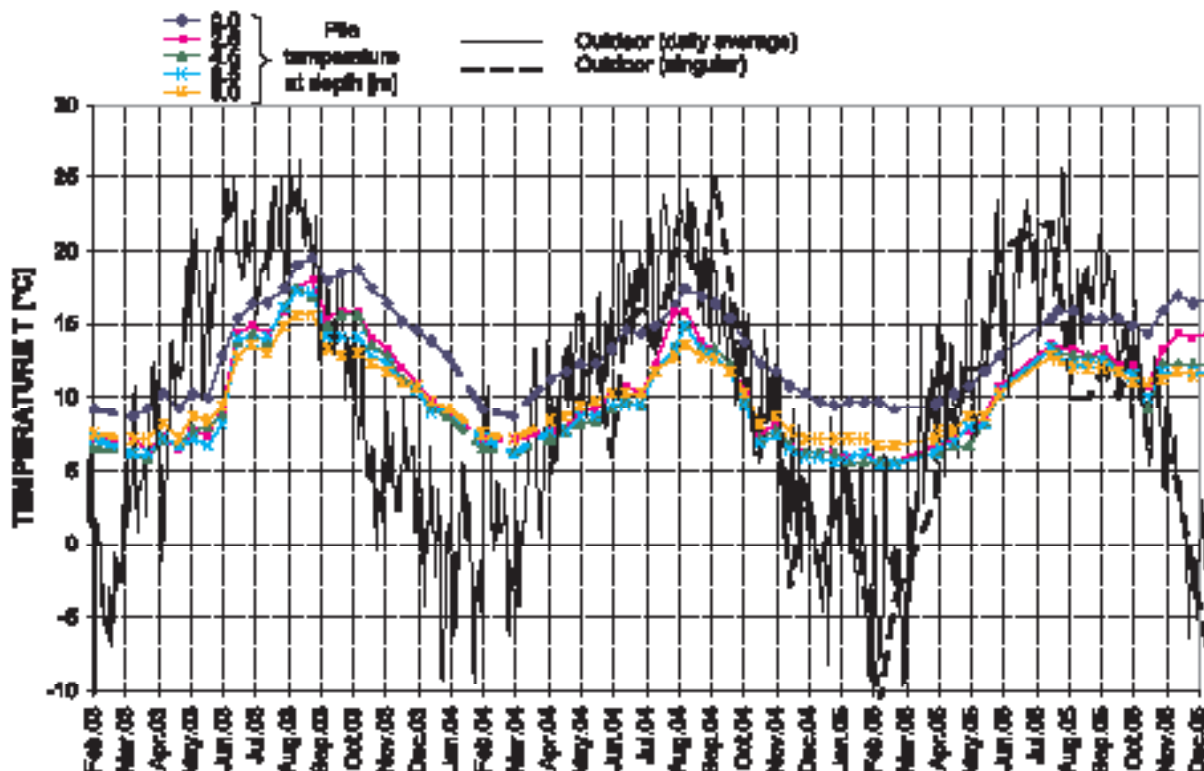


Figure 7. Outdoor temperature near a building with energy piles and temperature within a 'measuring pile'. Strong heatwave in summer 2003; more normal temperature distribution in 2004; cold summer and very warm autumn in 2005.

4 IN-SITU MEASUREMENT OF THERMAL GROUND PROPERTIES

In order to optimise the design of energy foundations or energy wells the thermal ground properties have to be considered. The most important parameter is the thermal conductivity λ . For the preliminary design of complex energy foundations, or for the detailed design of standard geothermal systems, it can be taken with sufficient accuracy from diagrams considering water content, saturation density and texture of the soil. However, for sophisticated design in-situ measurements are recommended, for instance the thermal response test. Its theory can be also applied to energy foundations and energy wells, thus providing a feedback referring to design assumptions and data collections for future projects.

A defined energy is applied to a vertical heat exchanger, and the inflow and returnflow temperatures of the heat carrier fluid are registered. Therefore, the measurements involve the entire length of the ground heat exchanger, thus providing an effective value for the thermal conductivity considering borehole refilling (or pile properties), heterogeneous ground conditions and groundwater situation. In addition, the thermal borehole resistance R_b is determined which is another parameter for designing earth-contact thermo-active elements.

Heat transfer from/to a vertical heat exchanger causes a temperature change in the surrounding soil. The temperature field as a function of time and radius around a borehole can be described as a line heat source with constant heat storage/extraction (Hellström, 1991):

$$\Delta T(r_b, t) = \frac{\bar{q}}{4\pi\lambda_g} \int_{\frac{r_b}{2a}}^{\infty} \frac{e^{-\beta}}{\beta} d\beta \quad (4)$$

where

- $\Delta T(r_b, t)$ = temperature increase [K]
- \bar{q} = heat storage rate per unit borehole length [W/m]
- λ_{eff} = effective thermal conductivity
- L_b = effective borehole length [m]
- t = time after storage/extraction of heat has started [s]
- a = thermal diffusivity ($\lambda/\rho c$ where c is the heat capacity)
- r = radial distance from the centre line of the borehole [m]
- r_b = borehole radius [m]
- $\bar{\beta}$ = integrating variable [-]

For the thermal response test, Eq. (4) can be approximated for the temperature field around a borehole. The theory is based on Gehlin (1998) as follows:

$$\Delta T(r_b, t) = \frac{\bar{q}}{4\pi\lambda_g} \left(\ln \frac{4at}{r_b^2} - \gamma \right) \text{ provided that } t > \frac{5r_b^2}{a} \quad (5)$$

where γ is Euler's number (0.5772...)

The above derivation assumes

- Constant temperature along the borehole which is not exactly the case in practice. However, the axial temperature gradient is small in relation to the radial quotient; thus, the approach provides only negligible deviation.
- Infinite length of the borehole. In practice, the borehole length is considerably larger than the borehole radius. Therefore, for short periods of time (as in the case of response tests) the borehole end effects can be ignored (Gehlin, 1998).

Another important factor for the design of heat exchanger systems is the thermal resistance between the heat carrier fluid and the borehole wall. It dictates the temperature difference between the fluid temperature (T_m) and the borehole wall (T_b) for a certain heat flux \bar{q}

$$T_m - T_b = R_b \bar{q} \quad (6)$$

The thermal borehole resistance R_b depends on the arrangement of the absorber pipes and on the material involved, i.e. pipe plastic and surrounding borehole fill material or concrete (in the case of energy piles). R_b causes temperature losses that affect the heat transfer. The equation for the temperature field considering the thermal borehole resistance can be written

$$\Delta T(r_b, t) = \bar{q} \left[R_b + \frac{1}{4\pi\lambda_g} \left(\ln \frac{4at}{r_b^2} - \gamma \right) \right] \quad (7)$$

Further transformation of equation 7 leads to equation 8 that approximates the transient process around a vertical heat exchanger (Fig. 8):

$$T_m = \frac{\dot{Q}}{4\pi\lambda_g L_b} \ln(t) + \left[\frac{\dot{Q}}{L_b} \left(\frac{1}{4\pi\lambda_g} \left(\ln \left(\frac{4at}{r_b^2} \right) - \gamma \right) - R_b \right) + T_0 \right] \quad (8)$$

where

$$T_m = \frac{T_{inflow} - T_{returnflow}}{2} \quad [^\circ\text{C}] \text{ is the mean heat carrier fluid temperature}$$

\dot{Q} = constant heat power [W], stored or extracted [W]

T_0 = undisturbed initial temperature of the ground [$^\circ\text{C}$]

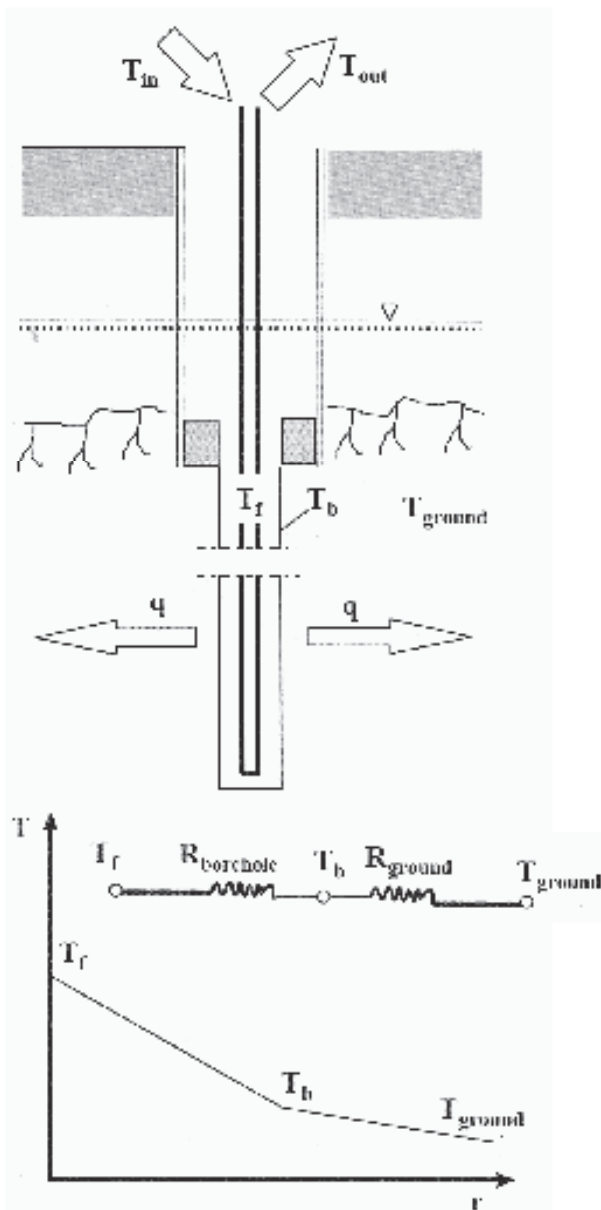


Figure 8. Temperature loss due to the thermal resistance of absorber and fill-material in a borehole (Gehlin).

Equation 8 can be simplified to a linear relation between T_m and $\ln(t)$:

$$T_m = k \ln(t) + m \quad (9)$$

with

$$k = \frac{\dot{Q}}{4\pi\lambda_{eff}L_b} \quad (10)$$

and

$$m = \frac{\dot{Q}}{L_b} \left(\frac{1}{4\pi\lambda_{eff}} \left[\ln\left(\frac{4z}{r_b^2}\right) - \bar{\gamma} \right] - R_b \right) + T_0 \quad (11)$$

By plotting the mean fluid temperature versus the dimensionless time parameter $\tau = \ln(t)$ the inclination k of the graph is obtained, hence leading to the thermal conductivity λ from equation 10. This finally provides the thermal resistance R_b between the heat carrier fluid and the borehole wall

$$R_b = \frac{L_b}{\dot{Q}}(T_m - T_0) - \frac{1}{4\pi\lambda_{eff}} \left(\ln(t) + \ln\left(\frac{4z}{r_b^2}\right) - \bar{\gamma} \right) \quad (12)$$

in [K/(W/m)]

The higher the thermal borehole resistance, the higher is the temperature step between the heat carrier fluid and the surrounding ground, hence the temperature loss. This is also the case for energy piles or energy diaphragm walls.

5 ENERGY WELLS - AN OVERVIEW

There are three different groups of geothermal wells that serve for environmentally friendly heating/cooling at low cost:

- (a) Exploiting hot water from the ground by boreholes reaching to a depth up to about 2000 m;
- (b) Conventional ground heat exchanger boreholes drilled up to about 300 m depth;
- (c) Wells that are anyway required for temporary groundwater lowering serve simultaneously as a heat extraction/storage system;
- (d) Near-surface open systems.

Drilling deep geothermal boreholes for (a) and (b) requires specialized equipment, considerable chill and experience. Such systems only serve for heat exchanging. Energy wells of group (c), however, represent a two-purpose system, hence a technology containing geotechnical and geothermal engineering: Many construction sites require wells for groundwater lowering. Sometimes discharge wells are coupled with recharge wells in order to minimize ground settlement. These temporary measures can be also used for heating and cooling adjacent buildings. This may be performed temporarily during the construction period but also permanently after ceasing groundwater lowering. Experience has revealed that the public acceptance of metros, railways and roads by neighbouring people increases if they are provided by cheap, renewable energy from such energy wells or other geothermal systems.

Thermo-active foundations, tunnels etc., hence earth-contact structural elements and related energy wells exhibit closed circuits. In contrast, open systems use water from an aquifer which is pressed through a heat exchanger or heat pump. These are simpler but hardly used in Austria because of operational problems such as clogging or bio-fouling in the wells and heat exchangers. Clogging may occur by precipitation of dissolved minerals caused by temperature changes and precipitation of iron-manganese hydroxides. It increases with temperature variations in the aquifer and with air entering the wells or pipework. The latter can be avoided by operating the system with a slight overpressure. Furthermore, such wells need submersible pumps that can be lifted for maintenance.

In order to gain sufficient energy from open systems a great number of wells may be needed, thus extracting a high quantity of groundwater. The groundwater-based cooling and heating system of the Technical University of Eindhoven, for instance, circulates about 3,000 m³/h from 48 wells (Holdsworth, 2003). In several countries this may cause legal problems, because a considerable quantity of water is extracted from an aquifer and recharged at a different temperature. Moreover, groundwater extraction may cause settlement of adjacent buildings, unless it is properly coupled with the groundwater recharging scheme. TU Eindhoven has solved this problem by placing the wells in “mirrored” clusters, so

that when one set is extracting water the others inject. In the first phase of this scheme (with 32 wells) more than 20 MW of energy were delivered, leading to estimated annual savings of 2,600 MWh of electricity and 1.2 Mm³ of natural gas, as well as reducing annual carbon dioxide emissions by 2,800 t.

6 PILOT RESEARCH PROJECT

6.1 FIELD TESTS

Fig. 9 shows the scheme of a large-scale test with energy wells for heating and cooling. Simultaneously, these wells were used for a long-term groundwater lowering along a new railway line under construction. Hence, the tests could run from 2001 to 2003.

The following investigations were carried out for research purposes and to optimise an adjacent energy tunnel in cut and cover:

- In-situ determination of thermal soil parameters (thermal conductivity, specific heat capacity);
- Maximum amount of extractable heat and energy influx, and storage capacity;
- Long-term behaviour and temperature conditions;
- Influence of groundwater flow.

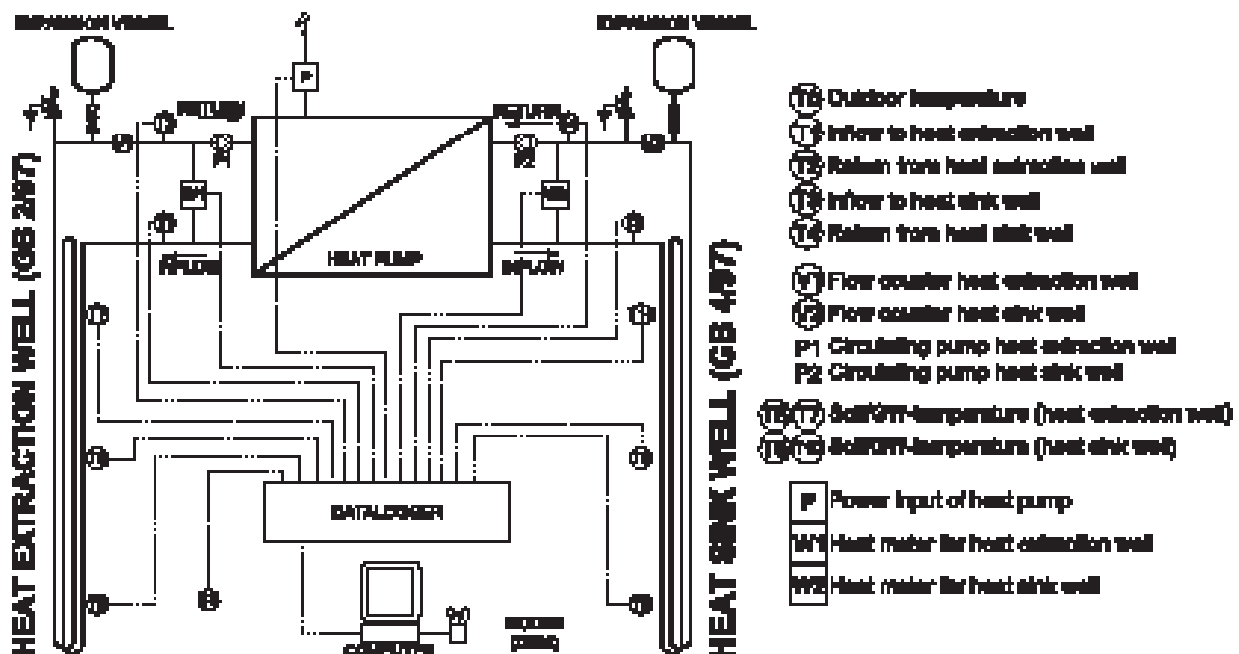


Figure 9. Scheme of testing plant “Energy well H” with GB 2/97 as heat extraction well and GB 4/97 as heat sink well.



Figure 10. Installation of absorber pipes into the filter pipe of a well used for groundwater lowering during a cut and cover tunnel construction.



Figure 11. Detail of Fig. 10 showing the U-shaped toe zone of absorber pipes.

During the tests several parameters were changed to investigate their influence, i.e. capacity of the circulating and heat pump, circuit temperatures, operation scheme (permanent, intermediate), ground temperature regeneration period between energy extraction, and storage. Moreover, the measurement should serve to compare numerical calculations with semi-analytical calculations.

The 45 m deep test wells were installed in 50 m deep boreholes of 600 mm diameter. The subsoil consisted of manmade fills (down to 4.7 m) underlain by heterogeneous tertiary sediments: silty clay, sand, sandy silt, gravel and wide-grained silty-sandy gravel, locally with sandstone and boulders. Below 23.0 m stiff cohesive layers with interlayers of sand and clay dominate.

The hydraulic conductivity was extremely scattered: locally from $k = 10^{-3}$ to 10^{-10} m/s with an overall value of about $k = 10^{-6}$ m/s. Due to the layered ground profile the horizontal permeability exceeded the vertical one, hence $k_h = 10 k_v$ to $50 k_v$.

Seepage water occurred between 9.5 to 13.4 m depth, the closed groundwater table lay at 20-23 m depth (seasonal amplitude), and in 36 m depth artesian groundwater was found.

Both boreholes were fitted with U-pipe heat exchangers consisting of HDPE-pipes of 25 mm outer diameter and located within the filter tube of the wells (Figs. 10 and 11). In order to achieve an optimal heat exchange between absorber and surrounding soil the spacing is typically filled with a cement-bentonite suspension for common energy wells. However, in this case only sand and gravel was used because the wells should be used again, at least temporarily, for groundwater extraction, too. Moreover, the influence of different contact-media should be investigated. In well GB 2/97 (Fig. 9) sand was filled between the tube and the filter, in well GB 4/97 the heat transfer into the absorber pipes should mainly occur by the contact with ground water.

Thermal energy was taken from the heat source GB 2/97 (discharge well), transported to a heat pump where the energy was raised to a higher temperature level, and then transferred back to the ground by the heat sink GB 4/97 (recharge well) - Fig. 9.

The following data were measured:

- Outdoor temperature [°C];
- Temperature of inflow and outflow [°C] of primary and secondary circuit;
- Temperature in both wells at different depths from 2.8 m to 45.6 m [°C];
- Volume flux in primary and secondary circuit [m^3/h];
- Cumulative heat volume in primary and secondary circuit [kWh];
- Electric performance of all electric equipment (heat pump, circulating pump, data-logger) [W].

The data-logger was connected to all measuring devices, registered in 20th and calculated / stored in 10³-intervalls. Instead of clean water a water-glycol mixture circulated in the absorber pipes thus influencing the measured heat quantity. This was taken into account by a reduction factor of 0.85.

Fig. 12 shows the temperature fluctuation in the absorber system after the start of operation on 28.03.2001. In the heat source (GB 2/97) the temperature

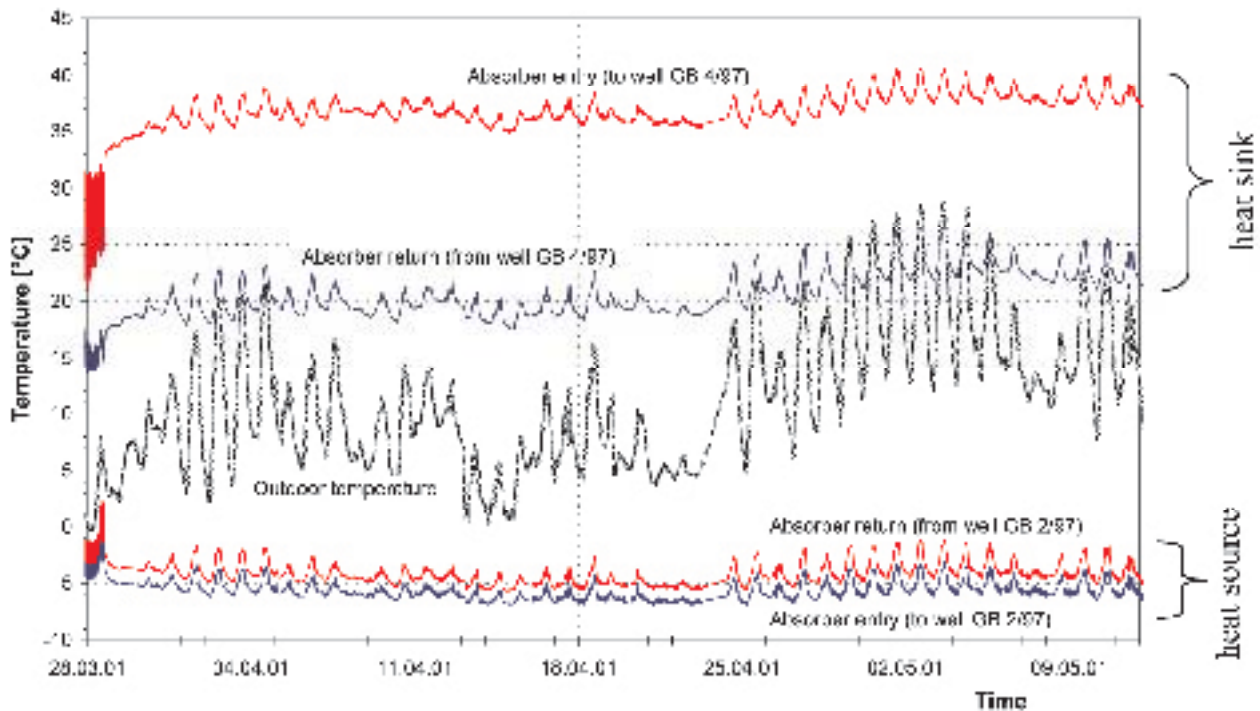


Figure 12. Operating temperatures in absorber system of energy well.

difference of the heat carrier fluid between absorber inflow and outflow was about $\Delta T=1.5^{\circ}\text{C}$, whereby the temperature level was very low and fluctuated at about $T=-5^{\circ}\text{C}$. This was caused by a high-performance circulating pump, which had too much power in relation to the relatively short absorber pipes in the well. But the over-capacity of the pump had been chosen deliberately to investigate the effects of an over-design.

Fig. 13 shows measured temperatures from February to June 2001. At the beginning of this period an intermediate operation was executed, whereby the heat pump was turned on and off within minutes. With such an operation only the temperature at the top of the heat sink is influenced. Temperatures of the heat source fluctuate in a range of about 1°C and interact strongly with the outdoor temperature.

At the end of March the operation scheme was changed from intermediate to continuous operation. The temperature set value of the secondary circuit was set to 55°C , so that the heat pump never turned off automatically. Fig. 13 shows that the lowest temperature of the heat carrier fluid was $T=-7^{\circ}\text{C}$ in the mid of April and the highest temperature in the secondary circuit was $T=41^{\circ}\text{C}$ in the mid of May. All temperature curves exhibit daily fluctuations, which indicate the influence of outdoor temperature. The temperature level is nearly constant during the whole period. Fig. 14 illustrates that about 60 kWh energy could be extracted from the

ground with one well within 24 hours. This energy was raised to a higher temperature level by the heat pump, so that an energy of about 110 kWh/24h was transferred back to ground.

In order to test various operation procedures the schema of Fig. 9 was changed to that of Figs. 15 and 16 in December 2001. The former energy storage well (sink well) was transformed into an energy extraction well, thus increasing the primary circuit. The heat gained by this energy system was increased by a heat pump to a higher temperature level and then sent to a heating radiator. After the radiator was exhausted a continuous operation had been started. A comparison of Fig 13 and Fig. 17 shows that the temperature level of the primary circuit is much higher after the system modification. Fig. 17 shows big temperature fluctuation of the heat carrier medium in the secondary circuit. This is caused by the radiator, which transfers the heat directly to the air.

The heat output of the secondary circuit (radiator) was lower and the extracted heat (primary circuit) was just a little bit higher than before the system had been modified (see Fig. 14 and Fig. 18). Due to smaller circulating pumps the demand of external energy was lower than before the system modification. About 62 kWh energy within 24 hours could be extracted from the ground with both wells, and the radiator finally had an output of about 93 kWh/24h.

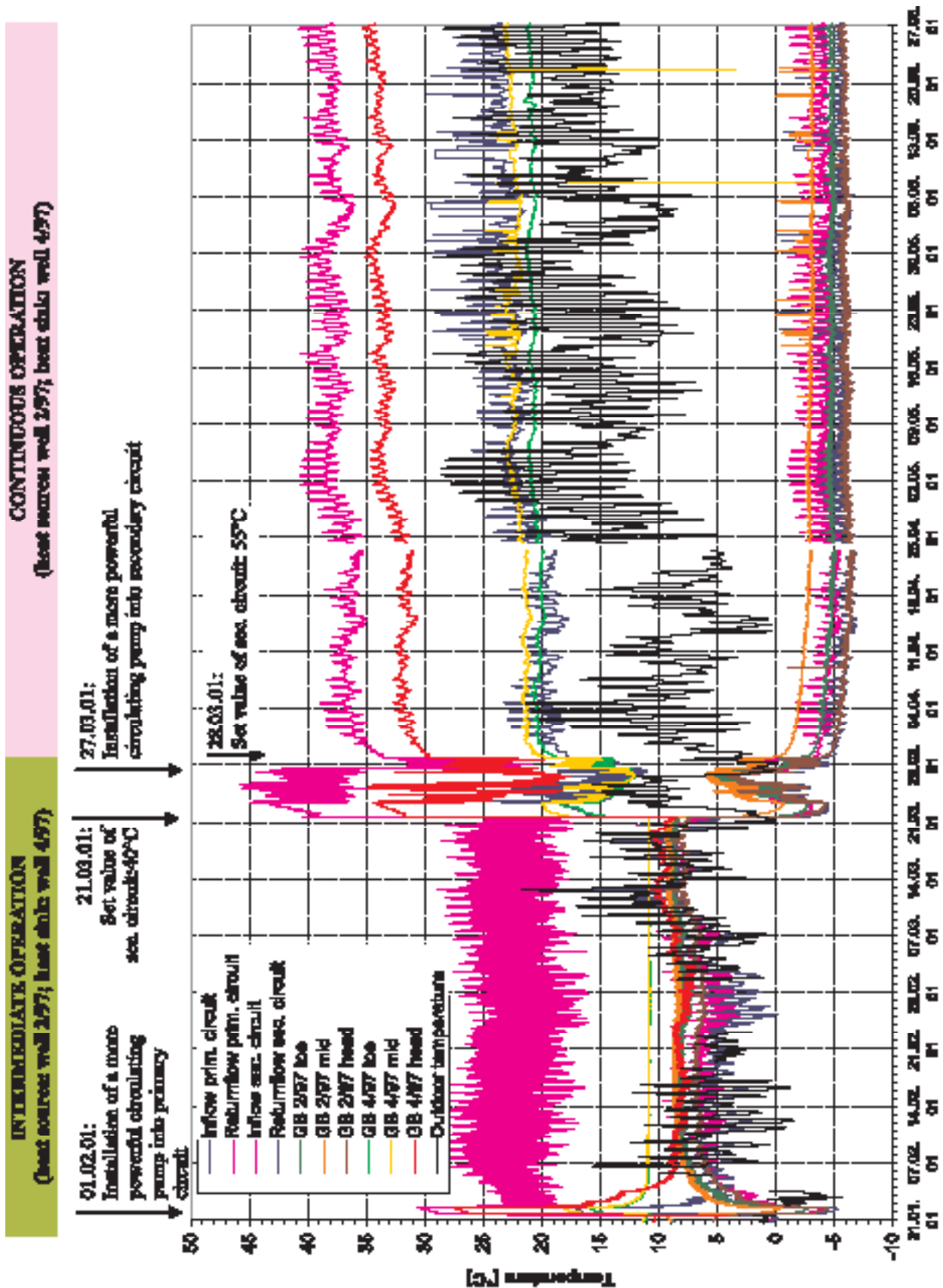


Figure 13. Measured temperatures from February to June 2001 (before system modification).

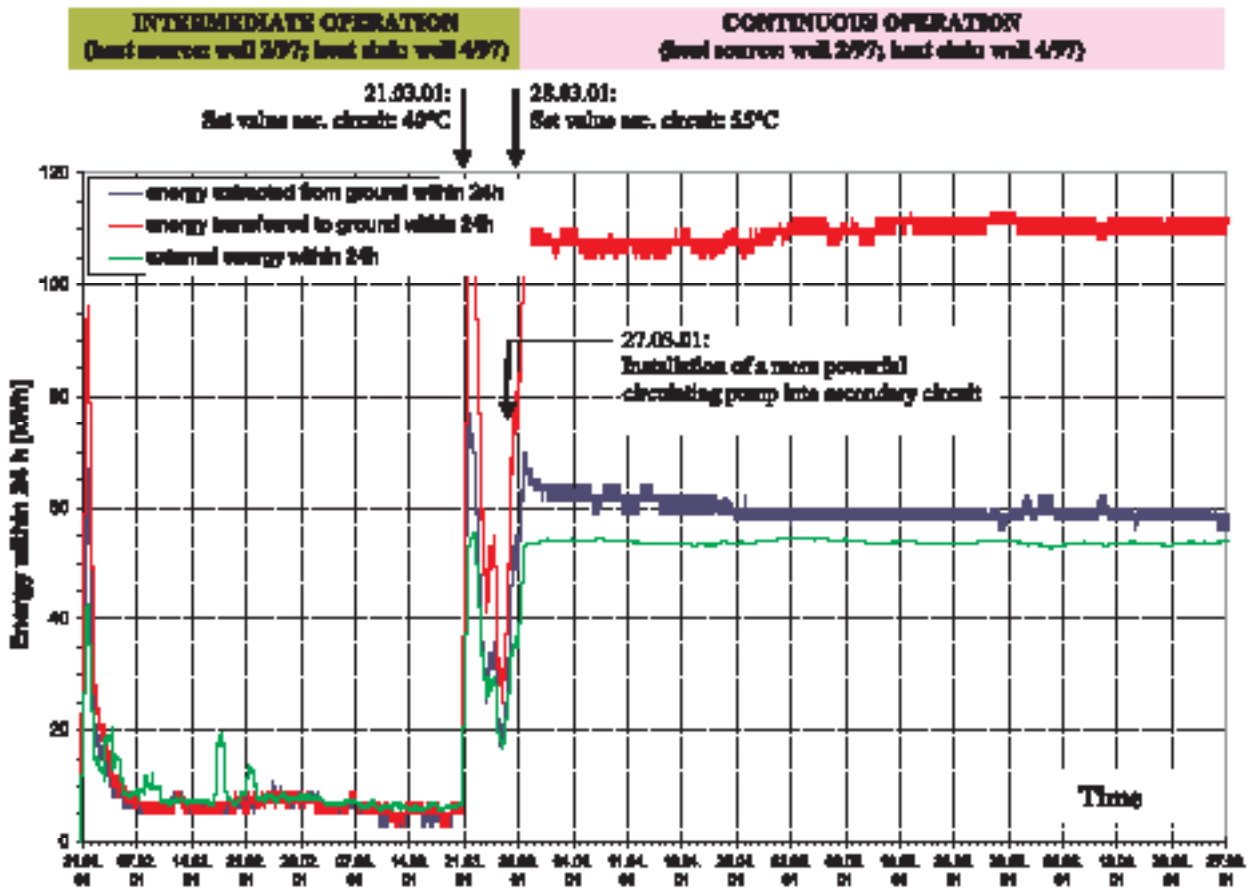


Figure 14. Measured energy within 24h from February to June 2001 (before system modification).

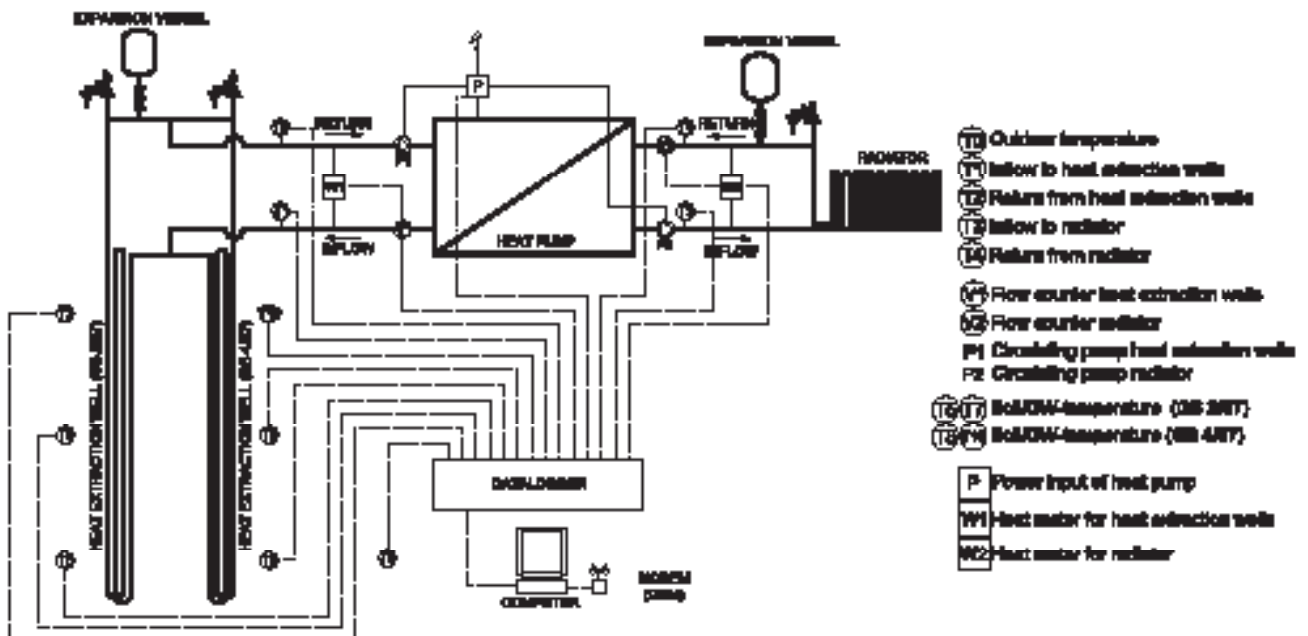


Figure 15. System modification of testing plant "Energy well H" with both GB2/97 and GB 4/97 as heat extraction wells. A second radiator serves as new heat sink that transfers heat to the outdoor air.

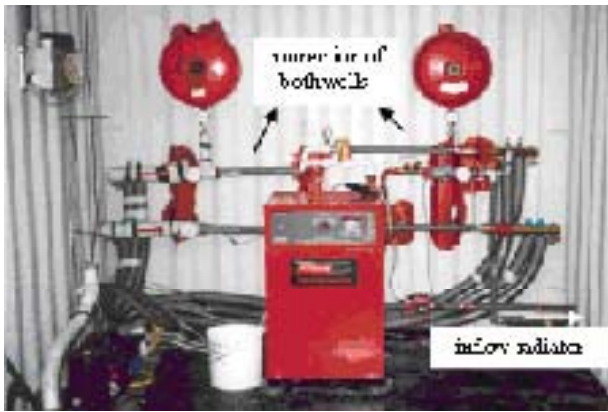


Figure 16. The testing plant “Energy well H” in a container on the construction site; details of Fig. 15.



Figure 16a. Data-logger with GSM-module; detail of Figs. 15 and 16.

Fig. 19 shows that in this period the seasonal performance factor was in the range of about $\beta = 2.4$, whereby the performance factor of the *Carnot*-process was calculated to $\epsilon_{Carnot} = 6.6$. This low performance factor confirmed that heat pumps of a too high coefficient of performance should be avoided.

At the end of April 2002 the system was modified again in order to investigate heat extraction from the energy well GB 4/97 only. Therefore the circuits to the well GB 2/97 were closed. Fig. 17 illustrates the regeneration process of this well after a long continuous operation period.

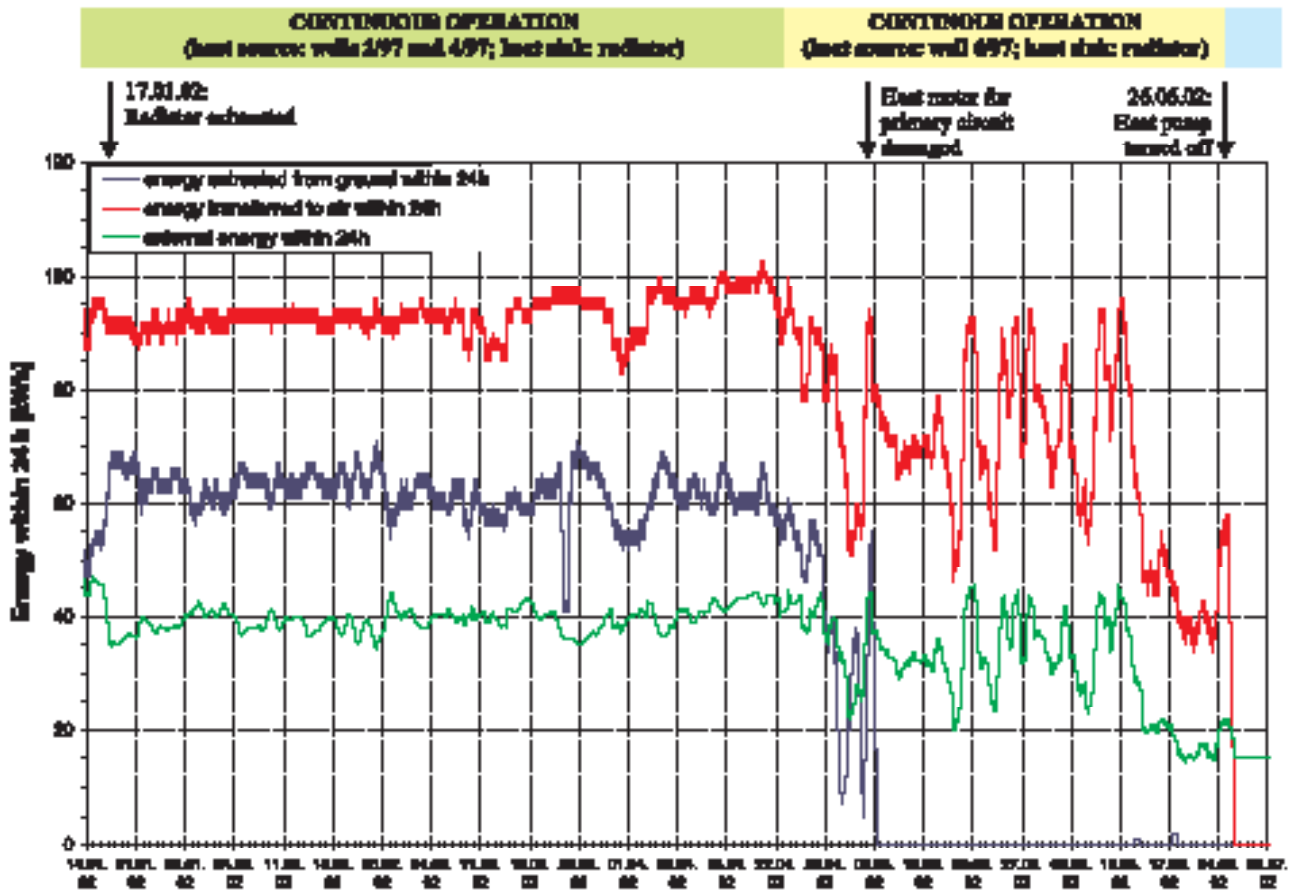


Figure 18. Measured energy within 24h from February to June 2002 (after system modification).

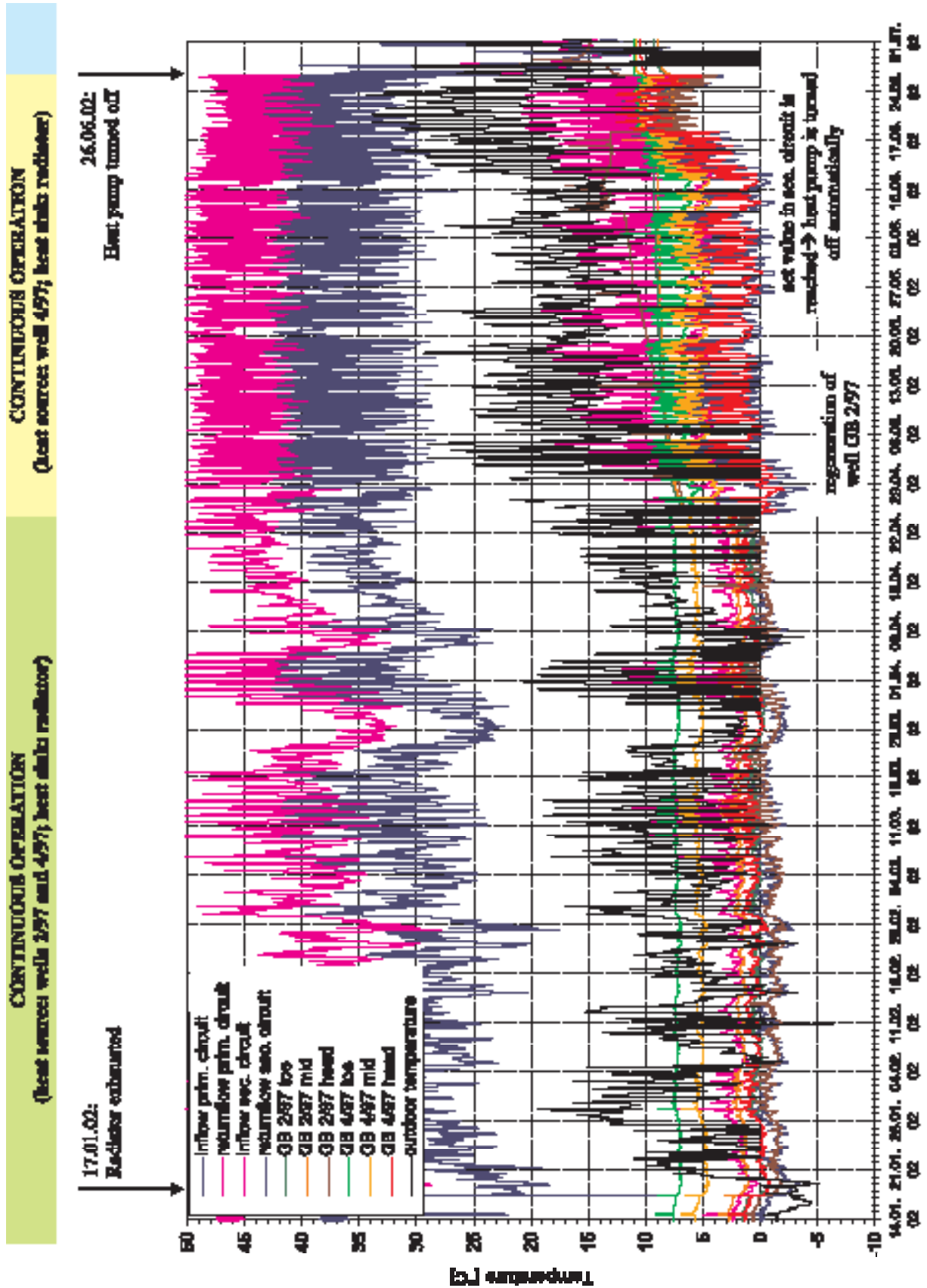


Figure 17. Measured temperatures from February to June 2002 (after system modification).

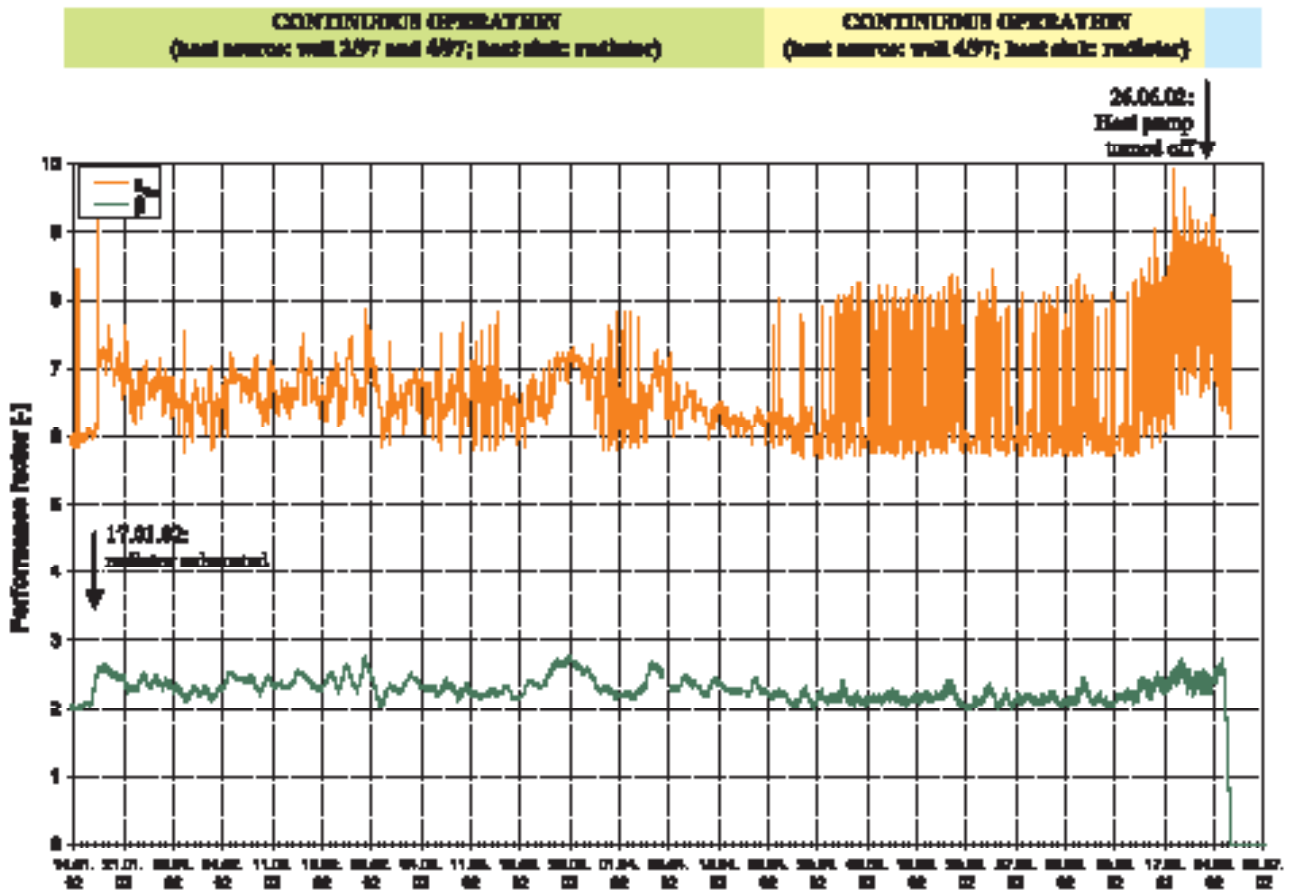


Figure 19. Measured performance factor from February to June 2002 (after system modification).

6.2 NUMERICAL SIMULATIONS COMPARED TO ANALYTICAL SOLUTIONS

An energy well is a vertical heat absorber of finite length embedded in a half-infinite soil body and it is a suitable model to prove all basic cases of heat conduction. For numerical simulations it is assumed that the temperature of the soil surface (half-infinite body) oscillates with a sinus function to simulate the annual temperature change. The temperature at the borders of the borehole is assumed to be periodically constant in order to calculate the maximum possible heat transfer (extraction and input, respectively).

A typical simulated temperature distribution is demonstrated in Fig. 20 representing the temperature field after five months of heat extraction. Different flux velocities of energy depending on the geometry and thermal soil parameters are indicated by the isotherms.

The accuracy of the numerical finite element model depends on numerous parameters, such as the refinement of the mesh and the polynomial order of the used elements. The basic cases 1 (semi-infinite body), 2

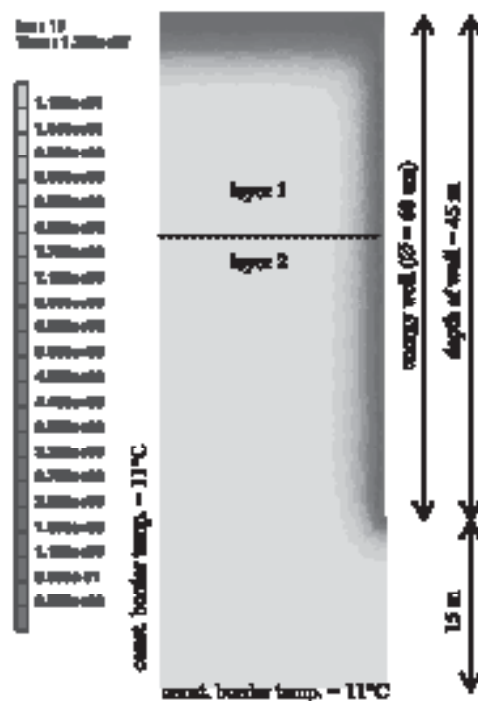


Figure 20. Temperature distribution around an energy well after 5 months of heat extraction.

(infinite body with cylindrical gap) and 3 (infinite body with spherical gap) in Table 1 can be used to simulate appropriately most of the commonly used absorber elements. With regard to the energy wells all basic cases interact: Case 1 refers to the ground surface, case 2 to the shaft interface of the well, and case 3 describes the spherical situation in the bottom of the well. Comparative calculations have shown that there are only minimal differences between the numerical and the analytical solutions as indicated in Fig. 21 for the example of Fig. 20. The corresponding parameters are given in Table 2. One of the results is that the soil temperature is influenced only to a depth of 7m at the maximum despite a simulated extreme energy flux in the wells.

Energy balances were also investigated with the numerical model. The simulation provided the power of extraction and the power of influx during a two-year simulation period for the 45 m deep test well. From Fig. 22 it can be seen that during the second heating period more energy could be extracted from the ground due to the energy influx in summer. These calculations can be also compared with measurements. Both calculations and measurements have resulted in a long-term extraction power of about 1.8 kW per well.

Table 1. Basic cases for heat conduction in soil

Basic case	Sketch	Differential Equation
1 Semi-infinite body		$\frac{\partial^2}{\partial x^2} \vartheta(x, t) = \frac{1}{a} \frac{\partial}{\partial t} \vartheta(x, t)$
2 Infinite body with cylindrical gap		$\frac{\partial^2}{\partial r^2} \vartheta(r, t) + \frac{1}{r} \frac{\partial}{\partial r} \vartheta(r, t) = \frac{1}{a} \frac{\partial}{\partial t} \vartheta(r, t)$
3 Infinite body with spherical gap		$\frac{\partial^2}{\partial r^2} \vartheta(r, t) + \frac{2}{r} \frac{\partial}{\partial r} \vartheta(r, t) = \frac{1}{a} \frac{\partial}{\partial t} \vartheta(r, t)$

Table 2. Exemplary parameters for calculating the basic cases of Table 1

Property	Value
Thermal conductivity λ	2.5 W/(M.K)
Density ρ	2,700 kg/m ³
Specific heat capacity c	800 J/(kg.K)
Temperature conductivity a	1.1574x10 ⁻⁶ m ² /s
Radius of cylindrical and spherical gap	0.3 m
Sudden temperature rise ϑ_s	25 K
Observed period t	a half year = 182.5 days

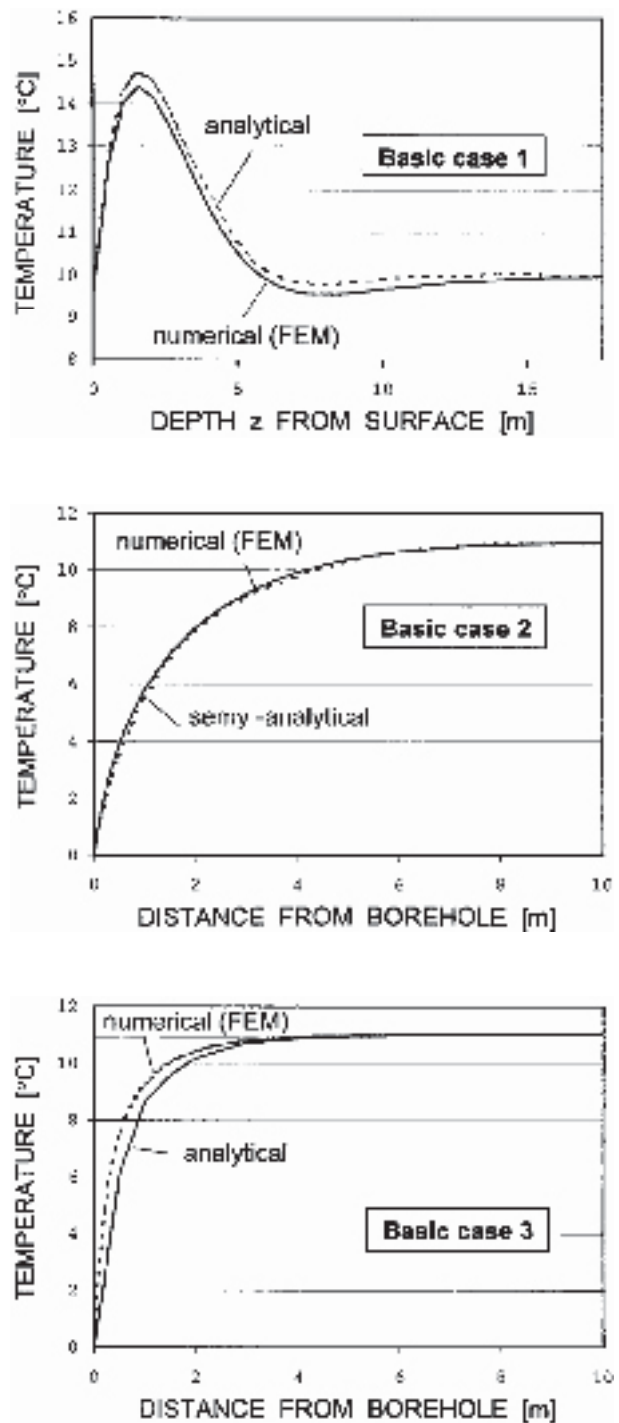


Figure 21. Temperature distribution at a certain time calculated with the FE-model (continuous line) and the analytical solution (dashed line) for basic cases 1, 2 and 3.

To sum up, parametric studies and comparative calculations have shown that both methods, numerical and analytical solutions, are suitable for thermal calculations. Complicated cases, however, can be only solved numerically.

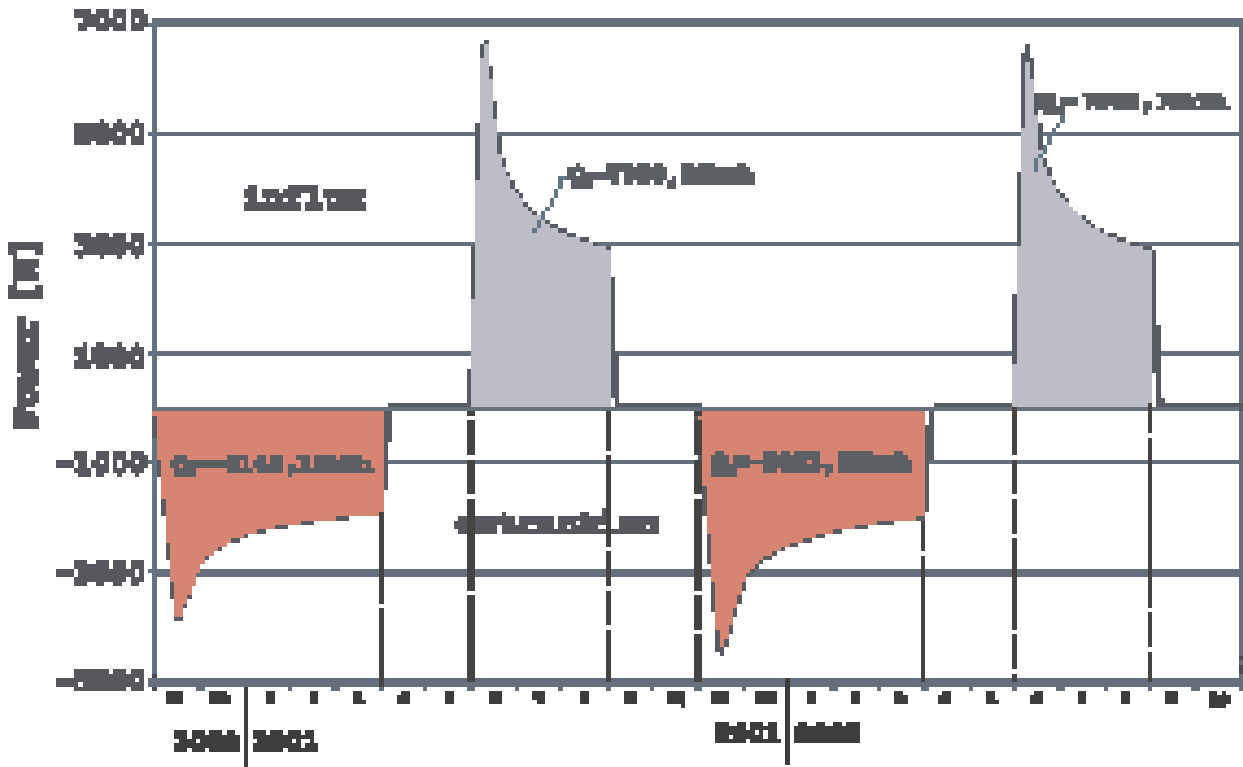


Figure 22. Results from FEM calculations for an energy well (example of Fig. 20). The covered areas represent the extracted energy (-) and the input energy (+) over a period of two years.

6.3 OPTIMISED OPERATION

Fig. 17 demonstrates that an intermediate operation with short intervals produces significantly less energy than a permanent, continuous operation of the energy system. Furthermore, it could be confirmed that the performance factor of the plant drops with increasing temperature difference between primary and secondary circuit, especially if the performance of the heat pump is not adapted to the temperature difference. A too high capacity causes a too strong cooling of the heat transfer fluid.

The Carnot-process represents the ideal heat pump process and has theoretically the highest thermal efficiency of all circulating processes between two given temperatures. Its coefficient of performance is

$$COP_{Carnot} = \frac{T_{cond}}{T_{cond} - T_{evap}} \quad (13)$$

where T_{cond} = temperature at condenser [K]

T_{evap} = temperature at evaporator [K]

When calculating COP_{Carnot} it should be considered that the evaporative temperature is by 3 to 5K lower than the outflow temperature of the heat source from the evaporator, and that the liquefaction temperature is at least 3K higher than the outflow temperature of the useable heat carrier from the liquefier. Consequently, the modified coefficient of performance of the Carnot-process becomes

$$COP_{Carnot} = \frac{T_{cond} + 3K}{(T_{cond} + 3K) - (T_{evap} - 5K)} \quad (14)$$

Calculations based on the measured temperatures provided performance coefficients of $\epsilon_{Carnot} \geq 6$. However, the real heat pump process usually achieves only about 55% of the performance coefficient of the Carnot-process due to significant compression losses, losses from friction etc.

This intensive heat extraction caused freezing in the discharge well, which should be usually avoided. Freezing increases the lateral pressure on the absorber pipes and may cause bulging. The measurements disclosed an increase in pressure caused by a constriction (necking) of the pipe. Such phenomena have been mainly observed

in rather dense granular soils whereas in soft cohesive soil lateral soil displacement prevails. Freezing, therefore, strongly stresses the PE-pipes, reduces gradually their cross section and may eventually cause a full drop out of a ground heat exchanger or heat exchanger bore-hole. Consequently, pressure and temperature are the main parameters influencing serviceability and life-time of HDPE absorber pipes in energy wells. Contrary to that, absorber pipes embedded in concrete (energy piles etc.) keep nearly “unlimited” function.

6.4 BACK CALCULATION OF THERMAL PARAMETERS

The in-situ determination of thermal soil parameters illustrates the strong influence of freezing, which should be investigated in the research programme because improper operation (excessive heat extraction) may occur in practice. The back-calculation is based on the following project data:

- Length of bore hole: $L_b = 45$ m;
- Type and material of heat exchanger: double U-tube absorber (HDPE);
- Radius of borehole: $r_b = 30$ cm;
- Measurements from the beginning of April 2001 (continuous operation of the test well) to determine the effective thermal conductivity. The period from start of pre-operation until April 2001 comprises 2081 hours (see Fig. 23).

The mean temperature of the heat carrier fluid is:

$$T_m = \frac{T_{inflow} + T_{outflow}}{2} \quad (15)$$

A reliable interpretation of the measured data requires a time-temperature regression line after a certain period of operation (t_{min}). This is obtained from a “minimum-time” criterion using the following soil parameters:

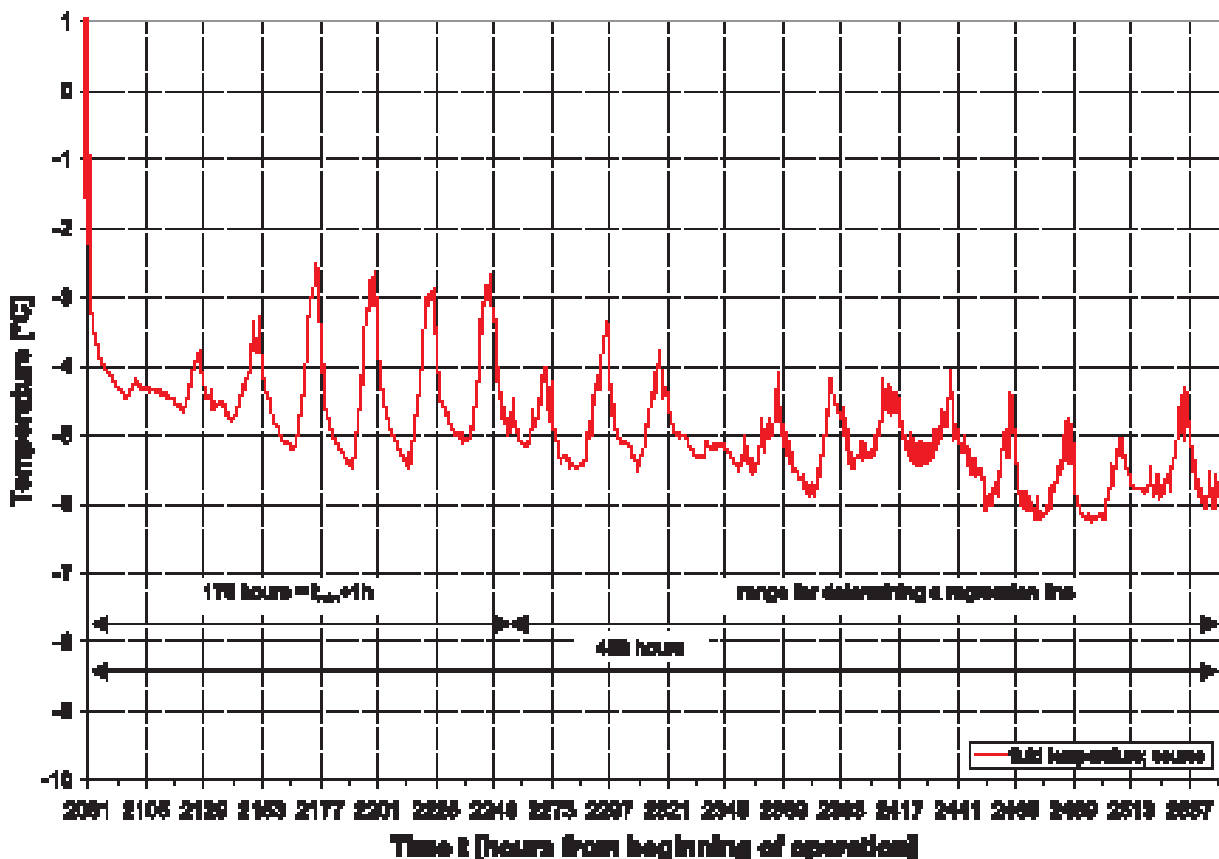


Figure 23. Mean heat carrier fluid temperature of the heat source. The temperature oscillation is caused by the outdoor temperatures. Also shown is the time range for determining a relevant regression line (see Fig. 24).

- Thermal conductivity:
 $\lambda_s = 4.0 \text{ W/m K}$
 - Density: $\sigma_s = 2800 \text{ kg/m}^3$
 - Specific heat capacity:
 $c_s = 1200 \text{ J/kg K}$
- $$\left. \begin{array}{l} \lambda_s = 4.0 \text{ W/m K} \\ \sigma_s = 2800 \text{ kg/m}^3 \\ c_s = 1200 \text{ J/kg K} \end{array} \right\} \sigma_s c_s = 3.36 \text{ MJ/m}^3 \text{ K}$$

The thermal diffusivity a_s is obtained from:

$$a_s = \frac{\lambda_s}{\rho_s c_s} = \frac{4.0}{3360000} = 1.19 \cdot 10^{-6} \text{ m}^2/\text{s} \quad (16)$$

The “minimum-time” criterion results in:

$$t_{min} > \frac{5r_d^2}{a_s} = \frac{5 \cdot 0.15^2}{1.19 \cdot 10^{-6}} = 630000 \text{ s} = 175 \text{ hours} \quad (17)$$

The regression line is derived from a time-temperature series of the daily mean temperature, whereby the temperature data starting one hour after the “minimum-time” (i.e. 176h) are used. On the abscissa the dimensionless time parameter $\tau = \ln(t)$ is drawn in a linear scale. As shown in Fig. 24, the inclination of the regression line results in $k = -1.02$, and the intersection

with the ordinate is at $m = 0.62$. The intersection point with the ordinate lies in the zero point of the diagram and is therefore not shown in Fig. 24.

Calculating the effective thermal conductivity $\lambda_{s,eff}$ needs the extracted amount of heat. According to the measurements a total heat volume of $\dot{Q} = 2605 \text{ W}$ was extracted from the soil, leading to:

$$\lambda_{s,eff} = \frac{\dot{Q}}{4\pi k L_s} = \frac{-2605}{4 \cdot \pi \cdot -1.02 \cdot 45} = 4.52 \text{ W/(m K)} \quad (18)$$

This high effective thermal conductivity (for comparison: concrete has a thermal conductivity of $\lambda_{concrete} = 2.1 \text{ W/(m K)}$) was caused by the site-specific conditions and temperatures. Measurements disclosed that the temperature of the heat carrier fluid was about -5°C (and lower) for a long time. Because of this deep temperature the groundwater close to the heat exchanger started to freeze. Finally, a continuous groundwater flow created a big ice block around the absorber pipes. Later measurements, which were taken after heat extraction in order to investigate the thermal regeneration capacity of the ground, proved this.

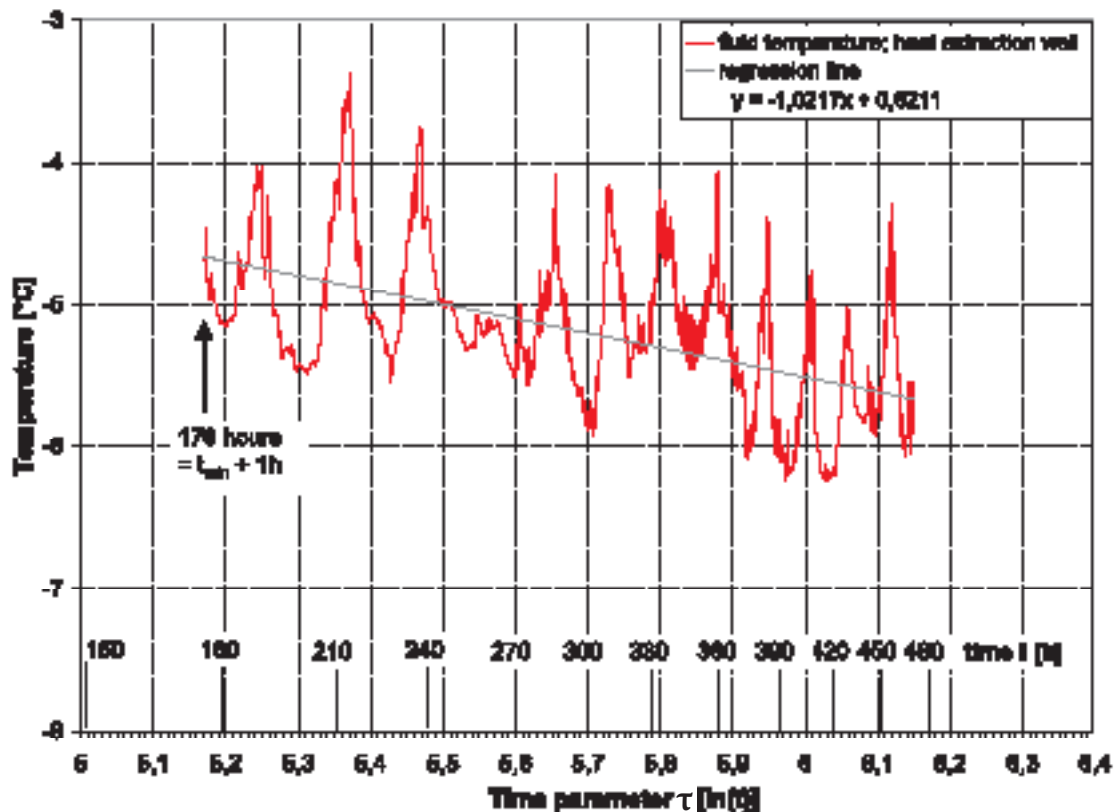


Figure 24. Mean temperature of the heat carrier fluid from the 176th hour until 486th hour after starting the test (Note: $\ln(176)=5.17$ and $\ln(468)=6.15$).

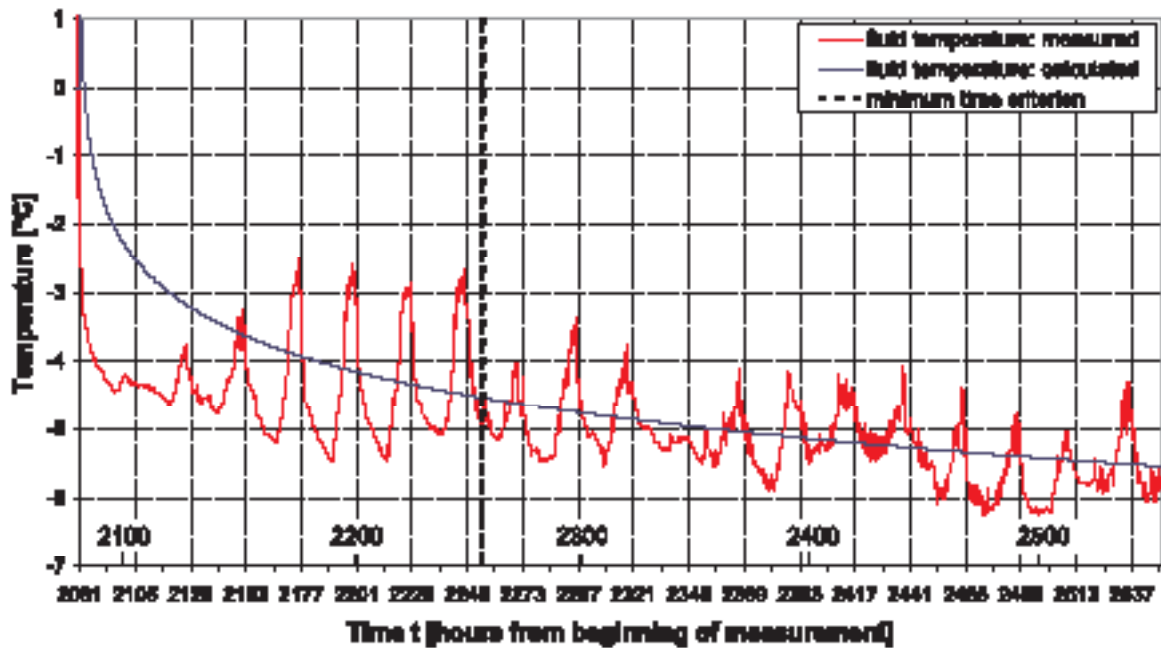


Figure 25. Measured and calculated (with $R_b=0.19$ K/(W/m)) mean temperature of the heat carrier fluid for the testing plant “Energy Well”.

During freezing of water energy is extracted until the water becomes ice. This so called latent heat is the significant reason for the calculated high effective thermal conductivity: thermal conductivity of water $\lambda_{water} = 0.56$ W/(m K) and thermal conductivity of ice $\lambda_{ice} = 2.23$ W/(m K). In addition to that a groundwater flow results in a high effective thermal conductivity because of a continuous heat supply by convection.

The temperature loss from the borehole wall to the heat carrier fluid is described by the thermal borehole resistance which typically lies about $R_b = 0.1$ K/(W/m). It can be determined by a variation of t and T_m using equation (12) with the following parameters:

- Undisturbed temperature of the soil: $T_s = T_0 = 11^\circ\text{C}$;
- Thermal conductivity: $\lambda_{s,eff} = 4.5$ W/m K;
- Thermal diffusivity: $a_s = 1.34 \cdot 10^{-6}$ m²/s.

The thermal borehole resistance at the testing plant varied between 0.179 to 0.202 with an average value of $R_b = 0.19$ K/(W/m). This high value was due to the improperly excessive heat extraction that lead to freezing. Eq. (12) shows that this parameter depends on the mean temperature of the heat carrier fluid, which for its part fluctuates in relation to the outdoor temperature.

With the determined effective thermal conductivity and thermal borehole resistance the time-mean fluid temperature curve can be back-calculated analytically.

In Fig. 25 both the calculated and measured values are shown.

Field tests and numerical simulations confirmed that there is a clear analogy between energy wells and hydraulic wells. The rate of pumping corresponds to heat extraction: The groundwater drawdown curve is analogous to the temperature change in the ground depending on the distance from the well, time, ground properties and on the pumping rate or extracted heat respectively.

Moreover, it could be found that energy extraction and sink wells should have a distance of at least 15 m. For 10 kW of usable energy about 1.5 to 1.8 m³/h of groundwater is required.

7 PROMOTION OF GEOTHERMAL ENERGY UTILISATION

Early ecological energy planning for buildings can prevent in many cases costly refurbishment and renovation in the future. High-quality energy design involves not only heating and cooling (rooms, water) but also lighting.

Geothermal geotechnics offers a promising alternative to conventional heating/cooling systems, providing solutions to the challenges of today's energy policies. The

targets for renewable energy and for energy buildings can be generally reached only by political measures.

- High taxes on fossil fuels are the most important prerequisite for energy saving and promotion of renewable energy sources.
- In order to promote the installation of thermo-active systems or other heating/cooling systems based on renewable energy, the economic incentives for private investors, house owners, companies, and also for public administrators to invest in renewable energy systems should be improved in many countries. Strong support by European Union policy is necessary.
- Legislation.
- Public grants.

Since January 2004 each person who wants to build a family house in Austria has received financial support by the local government only if they present an energy performance certificate with a low energy number. This number describes the energy consumption (provided by heating energy minus heating losses) and is expressed in kWh/m² and year.

Promotion by public funds is granted only if this energy number is smaller than 50 kWh/m² for each floor. At values less than 40, 30, 25, 20 and 15 kWh/m² the grant increases step by step.

However, if a building is heated/cooled by means of clean, renewable energy, for example by geothermal systems, the allowable limit value for energy consumption may be increased. The target of multidisciplinary innovation should approach heat-and-light systems combined with ground-sourced or solar residual heating/cooling.

Thermo-active structures (including energy foundations and energy wells) are therefore very helpful in reaching this low energy number. Their installation is widely supported by politicians and media. Consequently, about 500 buildings with energy foundations or retaining/basement walls already exist in Austria. This philosophy is fully supported by Directive 2002/91/EC of the European Parliament and of the Council on the energy performance of buildings, which will come into force in the European Community on 4 January 2006 at the latest. Thus an energy performance certificate has to be presented if a building with more than 500 m² is sold or rented.

8 CONCLUSIONS

Global energy consumption is increasing tremendously. The "World Energy Outlook 2005" estimates that in 2030 about 16.5 billion oil units will be needed annually if the present energy strategies do not change globally. World supplies of fossil fuels are rapidly being depleted. Consequently, multidisciplinary efforts are needed to develop innovative building practices using renewable energy, including new energy storage technologies. Near-surface geothermal and deep geothermal energy, solar photovoltaic and solar thermal energy, and wind energy are promising alternatives (like conventional hydropower energy). Optimum economical efficiency and environmental protection are gained in most cases by an 'energy mix' from different sources. Local climate and ground properties, technological level, the specific use of a building, seasonal fluctuations, environmental conditions and actual energy prices are the main influencing parameters.

Integral planning and balancing of buildings means considering the technical, economic, aesthetic and ecological aspects. An integral design, therefore, is always a sustainable design too, and it requires multi-objective optimisation. Balancing refers to materials, energy, emissions, waste water, waste/rubbish and its disposal or recycling, costs (investment, maintenance, demolition), and life cycle.

Both thermo-active ground structures (energy foundations, retaining walls, tunnels) and energy wells are the geotechnical contribution to renewable energy production. A significant advantage of such systems is that they are installed within elements that are already needed for statical/structural or geotechnical reasons. Hence no additional structural or hydraulic measures are required. Foundations, walls (below and above ground) and tunnel linings can be used directly for the installation of absorber pipes for heat exchange. Wells for groundwater lowering may also be simultaneously used for heat extraction/storage, thus becoming energy wells. This innovation is a key improvement over the conventional geothermal methods such as (deep) borehole heat exchangers or near-surface earth collector systems. At a certain depth, ground temperature remains widely constant throughout the year (e.g. 10–15°C below 10–15 m in most European regions), and a heat exchanger allows it to be used as a heat source in winter and for cooling in summer.

REFERENCES

- [1] Adam, D., Markiewicz, R. (2002). Nutzung der geothermischen Energie mittels erdberührter Bauwerke. *Österr. Ingenieur- u. Arch. Zeitschrift* 147, No. 4, 5 and 6.
- [2] Brandl, H. (1998). Energy piles and diaphragm walls for heat transfer from and into ground. *Proc. 3rd Int. Geotech. Seminar, Deep Foundations and Auger Piles III, Ghent, A.A. Balkema, Rotterdam*, 37-60.
- [3] Brandl, H. (2003). Geothermal heating and cooling of buildings. 4th Šuklje Lecture. Slovenian Geotechnical Society. *Proceedings*, pp. 3-27
- [4] Brandl, H. (2006). Energy foundations and other thermo-active ground structures. *Geotechnique*, Vol. LVI, No. 2, 79-122
- [5] Brandl, H., Adam, D. and Markiewicz, R. (2006). Energy geocomposites for tunnels. *8th International Conference on Geosynthetics (IGS)*. Yokohama, Proceedings in press.
- [6] Gehlin, S. (1998). *Thermal Response Test – In-Situ Measurements of Thermal Properties in Hard Rock*. Division of Water Resources Engineering, Department of Environmental Engineering, Lulea University of Technology, Sweden.
- [7] Hellström, G. (1991). *Ground heat storage: thermal analyses of duct storage systems I. Theory*. Doctoral dissertation, Lund Institute of Technology, Department of Mathematical Physics, Lund University, Lund, Sweden.
- [8] Hofinger, J. (2000). *Nutzung geothermischer Energie und Umweltwärme auf niedrigem Temperaturniveau mittels erdberührter Bauteile*. Diplomarbeit. Technische Universität Wien.
- [9] Holdsworth, B. (2003). Cool thinking. *European Foundations*, Spring, 10–11.
- [10] Markiewicz, R. (2004). *Numerische und experimentelle Untersuchungen zur Nutzung von geothermischer Energie mittels erdberührter Bauteile und Neuentwicklungen für den Tunnelbau*. Dissertation. Technische Universität Wien.
- [11] Markiewicz, R., Adam, D. et al. (2005). Extraction of Geothermal Energy from Tunnel. *16th Int. Conference of ISSMGE, Osaka, Proceedings*, 1629 – 1635.
- [12] Sanner, B. Reuß, M. Mands, E. and Müller, J. Erfahrungen mit dem Thermal Response Test in Deutschland. <http://www.ubeg.de/Downloads/GeRTGerm.pdf>.

GRANULOMETRIJA KOT FUNKCIJA SPEKTRALNE AMPLITUDE: NOV REGRESIJSKI ZAKON ZA MORSKE SEDIMENTE

NELLY ZANNETE ĪN DARINKA BATTELINO

o avtorjema

Nelly Zannete
Dipartimento di Ingegneria Civile,
Università degli Studi di Trieste
p.le Europa 1, 34127 Trst, Italija

Darinka Battelino
Dipartimento di Ingegneria Civile,
Università degli Studi di Trieste
p.le Europa 1, 34127 Trst, Italija
E-pošta: battelino@dic.univ.trieste.it

izvleček

V članku je prikazana geofizikalna metoda, katera omogoča analizo poroznih, saturiranih morskih sedimentov z uporabo širjenja akustičnega valovanja in primerjava dobljenih rezultatov z rezultati konvencionalnih geomehanskih preiskav. Akustične meritve so bile izdelane v SACLANT-NATO v kraju Spezija (I), z uporabo Vertikal Multi Sensor Core Logger (V-MSCL). Rezultati akustične preiskave so bili primerjani z granulometrijskimi krivuljami analiziranih morskih sedimentov in karakteristikami širjenja valov, kot so hitrost in dušenje valovanja ter poroznost materiala. Analiza rezultatov je bila izdelana na osnovi različnih matematičnih modelov, podanih v literaturi, s katerimi bi bilo možno določiti fizikalno odvisnost med širitvijo valovanja v poroznem, saturiranem materialu in njegovo granulometrijo. Rezultat študije je nov pristop, ki omogoča iz izmerjenih vrednosti spektralne amplitude oziroma spektralne analize širjenja valov v poroznem in saturiranem materialu, neposredno določanje velikosti posameznih zrn z matematično eksponentno funkcijo.

ključne besede

akustični valovi, drobno zrnate zemljine, krivulja zrnivosti

MEAN GRAIN SIZE AS FUNCTION OF SPECTRAL AMPLITUDE: A NEW REGRESSION LAW FOR MARINE SEDIMENT CORES

NELLY ZANNETE and DARINKA BATTELINO

About the authors

Nelly Zannete
Dipartimento di Ingegneria Civile,
Università degli Studi di Trieste
p.le Europa 1, 34127 Trieste, Italy

Darinka Battelino
Dipartimento di Ingegneria Civile,
Università degli Studi di Trieste
p.le Europa 1, 34127 Trieste, Italy
E-mail: battelino@dic.univ.trieste.it

Abstract

Geophysics has been developed in order to supply indicative estimations in soil mechanics like the grain size distribution of finely grained soils as clay, silt and fine sands. The paper describes the attempt to characterize porous and saturated marine sediments with a non destructive technique which is the acoustic wave, in order to determine the correlation with geotechnical measurements. The characterization of physical parameters of marine sediments was based on research methods which permit to describe the parameters defining different types of sediment and zones of sedimentation; to determine fundamental parameters that influence the propagation of the acoustic waves in saturated and porous means; to define quick and indicative methods for characterization of physical parameters of analysed means. The acoustic measurements were carried out at SACLANT-NATO of La Spezia (I), where the Vertical Multi Sensor Core Logger (V-MSCL) was used. The results of acoustic tests were compared to the grain size curves of the sediments and the propagation characteristics such as velocity, density, porosity and absorption of experimentally determined data. The analyses are based on various mathematical models presented in literature, in order to predict and to describe physical mechanisms of the wave propagation using a simplification of the sediment structure. The target of the study was to determine a new mathematical law that linked the mean grain size to a directly

measurable parameter such as the spectral amplitude, and to offer the possibility to obtain the first indicative value of the sediment mean grain size.

The determined exponential law represents an innovative and quick approach to determine a physical characteristic of saturated and porous sediments such as the grain size in a non destructive way based on the spectral analysis of the wave propagation form.

Keywords

acoustic waves, finely grained soil, grain-size curve

1 INTRODUCTION

With the innovative laboratory test presented in this paper, using frequencies, it is possible to estimate the physical characteristics (density, porosity, permeability, mean grain size) of the sediment and the microstructure of its matrix up to the order of a millimetre. The wavelength and the frequency of the used acoustic waves are function of the grain size of the sediment. Using different intervals of frequency, with different signal penetration, fine structures of the sediment can be distinguished from the coarse ones.

The mathematical and physical principles of the acoustic waves propagation in saturated porous media are known from Biot's theory. Compressional and shear velocities can be calculated by the elastic theory from the density, shear, and bulk modulus of the sediment. The problem is how to determine them from the properties of the constituent parts. Biot showed that composite properties could be determined from the porosity and the physical properties (density and moduli) of the fluid, the solid material, and the frame of the sediment. To account for different frequencies of propagation, it is necessary also to know the frequency, the sediment permeability and the fluid viscosity. Biot theory takes into account frequency variations, and allows for relative motion between fluid and the sediment frame. As a result, it predicts some of the observed changes of velocity as

function of frequency. It also predicts the existence of a so-called slow compressional wave in addition to the shear wave, and a compressional, or fast wave. The slow wave arises when the fluid and the sediment frame move in opposite phases with each other. Its velocity is related to fluid mobility, but unfortunately it has been only observed in the laboratory, not in in-situ measurements, where it degenerates into a diffusion phenomenon apparently too highly attenuated to be observed. With Biot's theory, it is also possible to evaluate the attenuation coefficient, the loss of energy or the amplitude of waves as they pass through media. The attenuation and the velocity of propagation of the acoustic waves depend on frequency. The grain size and the porosity can influence the attenuation of the P-waves; in particular, the attenuation is proportional to the grain size and inversely proportional to the porosity. High attenuation is related to coarse grains and low porosity

[1-2]. The variety of the examined cores of sediment shows a different influence of the lithology on the shapes of the acoustically transmitted signals. The comparison between the attenuation, estimated from acoustic measurements, and the curves of Biot's model shows that the main attenuation mechanism is a global viscous flow of the interstitial water [3].

2 DATA BASE

The geophysical and geotechnical analysis performed on marine sediment cores, collected during the survey "Boundary 2003" in the Channel of Malta (Figure 1) will be presented [10]. The analysis was carried on by the Undersea Research Centre SACLANT-NATO of La Spezia.

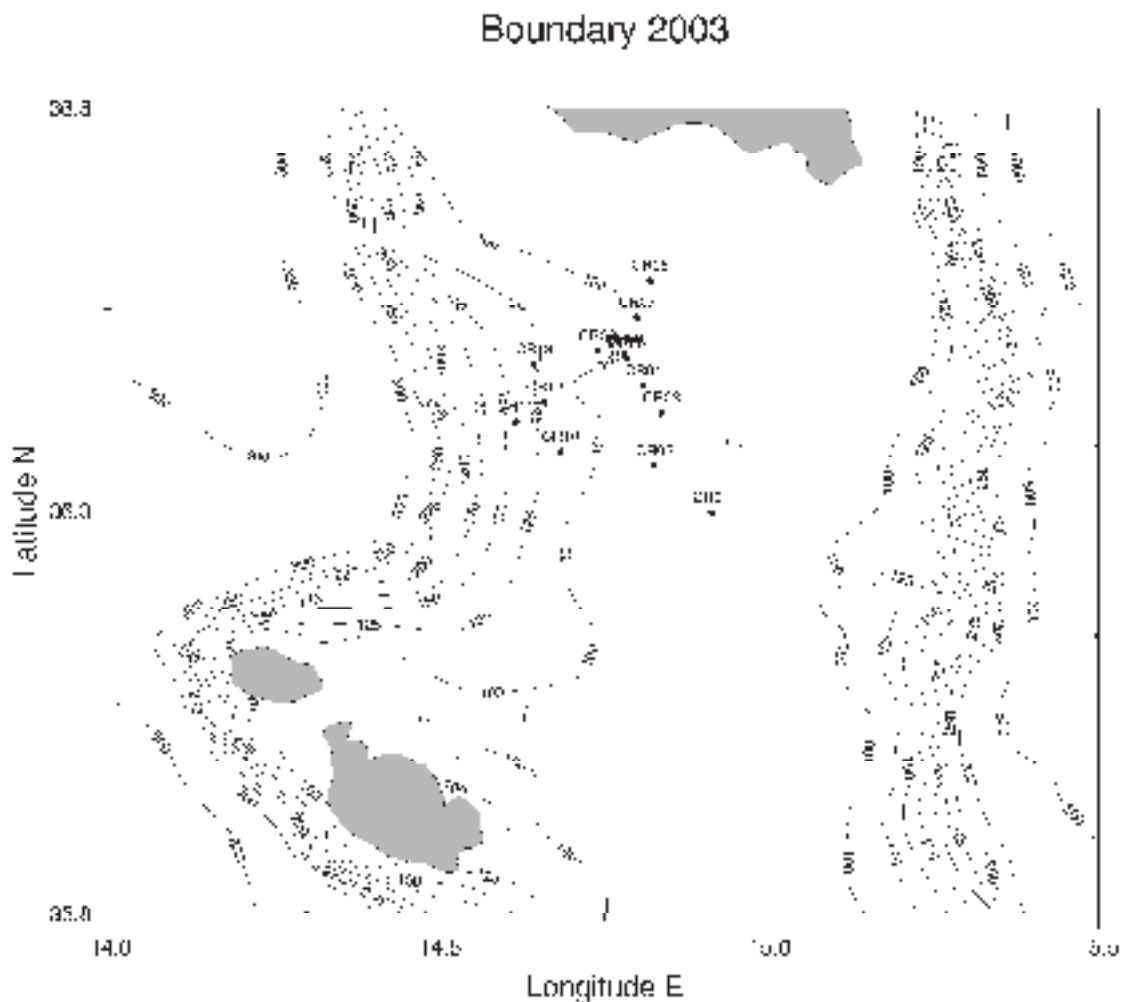


Figure 1. Boundary 2003.



Figure 2. Saclant Nato V-MSCL.

The sediment cores, of the diameter of 11 cm and length of 120 cm, were collected preserving the water-sediment interface. The analyses were performed with the Vertical Multi Sensor Core Logger (V-MSCL) [4]. The measurements of acoustic (P-wave velocity, impedance, wave form) and physical properties (density, porosity) were recorded completely automatically. The instrument is a prototype, which was produced especially for the Undersea Research Centre SACLANT-NATO of La Spezia, for logging the core in a vertical position. It is suitable for studying cores with preserved water-sediment interface (Figure 2).



Figure 3. Core 5.

The analyses were performed without extruding the sediment from the casing, with an interval sampling of 1 cm. The P-wave analyses were carried on using a couple of acoustic rolling transducers with the frequency interval between 50 to 500 kHz and the fundamental frequency of 250 kHz. Radial P-waves were transmitted through sediment cores and digitally recorded.

In Figure 4 the signals passing through the most representative gravity core (CORE 5) are shown. The water signal of greater amplitude wraps all the other wave forms.

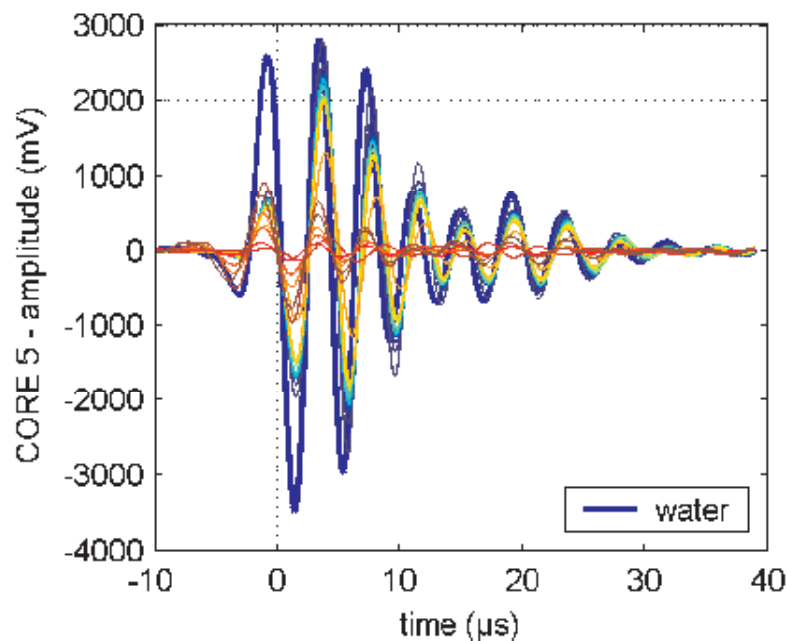


Figure 4. P-wave forms collected along the Core 5.

3 RESULTS

The attenuation of the acoustic signal depends on porosity, grain size and permeability of the sediment.

Both acoustic parameters (the P-wave velocity and the coefficient of attenuation) can be used for estimating the mean grain size. Biot's theory was used to model the velocity and attenuation data of gravity cores from the Channel of Malta. Data were compared to physical parameters of marine sand, silt and clay sediments of continental terrace from Hamilton [5-8], who discussed, in several reports, elastic properties of marine sediments from major locations in the North Pacific Ocean, in relation to a wide variety of laboratory and in-situ measurements.

Figure 5 and Figure 6 present a comparison of analyzed P-wave velocity and attenuation at four different traces along the gravity core 5, and the theoretical P-wave velocity and attenuation based on Biot's model.

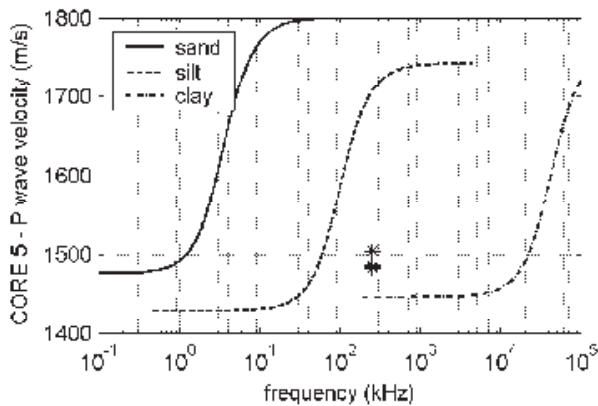


Figure 5. Comparison of theoretical data with velocity data of CORE 5 according to Biot's theory.

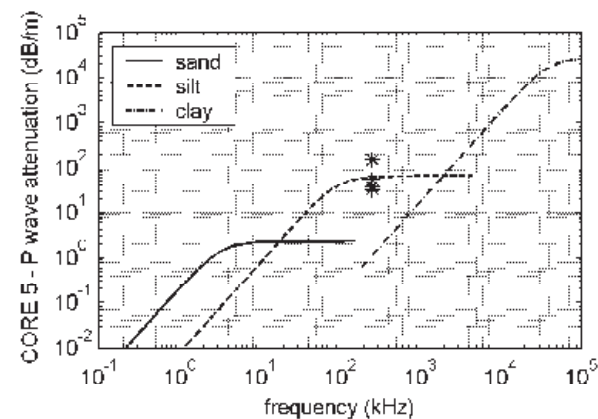


Figure 6. Comparison of theoretical data with attenuation data of CORE 5 according to Biot's theory.

The same four traces along the gravity core 5 were used to obtain the grain-size distribution curve (Figure 7) with laser grain size analysis in comparison with the acoustic measurements obtained with V-MSCL [9-11-12-13-14].

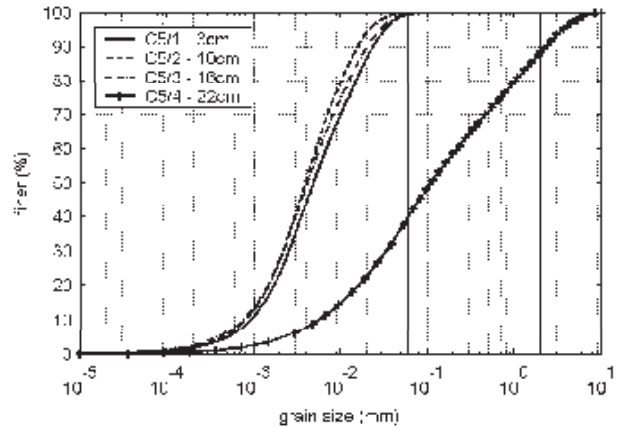


Figure 7. Grain-size distribution curve for CORE 5.

Gravity core 5, from the comparison with Biot's model, can be classified as a silty-clay sediment. An interpretative description of possible attenuation mechanism is based on the technique of spectral difference method, which is used to obtain the attenuation of the gravity cores. If $A_1(f,x)$ and $A_2(f,x)$ are the amplitude spectra of an unattenuated reference, the water signal wave form, and an attenuated signal, the generic trace of the sediment, the attenuation can be computed as:

$$attenuation(f) = \frac{\ln(A_1(f,x)) - \ln(A_2(f,x))}{x} \quad (1)$$

where f is the fundamental frequency of the V-MSCL and x is the travel path that corresponds to the diameter of the gravity core liner.

Spectral amplitude is calculated on the basis of Welch's method, which divides time series data into segments, overlapping and computing a modified periodogram of each segment, averaging the power spectral density estimates [15].

Figure 8 presents a quantitative image of the attenuation characteristics of the complete gravity core 5 through an attenuation surface. The frequency dependent attenuation of each trace (1 cm) is displayed versus the core depth. In the resulting three-dimensional shading surface the finely grained sediments, weakly attenuated, are represented by a valley, whereas coarsely grained sediments, highly attenuated, occur as a steep hill.

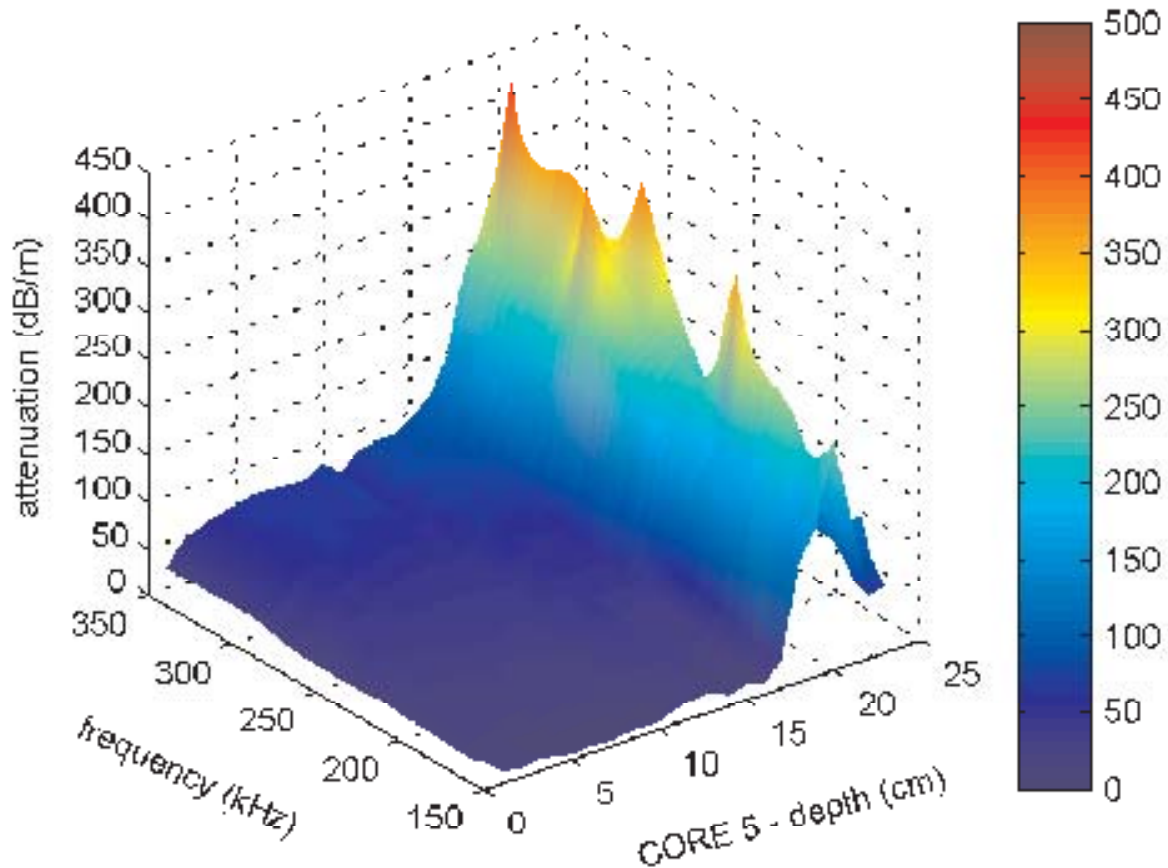


Figure 8. Attenuation surface of gravity core 5.

4 CONCLUSIONS

A correlation between the grain size distribution and the spectral amplitude of P-wave was used to establish a regression law which allows to predict the mean grain size of the sediment if the P wave spectral amplitude is given.

Therefore, the spectral amplitude values are correlated with the mean grain size and arranged with respect to the sorting of the sediment.

An exponential law:

$$m.g.s. (mm) = 2.2 \cdot 10^3 s.a. (dB)^{0.2} \quad (2)$$

which describes the mutual relationship between the spectral amplitude and mean grain size, was fitted to the data points of the Channel of Malta and used for the mean grain size prediction.

Figure 9 presents the regression curve, derived from the exponential law, which lies quite close to the measured data points.

The exponential law and the derived regression curve prove that the P wave spectral amplitude can be used as a reference parameter for a fast prediction of the mean grain size.

On the basis of the presented results it is possible to claim that V-MSCL permits to determine the widest possible range of information from core samples in a consistent, accurate, cost- and time-effective manner. At the same time, elaborated measurements and presented results confirm the appropriateness of the chosen frequency and the correlation of the results with Biot's model.

This spectral amplitude analysis provides a tool to reduce a time-consuming grain size analysis, and a non-destructive and fast approach to evaluate physical

properties of sediment of an intact core which represents a local and punctual parameter to predict regional parameters.

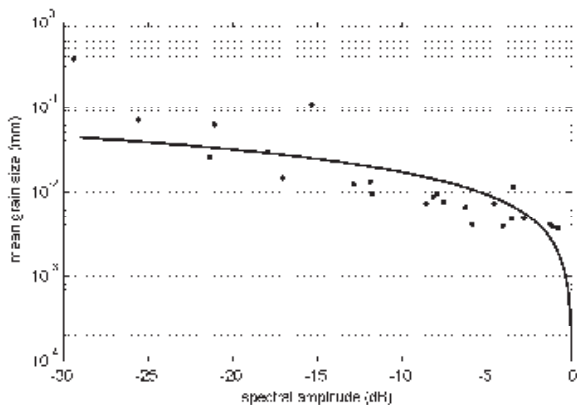


Figure 9. Regression law.

ACKNOWLEDGMENTS

The authors wish to thank the Undersea Research Centre SACLANT-NATO of La Spezia (Italy) for the possibility to use their laboratory and measurement device.

All the experimental data have been collected in the cooperation of Dr. Michelozzi to whom the authors are also grateful for discussions and useful suggestions.

REFERENCES

- [1] Biot, M. A. (1956a). Theory of propagation of elastic waves in a fluid-saturated porous solid, I, Low frequency range. *J. Acoust. Soc. Am.*, 28, 168-178.
- [2] Biot, M. A. (1956b). Theory of propagation of elastic waves in a fluid-saturated porous solid, II, Higher frequency range. *J. Acoust. Soc. Am.*, 28, 179-191.
- [3] Breitzke, M., Grobe, H., Kuhn, G., Muller, P. (1996). Full waveform ultrasonic transmission seismograms: a fast new method for the determination of physical and sedimentological parameters of marine sediment cores. *Journal of Geophysical Research*, 101, B10, 123-141.
- [4] GEOTEK MSCL Manual (2000). Multi-Sensor Core Logger. UK.
- [5] Hamilton, E. L. (1971a). Elastic properties of marine sediments. *Journal of Geophysical Research*, 76, 2, 579-604.
- [6] Hamilton, E. L. (1972). Compressional wave attenuation in marine sediments. *Geophysics*, 37, 4, 620-646.
- [7] Hamilton, E. L. (1979). Sound velocity gradients in marine sediments. *J. Acoust. Soc. Am.*, 65, 4, 909-922.
- [8] Hamilton, E. L., Bachman, R. T. (1982). Sound velocity and related properties of marine sediments. *J. Acoust. Soc. Am.*, 72, 6, 1891-1904.
- [9] Marple, S. L. (1987). *Digital Spectral Analysis and with applications*. Englewood Cliffs, NJ, Prentice-Hall, 492.
- [10] Max, M. D., Kristensen, A., Michelozzi, E. (1992). Small-scale Plio-Quaternary sequence stratigraphy and shallow geology of the West-Central Malta Plateau. *Proceedings of the International Scientific Meeting – Geological Development of the Sicilian-Tunisian Platform*, University of Urbino, 58, 117-122.
- [11] McCann, C., McCann, D. M. (1969). The attenuation of compressional waves in marine sediments. *Geophysics*, 34, 6, 882-892.
- [12] Smith, S. W. (1999). *The Scientist and Engineer's Guide to Digital Signal Processing*. California Technical Publishing, San Diego, California, 650.
- [13] Stoll, R. D. (1989). *Sediment Acoustic*. Springer-Verlag, New York, 153.
- [14] Urick, R. J. (1983). *Principles of Underwater Sounds*. McGraw Hill, New York, 423.
- [15] Welch, P. D. (1967). *The Use of Fast Fourier Transform for the Estimation of Power Spectra: A Method based on Time Averaging over Short Modified Periodograms*. *IEEE Trans. Audio Electroacoust.*, AU-15, 70-73.

ANALITIČNA METODA ZA ANALIZO GRUŠČNATIH KOLOV Z UPOŠTEVANJEM ROWOVE TEORIJE RAZMIKANJA

BOŠTJAN PULKO IN BOJAN MAJES

o avtorjema

Boštjan Pulko
Univerza v Ljubljani,
Fakulteta za gradbeništvo in geodezijo
Jamova 2, 1000 Ljubljana, Slovenija
E-pošta: bostjan.pulko@fgg.uni-lj.si

Bojan Majes
Univerza v Ljubljani,
Fakulteta za gradbeništvo in geodezijo
Jamova 2, 1000 Ljubljana, Slovenija
E-pošta: bojan.majes@fgg.uni-lj.si

izvleček

V članku je predstavljena nova metoda za analizo obnašanja togih temeljev na z gruščnatimi koli izboljšanih tleh. Gruščenat kol in okolna zemljina sta analizirana v pogojih osne simetrije kot enotna celica. Za gruščnat kol je predpostavljeno, da se obnaša kot Mohr-Coulombov togo-plastičen material z upoštevanjem neasociativnega tečenja po Rowovi teoriji razmikanja. Za zemljino je privzeto, da se obnaša kot linearno elastičen material. Te predpostavke, skupaj z ravnotežnimi in kinematičnimi enačbami, vodijo k preprosti analitični rešitvi za napoved obnašanja togih temeljev na z gruščnatimi koli stabiliziranih tleh. Prikazana je parametrična študija, ki analizira vpliv razmikanja gruščnatega materiala na deformacije in napetosti v temeljnih tleh ter ugoden vpliv na redukcijo posedkov. Rezultati nove metode so primerjani z nekaterimi drugimi analitičnimi metodami in objavljenimi rezultati terenskih testov in opazovanj.

ključne besede

izboljšanje tal, gruščnati koli, posedki tal, teorija razmikanja

ANALYTICAL METHOD FOR THE ANALYSIS OF STONE-COLUMNS ACCORDING TO THE ROWE DILATANCY THEORY

BOŠTJAN PULKO and BOJAN MAJES

about the authors

Boštjan Pulko
University of Ljubljana,
Faculty of Civil and Geodetic Engineering
Jamova 2, 1000 Ljubljana, Slovenia
E-mail: bostjan.pulko@fgg.uni-lj.si

Bojan Majes
University of Ljubljana,
Faculty of Civil and Geodetic Engineering
Jamova 2, 1000 Ljubljana, Slovenia
E-mail: bojan.majes@fgg.uni-lj.si

abstract

In this paper a new analytical method to analyse the behaviour of rigid foundations stabilized by end bearing stone-columns is proposed. The stone column and the surrounding soil are treated in axial symmetric conditions as a unit cell. The stone column is assumed to behave as an Mohr-Coulomb rigid-plastic material with non-associative flow rule according to the Rowe stress dilatancy theory and the soil as an elastic material. These common assumptions, combined with equilibrium and kinematic conditions, lead to the simple analytical closed-form solution for the prediction of the behaviour for rigid footings resting on stone-column reinforced ground. The parametric study is presented to show the effect of dilatancy of the granular material on the deformations and stresses in the ground and its beneficial effect on settlement reduction. The results of the new method are compared with some already known analytical methods and some published field test results and observations.

keywords

ground improvement, stone columns, ground settlements, dilatancy theory

1 INTRODUCTION

Stone columns or granular piles are frequently used for the stabilization of soft clays and silts and loose silty sands with large amount of fines. For low-rise buildings, highway facilities, storage tanks, embankments, bridge abutments and other structures that can tolerate some settlements, stone columns are one of the most frequently used methods of support due to the cost, effectiveness and ease of the installation. The beneficial effects of stone columns are increased stiffness, reduced settlements, increased time rate of settlements, increased shear strength and reduction of the liquefaction potential of soft ground.

The available methods for the estimation of the behaviour of foundations resting on soft soil stabilised by a large number of end-bearing stone-columns can be classified as either approximate methods with important simplifying assumptions or sophisticated methods based on elasticity and/or plasticity theory such as finite element model.

The majority of the proposed approximate methods assume infinitely wide, loaded area with end-bearing stone columns having constant diameter and spacing. For such loading and geometry conditions the stone column and the surrounding soil can be treated in axial symmetric conditions. This approach is commonly known as a unit cell concept and was adopted by several researchers.

Several approximate analytical solutions are available to estimate the settlement reduction of stabilized ground and stress concentration in the stone-columns. Many of them [1-3] are based on elastic approach considering the stone-column and the surrounding soil as elastic materials. However, elastic methods give the ratio between the vertical stress in the column and in the soil (also known as stress concentration factor) approximately equal to the ratio of constrained modulus of both materials. This ratio was found to be considerably higher than measured in the field and it is believed that elastic methods may easily overestimate the effects of stone columns on settlement reduction [4].

The elastic and elasto-plastic solutions presented by Balaam and Booker [2, 5] indicate that the problem can be idealized by assuming that the stone column is in a triaxial state and perhaps yielding, that there is no shear stress at the stone-soil interface, and that there is no yielding in the soil. These common assumptions have been implemented in many methods where stone column is considered to be in a state of plastic equilibrium and under a triaxial stress state [5-8]. In the majority of these methods it is assumed that when loaded, stone-column yields at constant volume. However, in the work by Van Impe and Madhav [8] the nonlinear analytical solution is presented, showing the beneficial effect of the stone-column dilation on the deformation behaviour of the stabilized ground.

The objective of this paper is to present an analytical closed-form elastic-rigid-plastic solution which takes into account confined yielding of the stone material according to the Rowe stress-dilatancy theory [9] and to show the beneficial effects of dilation on the settlement reduction.

2 METHOD OF ANALYSIS

If stone-columns are evenly distributed, a regularly shaped area around the stone-column may be consid-

ered as a “unit cell”, consisting of stone-column and the surrounding soft soil in a zone of influence (Fig. 1). To simplify the analysis the zone of influence is approximated by a circle with a diameter d_e equal to $1.05s$, $1.13s$ and $1.29s$, for triangular, square or hexagonal pattern, respectively, where s is the column spacing.

The ratio between the area of column A_c and the area of the zone of influence A_e is represented by the area replacement ratio A_r , defined as

$$A_r = \frac{A_c}{A_e} = \frac{d_c^2}{d_e^2} = \frac{r_c^2}{r_e^2} \quad (1)$$

Let us consider a unit cell on smooth rigid base loaded with uniform load through the smooth rigid raft. The high drainage capacity of the granular material ensures that it deforms under drained conditions. The immediate settlement of soil in undrained conditions is negligible compared to the total final settlements, and thus it will not be considered in the analysis [5].

It is assumed that the dense granular material in the column is in triaxial stress state, reaching its peak resistance and thus dilating. The self weight of the soil and the column is neglected, which is one of the main drawbacks of the proposed method.

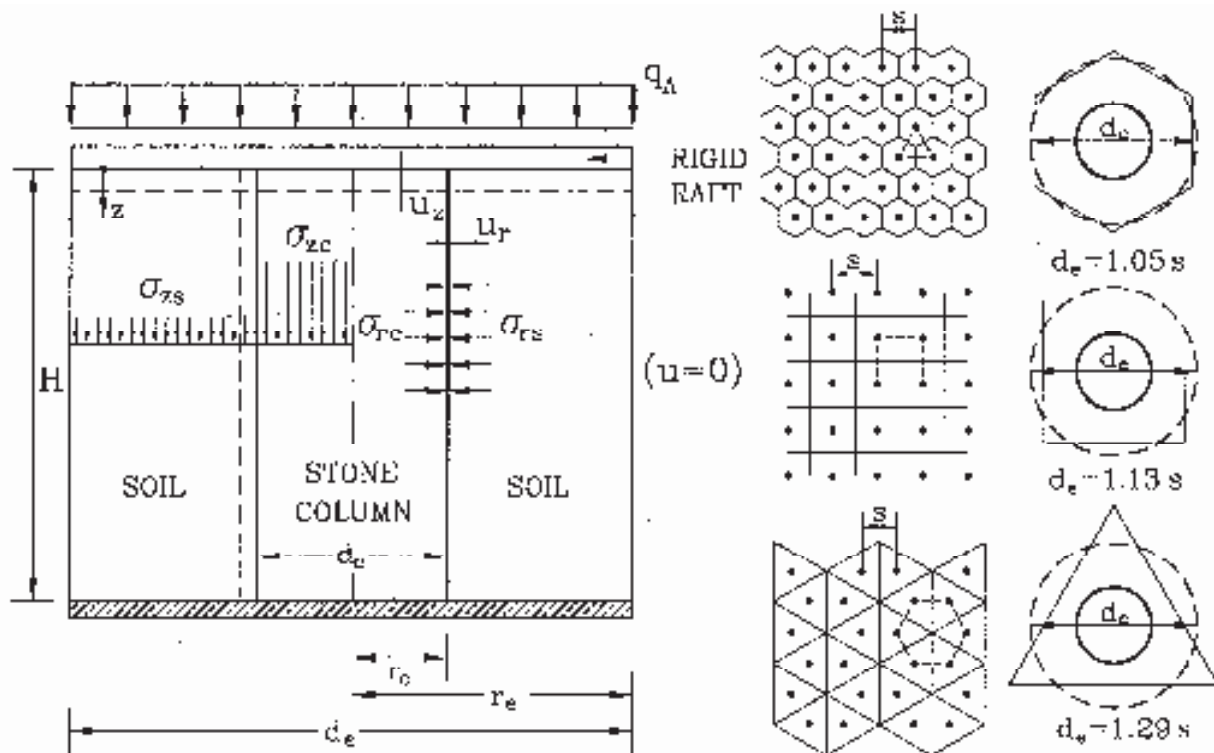


Figure 1. Basic features of the model based on regular patterns of stone-columns

Under uniform load q_A applied through rigid raft the end bearing stone-column and the surrounding soil will undergo the same vertical displacement u_z and radial displacement u_r , thus at the soil-column interface no slippage is expected between the soil and the granular material. The vertical, radial and volumetric strains of the stone-column are defined as

$$\epsilon_z = \frac{u_z}{H} \quad (2)$$

$$\epsilon_r = -\frac{u_r}{r_c} \quad (3)$$

$$\epsilon_v = \epsilon_z + 2\epsilon_r \quad (4)$$

where H is the height and r_c the radius of the column.

The relation between vertical and radial stress at the soil-column interface, σ_{zc} and σ_{rc} , in triaxial stress state can be simply obtained for the column material at yield:

$$\frac{\sigma_{zc}}{\sigma_{rc}} = \frac{1 + \sin\varphi_c^*}{1 - \sin\varphi_c^*} = K_{rc} \quad (5)$$

where φ_c^* represents the peak triaxial shear angle of the column material. According to the Rowe stress dilatancy theory [9], Equation (5) can also be modified to:

$$\frac{\sigma_{zc}}{\sigma_{rc} \left(1 - \frac{\epsilon_v}{\epsilon_r}\right)} = \frac{1 + \sin\varphi_{rc}^*}{1 - \sin\varphi_{rc}^*} \quad (6)$$

where φ_{rc}^* is a triaxial shear angle of the stone material at constant volume. The relationship between the angle of dilatancy ψ and the peak friction angle φ_c^* can be obtained using Rowe's equation [9]:

$$\sin\psi = \frac{\sin\varphi_c^* - \sin\varphi_{rc}^*}{1 - \sin\varphi_c^* \sin\varphi_{rc}^*} \quad (7)$$

Angle of dilatancy ψ can also be expressed in terms of the volumetric strain due to dilation and vertical strain of the column [10]:

$$\sin\psi = \frac{\frac{\epsilon_v}{\epsilon_r}}{2 - \frac{\epsilon_v}{\epsilon_r}} = -\frac{\epsilon_v}{2\epsilon_r - \epsilon_v} \quad (8)$$

The stress-strain behaviour of the column is entirely defined by Equations (5) and (8), and the two material parameters, which can be arbitrary selected between φ_c^* , ψ and φ_{rc}^* . The ratio between vertical and horizontal stresses in the column is defined by the strength of the

selected column material, while the ratio between the contained plastic strains of the stone-column material, ϵ_v and ϵ_r , is determined by the selected value of the dilation angle ψ .

The soil surrounding the stone-column can be analysed as a thick cylinder using Equations (9) and (10) relating vertical and radial displacements, u_z and u_r , at the soil-column interface with vertical stress in the soil and radial interaction stress, σ_{zs} and σ_{rs} [11]:

$$u_z = \frac{H}{E_{soil}} \left[\frac{C_2 \sigma_{zs} - C_1 \sigma_{rs}}{C_3} \right] \quad (9)$$

$$u_r = \frac{r_c}{E_{soil}} \left[\frac{\sigma_{rs} - k_0 \sigma_{zs}}{C_3} \right] \quad (10)$$

where E_{soil} is the oedometric modulus of the soil and C_1 , C_2 and C_3 are constants defined as

$$C_1 = \frac{2k_0 A_r}{1 - A_r}, \quad C_2 = \frac{1 - 2\nu_s + A_r}{(1 - A_r)(1 - \nu_s)}, \quad C_3 = C_2 - k_0 C_1 \quad (11)$$

where ν_s is Poisson's ratio of the soil and $k_0 = \nu_s / (1 - \nu_s)$.

Applied vertical load q_A must be in equilibrium with vertical stresses in the column and in the soil:

$$q_A A_c = \sigma_{zc} A_c + \sigma_{zs} (A_s - A_c) \quad (12)$$

Using the definition of the replacement ratio A_R given by Equation (1), Equation (12) can be rewritten as

$$q_A = \sigma_{zc} A_R + \sigma_{zs} (1 - A_R) \quad (13)$$

The stresses at the soil-column interface must be equal, thus $\sigma_{rs} = \sigma_{rc} = \sigma_r$. If kinematic relations (2), (3) and (4) are introduced in Equation (8), Equations (5), (8), (9), (10) and (13) represent a set of five equations for five unknowns: vertical stresses in the column σ_{zc} and in the soil σ_{zs} , radial stress at the soil-column interface σ_r , vertical displacement u_z and interface displacement u_r . This set of equations can be solved to obtain simple analytical closed-form solutions for displacements and stresses:

$$u_z = \frac{2Hq_A}{E_{soil} C_4} \quad (14)$$

$$u_r = \frac{r_c q_A K_4}{E_{soil} C_4} \quad (15)$$

$$\sigma_r = \frac{q_A (C_2 K_\psi + 2k_0)}{C_4} \quad (16)$$

$$\sigma_{sc} = \frac{q_A K_r (C_2 K_\psi + 2k_0)}{C_4} \quad (17)$$

$$\sigma_w = \frac{q_A (C_1 K_\psi + 2)}{C_4} \quad (18)$$

where constants K_ψ and C_4 are defined as follows:

$$K_\psi = \frac{1 + \sin \psi}{1 - \sin \psi}$$

$$C_4 = (1 - A_r)(C_1 K_\psi + 2) + A_r K_r (C_2 K_\psi + 2k_0)$$

Constant C_4 depends only on material and geometrical properties of the column and the surrounding soil.

If the area of the applied load is sufficiently large, then the settlement of the untreated soil can be estimated as

$$w_{s,0} = \frac{q_A H}{E_{soil}} \quad (20)$$

Combining Equation (20) with Equation (14), a settlement reduction factor β , which is usually used as a measure for the improvement of the ground, can be calculated as

$$\beta = \frac{w_s}{w_{s,0}} = \frac{2}{C_4} \quad (21)$$

Stress concentration factor η defined as a ratio between vertical stresses in the soil σ_{zc} and in the column σ_{sc} can be calculated as

$$\eta = \frac{\sigma_{sc}}{\sigma_w} = \frac{K_r (C_2 K_\psi + 2k_0)}{C_1 K_\psi + 2} \quad (22)$$

Similarly, stone-column stress concentration factor η_c defined as a ratio between vertical stress in column σ_{sc} and the applied load q_A can be calculated as

$$\eta_c = \frac{\sigma_{sc}}{q_A} = \frac{K_r (C_2 K_\psi + 2k_0)}{C_4} \quad (23)$$

According to the above analysis the settlement reduction and the stress concentration factor depend mainly on area replacement ratio A_r , on material properties of the column material represented by the peak shear angle φ_c^* , the angle of dilatancy ψ and on Poisson's ratio ν_s of the soil.

3 RESULTS AND DISCUSSION

3.1 PARAMETRIC STUDY

A parametric study has been made to show the effect of area replacement ratio A_r , peak shear strength φ_c^* and especially the effect of dilation on settlement reduction and stress concentration. In stone column construction usually 15 to 35 percent of the soft soil is replaced [4]. However, the replacement ratios A_r from 5 up to 50 percent were considered in the present study.

When selecting basic input parameters of the method, such as peak and dilation angle of the column material, one should consider that the values for peak, critical and the dilation angle of the granular soil are not independent. The critical state shear angle φ_{cs}^* of granular material, which is sheared under constant volume, is in general a function of mineralogy and can be treated as material property. The relationship between the peak shear angle φ_c^* , the critical state shear angle φ_{cs}^* and the angle of dilatancy ψ is theoretically given by Equation (7), which can be rewritten in the following form:

$$\sin \varphi_c^* = \frac{\sin \varphi_{cs}^* + \sin \psi}{1 + \sin \varphi_{cs}^* \sin \psi} \quad (24)$$

In practice the difference between peak and critical state shear angle can also be correlated to the material's relative density and principal stress. According to the work of Bolton [12] the peak triaxial shear angle correlates to the relative density of the granular material and to the mean effective stress p^* as follows:

$$\varphi_c^* \approx \varphi_{cs}^* + 3I_R \quad (25)$$

where I_R is a relative dilatancy index defined as

$$I_R = D_x (10 - \ln p^*) - 1 \quad (26)$$

The relative dilatancy index I_R can also be used for the prediction of the angle of dilatancy as proposed by Schanz and Vermeer [10]:

$$\sin \psi = \frac{I_R}{6.7 + I_R} \quad (27)$$

In the case that no laboratory data are available on the dilatancy behaviour, the strength and dilation properties of the column material can be estimated by the above relationships.

To investigate the effect of the dilation of the column material on the displacements and stresses, the angle of dilatancy equal to $\psi = 0^\circ, 5^\circ, 10^\circ, 15^\circ$ and the representative value of the critical state shear angle $\varphi_{cs}^* = 35^\circ$ were adopted. Another input parameter of the method is Poisson's ratio of the soil ν_s , which was selected to be 0.35.

The results of the parametric study are presented in Figures 2, 3, 4 and 5. The effect of area replacement ratio A_r and of angle of dilatancy ψ on settlement reduction factor β is shown in Figure 2. The spacing of the columns has dominant effect on settlement reduction. As the spacing of the columns increases, the replacement ratio A_r decreases, the unit cell becomes less stiff and the total settlement increases. The settlement reduction factors are generally low and not significant for area replacement ratios lower than 4 percent ($d_p/d_c > 5$).

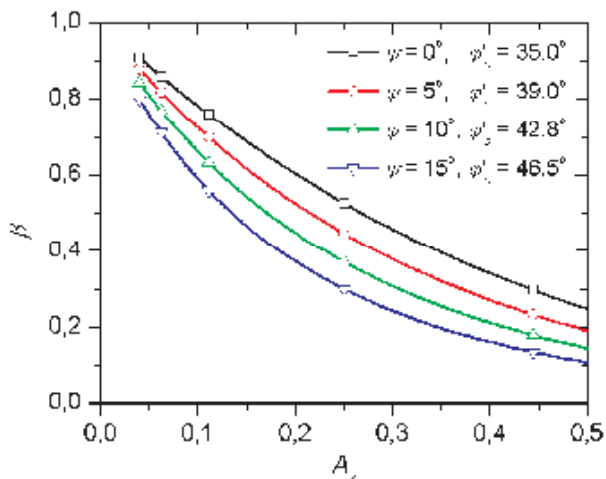


Figure 2. The effect of area replacement ratio A_r and angle of dilatancy ψ on settlement reduction factor β

The angle of dilatancy has also significant effect on settlement reduction factor β , clearly showing the importance of stone densification. High density of the column material yields high dilatancy index, hence higher dilation angle ψ could be achieved. The higher the value of dilation angle ψ , the greater is the peak shear angle φ_{cs}^* and more reduction of the settlement could be expected due to higher stress concentration in the stone-column (Fig. 2). However, the effect of the dilation of granular material at yield can not be clearly distinguished from the beneficial effect of peak shear strength of the stone column.

The effect of the dilation on settlement reduction is far more evident, if a constant value of peak shear strength is considered ($\varphi_{cs}^* = 46,5^\circ$) and different dilation properties of the granular material are taken into account. The

effect of dilation angle ψ on the settlement reduction for this case is depicted in Fig. 3. The volume increase of the granular material at yield has significant effect on the settlement reduction. For example, for the area replacement ratio A_r between 0.15 and 0.35 the total settlement for dilating stone-column ($\psi = 15^\circ$) is 16.5 to 28.0 percent lower than compared to the settlement when no dilation is taken into account.

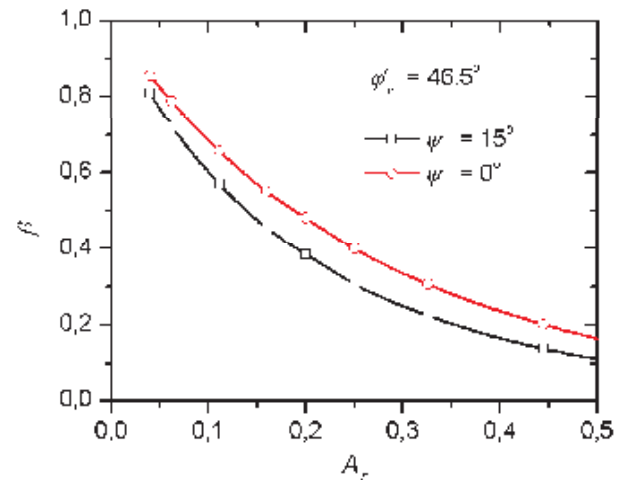


Figure 3. The effect of area replacement ratio A_r and dilation angle ψ on settlement reduction factor β

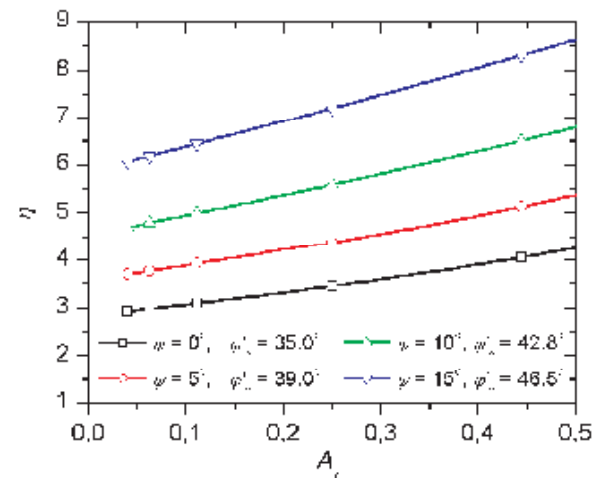


Figure 4. The effect of area replacement ratio A_r and angle of dilatancy ψ on stress concentration factor η

The effect of area replacement ratio A_r and angle of dilatancy ψ on stress concentration factor η is shown in Fig. 4. The importance of the dilation of the column material on the stress concentration in the column is clearly indicated. Well densified stone-column with high dilation angle ψ acts stiffer and can take greater proportion of the applied load. Stress concentration factors η are generally in the range from 3 to 8 for the area replacement ratios from 0.15 to 0.35.

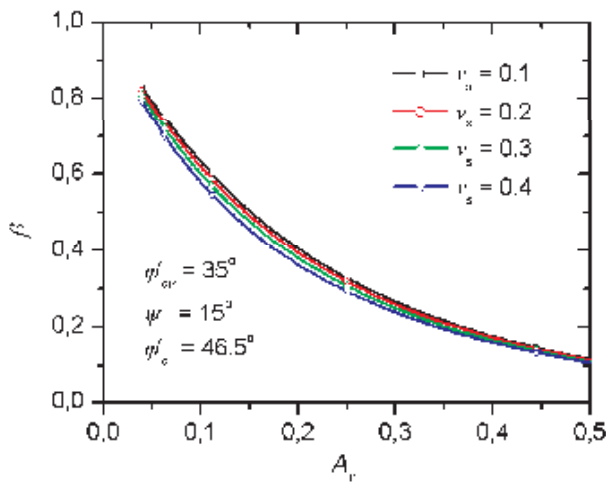


Figure 5. The effect of area replacement ratio A_r and Poisson's ratio of the soil on settlement reduction factor β

The effect of Poisson's ratio of soil is illustrated in Fig. 5, where settlement reduction factor β is depicted as a function of Poisson's ratio against the area replacement ratio A_r . The value of Poisson's ratio ν_s of soil has rather small effect on the settlement reduction, if the soil is considered under drained conditions. The effect of Poisson's ratio on the stress concentration factor η is also small.

3.2 COMPARISON WITH OTHER METHODS

It is interesting to compare the settlement reduction factors, obtained by the proposed analytical method, with some other known analytical solutions, based on similar approaches. A comparison was firstly made with elastic methods proposed by Aboshi et al. [1] and Balaam and Booker [2] and then with elastoplastic methods, which take into account the yield of the stone-column at constant volume as proposed by Priebe [6], Van Impe and De Beer [7], and finally with the method proposed by Van Impe and Madhav [8], which takes into account the yield and the dilation of the stone-column.

A direct comparison between the results is not possible because of different input parameters. However, a comparison can be made for a regular set of parameters for stone column material and for soil. The stone and soil modulus ratio $E_c/E_s = 30$, critical state shear angle $\varphi_{cr}^s = 35^\circ$, dilation angle $\psi = 15^\circ$ and Poisson's ratio $\nu_s = 0.3$ were adopted in the analysis. This combination of the critical shear angle and dilation angle of the column material leads to the peak shear angle $\varphi_c^s = 46.5^\circ$. This standard set of parameters was used in the prediction of settlements according to the above mentioned methods.

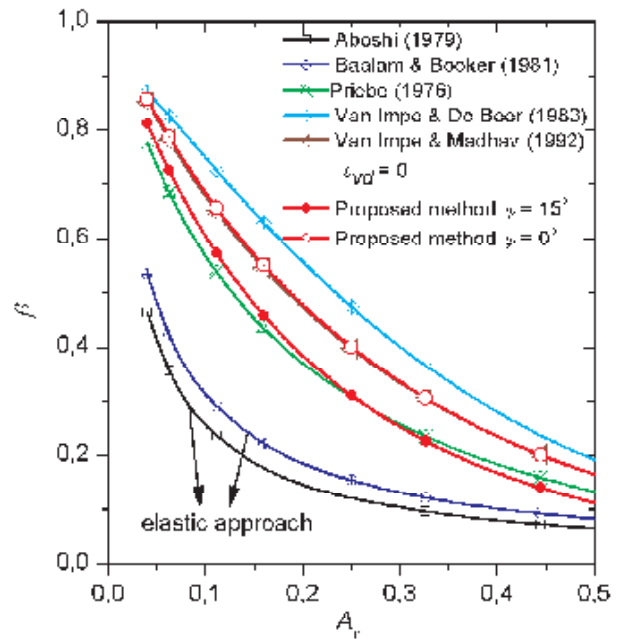


Figure 6. The comparison of settlement reduction factors according to different analytical methods

The comparison of settlement reduction factors is shown in Fig. 6. The differences in the settlement reduction factors obtained by different methods are quite significant, even if the general trend of the results is found to be similar.

The elastic methods [1, 2] give low settlement reduction factors due to supposed high stiffness of the stone column and consequently due to high stress concentration factors. If the column and soil are considered as elastic materials, then the ratio between the load carried by the column and by the soil is approximately the same as the stone and soil modulus ratio E_c/E_s . There is a simple approximate explanation why stress concentration factors are limited to a certain value. If vertical stress in the column σ_{zz} is a major principal stress in the column and vertical stress in soil, σ_{zz} is a minor principal stress in the soil and the radial stress $\sigma_r = \sigma_x = \sigma_y$ at soil-column interface is a minor principal stress in the column and major principal stress in the soil, then the maximum stress concentration factor at yield can be expressed as:

$$\frac{\sigma_{zz}}{\sigma_{zz}} = \frac{\sigma_x}{\sigma_y} = \frac{K_p}{1} = K_p \cdot K_p = \frac{1 + \sin\varphi_c^s}{1 - \sin\varphi_c^s} \cdot \frac{1 + \sin\varphi_c^s}{1 - \sin\varphi_c^s} = \eta_{max} \quad (28)$$

For example, peak shear angles of the granular material $\varphi_c^s = 45^\circ$ and soft soil $\varphi_c^s = 20^\circ$ give maximum stress concentration factor $\eta_{max} = 11.9$. If high

stone and soil deformation ratio E_c/E_s is considered in the elastic analysis and if the applied load q_A is high as compared to the initial (lateral) stresses in the soil, then the stress concentration factor may be too high and thus the calculated settlement underestimated. For this reason elastoplastic methods are believed to give better predictions of the settlement reduction and stress concentration factors [5].

The main difference between the proposed method and other elasto-plastic analytical methods [6-8], which also take into account column yield, is the assumption regarding the dilation of the column material. In the majority of rigid-plastic methods [6, 7] it is assumed that stone-column deforms at constant volume, thus no dilation takes place while deforming.

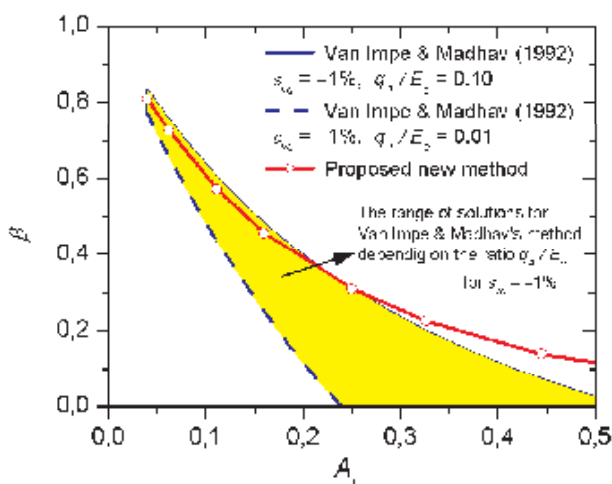


Figure 7. The comparison of settlement reduction factors for dilating stone-columns according to the proposed new and Van Impe and Madhav's method for a given set of parameters

The comparison of the results between the present and Van Impe and Madhav's method [8] is of special interest, since the dilatancy of the granular material is taken into account in both methods (Fig. 7). The present method is actually an extension of the Van Impe and Madhav's method [8] with three important differences. Small strains and vertical equilibrium of the undeformed geometry was assumed in the present method to simplify the problem and to get the closed form solution instead of nonlinear solution. These two differences have insignificant effect on the results as compared to the Van Impe and Mahav's method [8] as shown in Fig. 6, where the settlement reduction factors obtained with both methods are almost identical if no dilation is taken into account ($\varepsilon_{vd} = 0$ or $\psi = 0$).

The third, and most important difference relates to the dilation. In the proposed method the dilation of the granular material at yield was considered according

to the Rowe dilatancy theory [9]. In Van Impe and Madhav's method [8] the dilation is taken into account through the final value of the volumetric strain of the column ε_{vd} , which must be selected in advance as an input parameter. Inappropriate selection of the volumetric strain leads to a quite large range of settlement reduction factors for different ratios between the applied load and soil elastic modulus. If inappropriate volumetric strain is selected, it can also lead to the negative settlement reduction factor β (Fig. 7). There is a simple explanation for this phenomenon. If the load level q_A/E_s is low, causing only small vertical strain, it is very unlikely that large volumetric strain $\varepsilon_{vd} < 0$ would occur. If the final volumetric strain of column material $\varepsilon_{vd} < 0$ is taken in advance as a constant value, then, theoretically, the dilation angle ψ of granular material becomes directly dependent on the vertical strain (Fig. 8). Especially for small vertical strains the dilation angle will be unrealistically high and will consequently lead to unrealistic prediction of settlements.

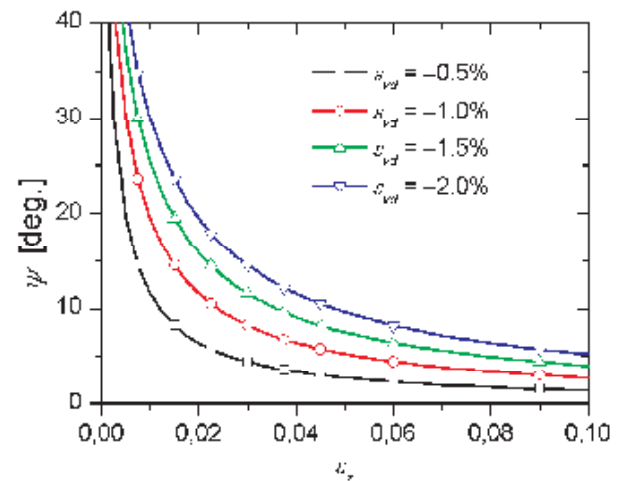


Figure 8. The effect of vertical strain ε_z on angle of dilatancy ψ and vertical deformation ε_z with the selected value of volumetric strain ε_{vd} according to Van Impe and Madhav's method

The correct value of volumetric strain at every level of axial strain can be determined from a triaxial test on the granular material. Nevertheless, Van Impe and Madhav's method [8] can be used in an iterative procedure. If the calculated vertical strain does not fit to the initially prescribed volumetric strain ε_{vd} , then the nonlinear calculation must be repeated with another value of the volumetric strain as an input parameter.

To overcome this problem, the ratio between plastic volumetric and vertical strain, defined by the dilation angle ψ according to Rowe's theory, was used in the proposed method, instead of assuming dilation volumetric strain ε_{vd} . In this way, the ratio between the volumetric and the vertical strain of the column at

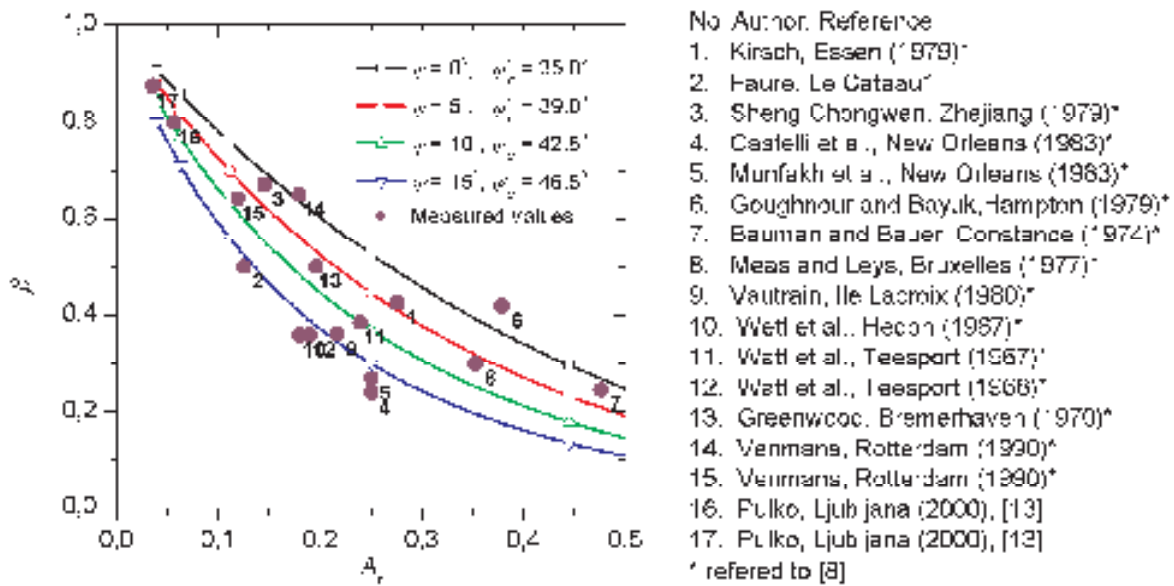


Figure 9. Comparison of settlement reduction factors β versus area replacement ratio A_r , with some field test results

yield remains constant and load independent. It should be noted, however, that the post-peak behaviour of the column material is not taken into account.

3.3 COMPARISON WITH FIELD TEST RESULTS

Figure 9 compares the predicted settlement reduction factors and corresponding area replacement ratios with some published field test results and observations. If dilation of the granular material is taken into account, then the present method is able to cover most of the field test data.

The results can not be completely conclusive due to the significant scatter of field test results and lack of well documented data in the literature. This scatter is most probably due to many factors that can affect stone-column performance, such as non-homogeneity of soil conditions, foundation shape and size, stone-column installation technique, properties of the granular material used, length of the column, different densification of the column material, different applied load, etc... Nevertheless, the predictions agree well with the field test data, thus validating the importance of the dilation in the presented method.

4 CONCLUSIONS

A simple but effective analytical method for the analysis of stone-column reinforced foundations is presented.

The stone-column and the surrounding soil are modelled as a unit cell, consisting of elastic soil and rigid plastic column material according to the Mohr-Coulomb failure law. The dilation of the column material according to the Rowe stress-dilatancy theory is directly incorporated into the method. An important feature of the method is a simple closed-form solution for the prediction of the effects of stone-columns on settlement reduction and stresses in the soil and column, which can be easily used in engineering practice.

Comparisons and some parametric analyses are presented to study the influence of area replacement ratio and material properties of the granular material on settlement reduction factor. The dilatancy of granular material has significant effect on the settlement reduction and stress concentration. Thus, densification of the column is not only important to achieve greater initial stiffness but also affects the column behaviour at yield and the overall performance of the stabilized ground.

The results are compared with some existing methods and with field test results and observations. The results of the present method agree well with most of the field data, showing the ability of the proposed analytical method to yield reasonable predictions of the behaviour of stone-column reinforced foundations. The present analytical model confirms the significance of the dilation of the column material and its effect on settlement reduction and on the stresses in the soil and column.

REFERENCES

- [1] Aboshi, H., Ichimoto, E., Enoki, M., and Harada, K. (1979). The compozer – a method to improve characteristics of soft clay by inclusion of large diameter sand columns. *Proceedings of International Conference on Soil Reinforcement - Reinforced Earth and Other Techniques*, E.N.P.C., 1, Paris, 211-216.
- [2] Balaam, N.P. and Booker J.R. (1981). Analysis of rigid rafts supported by granular piles. *International Journal for Numerical and Analytical Methods in Geomechanics*, 5, 379-403.
- [3] Shahu, T.F., Hayashi S., Madhav, M.R. (2000). Analysis of soft ground reinforced by non-homogeneous granular pile-mat system. *Lowland Technology International*, Vol. 2, No. 2., 71-82.
- [4] Barksdale, R.D. and Bachus, R.C. (1983). Design and construction of stone columns. Report No. FHWA/RD-83/026, Federal Highway Administration, Office of Engineering and Highway Operations, Research and Development, Washington D.C.
- [5] Balaam, N.P. and Booker J.R. (1985). Effects of stone columns yield on settlement of rigid foundations in stabilized clay. *International Journal for Numerical and Analytical Methods in Geomechanics*, 9, 331-351.
- [6] Priebe, H. (1976). Abschätzung des Setzungsverhaltens eines durch Stopfverdichtung verbesserten Baugrundes. *Die Bautechnik*, 5, 160-162.
- [7] Impe, W.F. and De Beer, E. (1983). Improvement of settlement behaviour of soft layers by means of stone columns. *Proceedings of 8th European Conference of Soil Mechanics and Foundation Engineering*, Helsinki, Vol. 1, 309-312.
- [8] Impe, W.F. and Madhav, M.R. (1992). Analysis and settlement of dilating stone column reinforced soil. *Österreichische Ingenieur und Architekten Zeitschrift (ÖIAZ)*, 137(3), 114-121.
- [9] Rowe, P.W. (1962). The stress-dilatancy relation for static equilibrium of an assembly of particles in contact. *Proceedings of Royal Society*, 269A, 500-527.
- [10] Schanz, T. and Vermeer, P.A. (1996). "Angles of internal friction and dilatancy of sand." *Géotechnique*, 46(1), 145-151.
- [11] Poulos, H.G. and Davis, E.H. (1974). *Elastic Solutions for Soil and Rock Mechanics*. Wiley, New York.
- [12] Bolton, M.D. (1986). The strength and dilatancy of sand. *Géotechnique*, 36(1), 65-78.
- [13] Pulko, B. (2000). The influence of stone columns on the mechanical properties of soft ground (in Slovene), *PhD Thesis*, University of Ljubljana, Ljubljana.

APPENDIX

NOTATION

The following symbols are used in the paper:

A_c	= area of column portion;
A_e	= area of soil portion (influence area);
A_r	= replacement ratio;
C_1, C_2, C_3, C_4	= geometrical and material constants;
d_c	= diameter of stone-column;
d_e	= diameter of influence area;
D_R	= relative density;
E_{oed}	= oedometric modulus of soil;
E_c	= elastic modulus of column material;
E_s	= elastic modulus of soil;
I_R	= relative dilatancy index;
H	= column height;
k_o	= coefficient of earth pressure at rest;
K_{pc}	= passive earth pressure coefficient (column);
K_{ps}	= passive earth pressure coefficient (soil);
K_ψ	= dilation constant;
q_A	= applied vertical load;
p'	= mean effective stress;
r_c	= radius of stone-column;
r_e	= radius of influence area;
s	= stone-column spacing;
u_r	= radial displacement of stone-column;
u_z	= vertical settlement;
$u_{z,0}$	= vertical settlement of untreated soil;
β	= settlement reduction factor;
ϵ_r	= radial strain;
ϵ_{vd}	= volumetric strain of column;
ϵ_z	= vertical strain;
η	= stress concentration factor;
η_c	= column stress concentration factor;
ψ_{σ}^*	= peak shear angle of soil;
$\psi_{\sigma_c}^*$	= peak shear angle of column material;
$\psi_{\sigma_c}^{*cr}$	= shear angle of column material at critical state;
ν_s	= Poisson's ratio of soil;
$\sigma_r, \sigma_{rs}, \sigma_{rc}$	= radial stress at soil-column interface;
σ_{zc}	= vertical stress in column;
σ_{zs}	= vertical stress in soil;
ψ	= angle of dilatancy.

INTERAKCIJSKA ANALIZA KONZOLNO VPETIH PODPORNIH KONSTRUKCIJ

STANISLAV ŠKRABL

o avtorju

Stanislav Škrabl
Univerza v Mariboru,
Fakulteta za gradbeništvo
Smetanova ulica 17, 2000 Maribor, Slovenija
E-pošta: stanislav.skrabl@uni-mb.si

izvleček

V članku so prikazane metode za geomehanske analize in projektiranje konzolnih podpornih konstrukcij. Vse podane rešitve temeljijo na metodi mejnih stanj in so uporabne pri analizah podpornih konstrukcij v tleh poljubnih geomehanskih lastnosti. Prikazana je posplošitev nekaterih obstoječih metod, ki temeljijo na predpostavki linearne porazdelitve vplivov in odporov, vendar za nekatere standardne primere nehomogenih tal ne dajejo zanesljivih rezultatov. Zato je podan predlog nove izboljšane metode, ki prav tako temelji na analizi mejnih stanj, vendar so pri razporeditvi aktiviranih vplivov in odporov upoštevane nekatere dodatne interakcijske soodvisnosti med podpornimi konstrukcijami in tlemi. Prednosti predlagane metode se kažejo predvsem pri analizah konstrukcij v heterogenih tleh, vpetosti v koherentne materiale in možnostih upoštevanja vplivov berme pred ter dodatnih površinskih obremenitev v zaledju podpornih konstrukcij. V takšnih bolj realnih primerih predložena metoda daje rezultate, ki so skladnejši z rezultati primerljivih elasto-plastičnih interakcijskih analiz po metodi končnih elementov ter so hkrati skladni tudi z rezultati že v literaturi objavljenih rešitev za primere v homogenih nekoherentnih tleh. Ker se v praksi skoraj vse podporne konstrukcije nahajajo v nehomogenih tleh, obstoječe metode pa dajejo natančne rešitve le za podporne konstrukcije v homogenih in nekoherentnih tleh, so prikazane rešitve bolj primerne in bolj uporabne za analize in projektiranje vpetih podpornih konstrukcij v geotehnični praksi.

ključne besede

podporne konstrukcije, vpetost, konzole, interakcija zemljina-stena, zemeljski tlak, razporeditev tlakov, trenje zemljina-stena, mejna analiza, strižne sile

INTERACTIONAL APPROACH OF CANTILEVER PILE WALLS ANALYSIS

STANISLAV ŠKRABL

About the author

Stanislav Škrabl
University of Maribor,
Faculty of Civil Engineering
Smetanova ulica 17, 2000 Maribor, Slovenia
E-mail: stanislav.skrabl@uni-mb.si

Abstract

This paper proposes a new method for the geomechanical analysis and design of cantilever retaining structures. It is based on the limit equilibrium method, but it uses some additional conditions for interaction between the retaining structure and the ground, when referring to the distribution of the mobilized earth pressures on the structure. The greatest benefit of the proposed method is shown in the analysis of structures of layered ground (heterogeneous above the dredge level and homogeneous below it), embedded in frictional and cohesive materials, and in the possibility of considering the influence of surcharge loadings on the active or passive side of the retaining structure. When analyzing such cases in practice, the proposed method gives results which are in better agreement with the results of FEM based elasto-plastic interaction analyses than with the results of currently used methods. At the same time, its results are in accordance with those published for homogeneous cohesionless ground. Since in practice almost all retaining structures are erected in layered ground (heterogeneous above the dredge level and homogeneous below it), the proposed method is very convenient and applicable for the analyses and design of cantilever structures under arbitrary geomechanical conditions.

Keywords

retaining walls, embedment, cantilevers, soil-structure interaction, earth pressure, pressure distribution, wall friction, limit analysis, shear forces

1 INTRODUCTION

In geotechnical practice, cantilever embedded retaining structures are specifically used for protecting permanent and temporary excavations, for highway construction, and sanitation of landslides. These structures are mostly sheet walls as temporary retaining structures, and pile walls and diaphragms as permanent retaining structures.

Embedded retaining structures sustain overturning moments and horizontal forces, which are caused by backfill soil, ground water and surcharge loading. The contact pressures and resistances are distributed over the embedment depth due to the backfill loading, so that the entire retaining structure remains in equilibrium. The limit state of the retaining structure is achieved when the distribution of contact pressures and extensive regions of plastification in the ground are re-established at the embedded part of the structure, and the structure is no longer capable of taking additional backfill loading. The limit state can be defined by the limit shear loading of the ground or bending moment and shear loading of the retaining structure, respectively. Therefore, only retaining structures, which have a comparable level of safety and reliability for the ultimate limit state of both the soil and the structure, can be optimal.

Bica and Clayton (1989) describe several different methods for the geomechanical analysis and design of embedded retaining structures. In these methods, different assumptions of soil pressure distribution, deformations and wall displacements are considered over the embedded part of the retaining structure. Most of the considered methods are limit equilibrium methods. They are based on a classical distribution of the limit soil pressure values. Some model studies of retaining structures are well known, e.g. Rowe (1951), Lyndon and Pearson (1985), Bica and Clayton (1993), as well as some empirical methods for the design of retaining structures.

King (1995) proposed an original approach to geomechanical analysis in homogenous cohesionless soil, which is based on the method of limit equilibrium,

polygonal distribution of soil pressures and one empirically determined parameter. This parameter is the depth, at which the net pressure is vanishing. King defined this depth by centrifuge test results. Day (1999) suggested improving King's method by determining the empirical parameter using the results of FEM analysis. Both methods, King's and Day's, are applicable only to analyses of retaining structures in homogeneous cohesionless ground without additional surcharge loading. This paper firstly presents a generalization of the existing standard methods for the analyses of rigid retaining structures embedded in frictional and cohesive layered ground (heterogeneous above the dredge level and homogeneous below it) with surcharge loading, and then compares the obtained results with the results of FEM-based analyses. Finally, it proposes a new method that considers significant interactive conditions between the retaining structure and the ground.

2 GENERALIZATION OF-CURRENT USED METHODS

The aim of the analyses based on the method of limit equilibrium is to determine the critical excavation depth and the critical values of bending moment and shear force at which the limit equilibrium state can be reached. The first important step of this approach is to determine the soil pressure, which can be activated at the ultimate limit state of the ground.

The soil pressures acting on the retaining structure at the ultimate limit state, depends on the complex properties of the interaction between the retaining structure and the ground. The most important interaction parameter represents equal displacements of both mediums along the contact surface between the retaining structure and the ground. As a rule, the retaining structures are designed by the limit values of soil pressures which cannot be activated over the whole region of interaction due to the condition of both mediums' equal displacements. The general shape of the mobilized earth pressures acting at the ultimate limit state of the homogeneous cohesionless ground is presented in Fig. 1. All standard methods are based on earth pressures at limit equilibrium. Methods differ only in the assumptions and simplifications used in the determination of these pressures.

A generalization of the existing methods to the case of a layered strata is presented in this section. Layered strata means multilayer above the dredge level and a single layer below it.

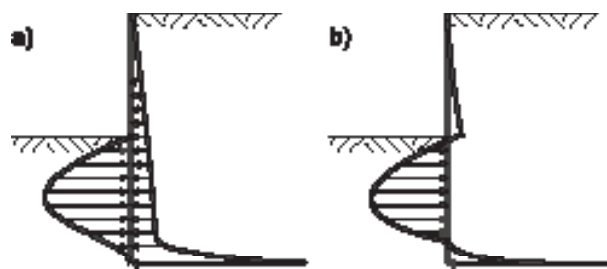


Figure 1. Activated Influences and Resistances: (a) Soil Pressure Distribution; (b) Net Soil Pressure Distribution

2.1 UK SIMPLIFIED METHOD^{6E}

This method, mostly used in Europe, is the simplest one. It is described in several publications (Padfield and Mair 1984, King 1995), and represents the basis of many computer codes for designing embedded retaining structures. The activation of all active pressures and passive resistances in this method is assumed, above the calculating rotation point 1 (Fig. 2). The resistances under the rotation point are not determined exactly; they are substituted with the fictitious concentrated force R.

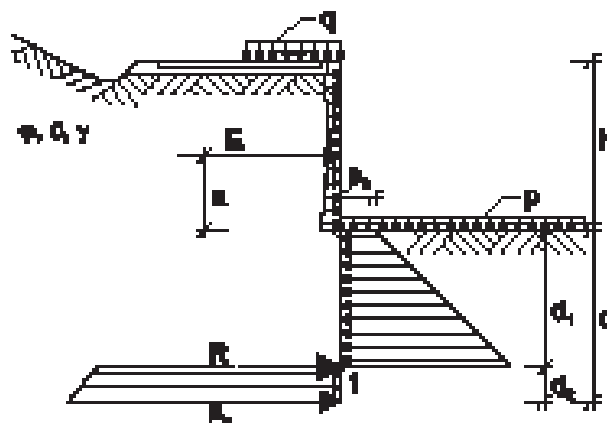


Figure 2. Influences and Resistances According to the UK Simplified, and UK Full Method

By considering the equilibrium condition of the moments around the rotation point 1, we obtain:

$$a_1^2 (K - 1) + 15 p_0^* a_1^2 - 3E^* (a^* + a_1^*) = 0 \quad (1)$$

where the normalized quantities are:

$$\begin{aligned} a_1^* &= a_1/h, & K &= K_{p1}/K_{a1}, \\ E^* &= 2E/(\gamma h^2 K_{a1}), & c^* &= 2c/(\gamma h) \\ p_0^* &= c^*(K_{a1} + K_{p1})/K_{a1} + p^* K_{p1}/K_{a1} - 2, \\ a^* &= 2q/(\gamma h), & a^* &= a/h \end{aligned} \quad (2)$$

K_{ay} , K_{py} , and K_{ac} , K_{pc} , and K_{pq} denote the coefficients of active and passive pressures for the influences of soil weight, cohesion and surcharge (Kérisel and Absi 1990). The letters γ , c and q in indices denote the unit weight, cohesion and surcharge loading of the soil layer in which the analyzed retaining structure is embedded. The required embedment depth d_1 up to point 1 is determined by solving (1). The analytical solution (3) can be applied only for a retaining structure in homogeneous cohesionless soil without surface or other additional loading.

$$a_1^* = 1/(\sqrt{K} - 1) \quad (3)$$

The total required embedment depth $d = d_1 + d_2$ is approximately:

$$d = 1.2a_1^*, \quad a^* = a/h \quad (4)$$

The maximum values of bending moment and shear force acting on the retaining structure are determined:

$$M_m^* = M_m^* \gamma h^2 K_{ay} / 2, \quad T_m^* = T_m^* \gamma h^2 K_{py} / 2 \quad (5)$$

where M_m^* and T_m^* are the normalized values of the maximum inner forces determined by using:

$$\begin{aligned} M_m^* &= E^* (a^* + x_m^*) - p_0^* x_m^{*2} / 2 - (K-1) x_m^{*2} / 3 \\ T_m^* &= E^* - p_0^* a_1^* - (K-1) a_1^{*2} \end{aligned} \quad (6)$$

where x_m^* denotes the distance between the point where the maximum bending moment acts and the dredge line:

$$x_m^* = \frac{(p_0^{*2} + 4(K-1)E^*)^{1/2} - p_0^*}{2(K-1)} \quad (7)$$

2.2 UK FULL METHOD^{9E}

UK full method additionally considers the influence of limit pressures under rotation point 1 (Fig. 2). The ground resistance at the toe of the embedded wall is determined:

$$p_3^* = 2p_3 / (\gamma h K_{ay}) = 2K\gamma^* + 2(K-1)a^* + c'(K_\mu - K_{ac}) / K_{ay} \quad (8)$$

where γ^* denotes the ratio of the average unit weight of the backfill ground above the dredge line for the considered problem to the unit weight of the ground under the dredge line.

After considering the equilibrium conditions of the horizontal forces and moments we obtain the following expressions:

$$\begin{aligned} a_2^* &= ((K(\gamma^* + a_1^*) - a_1^* + c'(K_\mu + K_{ac}) / 2K_{ay})^2 / (K-1)^2 + \\ & \quad ((K-1)a_1^{*2} + p_0^* a_1^* - E^*) / (K-1))^{1/2} \quad (9) \\ & \quad - (K(\gamma^* + a_1^*) - a_1^* + c'(K_\mu + K_{ac}) / 2K_{ay}) / (K-1) \end{aligned}$$

$$\begin{aligned} E^* (3a^* + 3a_1^* + 2a_2^*) - p_0^* a_1^* (1.5a_1^* + 2a_2^*) + K\gamma^* a_2^{*2} \\ - (K-1)(a_1^{*2} + 2a_1^{*2} - a_1^* a_2^{*2}) + 0.5c'(K_\mu + K_{ac}) a_2^{*2} / K_{ay} = 0 \quad (10) \\ a_2^* = a_2^* / h \end{aligned}$$

The required embedment depth $d = d_1 + d_2$ is calculated by solving the system of equations (9) and (10). The maximum values of bending moment and shear force acting on the retaining structure are determined using (5), (6) and (7).

2.3 USA METHOD^{9E}

The USA method, which was first introduced by Bowles (1988) for homogeneous soil, supposes that the entire passive resistance is mobilized at the toe of the retaining structure. In the region between depths d_1 and d (Fig. 3), the resulting resistances have the form of a straight line (polygonal net pressure distribution).

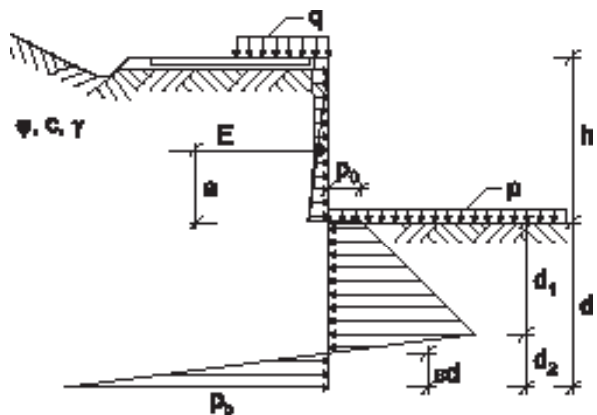


Figure 3. Influences and Resistances According to the USA, King, and Day Methods

The individual earth pressures and available passive pressures above the calculated embedment depth can be estimated for arbitrarily layered ground. The unknown embedment depth d in the soil at the toe of the pile wall is determined by using the equilibrium of horizontal forces (11), while the depth d_1 is determined by the moment equilibrium condition (12).

$$E^* + (\gamma^* K + (K-1)a^* + 0.5c'(K_\mu + K_{ac}) / K_{ay})(a^* - a_1^*) - 0.5p_0^*(a^* + a_1^*) - (K-1)a^* a_1^* = 0 \quad (11)$$

$$a_1^* = (E^* (3a^* + 2a_1^*) - 0.5p_0^* a^*^2) / ((K-1)a^*^2 - E^* + p_0^* a^*) \quad (12)$$

2.4 KING'S METHOD^{6E}

On the basis of centrifuge model tests, King (1995) established that not all available resistances at the toe of an embedded pile without anchors could be fully activated in the limit state. He, therefore, proposed modifying the USA method by considering a polygonal form of the active and passive pressures, and determining experimentally the value of parameter $\varepsilon = 0.35$. This parameter defines the depth at which the activated contact-stresses in front of and behind the embedded pile are balanced. King only gave solutions for homogeneous cohesionless ground. The critical embedment depth d for layered ground can be determined using (13).

$$E' (\alpha' (1 - \beta - \alpha_1') - 0.5 \beta_0' (\alpha'' (1 - 2\varepsilon) - \alpha_1'')) - (X - 1) \alpha_1' \alpha_1'' (\alpha' (1 - 2\varepsilon) - \alpha_1' (1 - \beta)) = 0 \quad (13)$$

The depth d_1 is determined by the moment equilibrium condition (12).

2.5 DAY'S METHOD^{6E}

Day (1999) found that King's method gave too conservative results, particularly for lower values of parameter K . If K is lower than 7.90, the solution does not practically exist.

He therefore proposed, on the basis of the interaction analysis results using FEM, introducing new value of parameter ε .

$$\varepsilon = 0.047 \ln(X) + 0.1 \quad (14)$$

In Day's method the unknown embedment depth is also determined using (12) and (13).

3 FINITE ELEMENT ANALYSESS

A set of two-dimensional plane strain analyses for the ultimate limit state of embedded retaining structures was performed to confirm the results of the described analytical methods. The critical excavation depth was determined by progressive removal of the excavated soils until the horizontal displacement of the wall was so high that further re-establishment of the retaining structure's global equilibrium could not occur anymore.

A relatively stiff elastic concrete retaining structure of the total length $h + d = 10.0$ m was considered in the analyses. Its characteristics were $E = 31 \cdot 10^6$ kPa, $I = 0.083$ m⁴/m and $A = 1$ m²/m. The cross-section of the analyzed excavation is presented in Fig. 4.

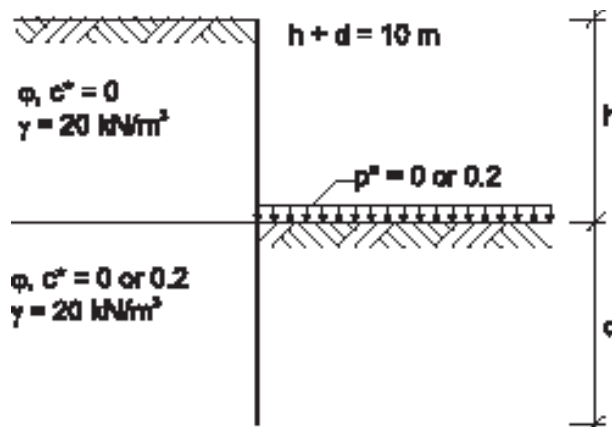


Figure 4. Cross-Section of the Analyzed Excavation

The elasto-plastic Hardening-Soil model with isotropic hardening (PLAXIS 1998) was used. The advantage of the Hardening-Soil model over the Mohr-Coulomb model is in the use of a hyperbolic stress-strain curve, and the stress dependency on soil stiffness. The Hardening-Soil model uses the theory of plasticity, includes dilatancy and introduces a cap yield surface. The following properties were considered: $E_{50}^{ref} = E_{oed}^{ref} = 40$ MPa, $E_{ur}^{ref} = 3E_{50}^{ref}$, $\nu_{ur} = 0.2$, $m = 0.5$, $R_f = 0.9$, $p^{ref} = \gamma h$, where h denotes the final excavation depth in the limit state. The analyzed region was discretized in 2.000 six-node triangle finite elements with a refined mesh near the retaining structure. The finite element mesh with the deformed mesh of the analyzed excavation is presented in Fig. 5.

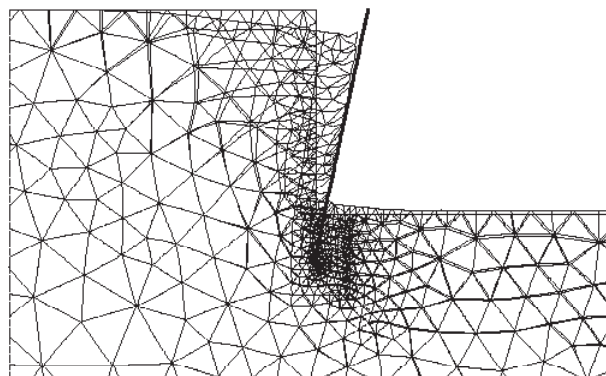


Figure 5. The Cutting Out of the Finite Element Mesh with the Deformed Mesh (scaled 10 times) of the Analyzed Excavation

The numerical analyses were performed for friction angles $\varphi = 10^\circ$ to $\varphi = 50^\circ$ in steps of 5° , normalized cohesions $c^* = 0$ and 0.2 , and normalized surcharges $p^* = 0$ and 0.2 . All analyses considered the friction between the retaining structure and the ground $\delta = \varphi$, dilatation $\psi = \varphi/2$ and unit weight of soil $\gamma = 20$ kN/m³.

The ultimate limit state, reflected in the critical excavation depth h_c , was considered as a state when no equilibrium could be ensured anymore or when numerical results could not converge.

The results of analyses have shown that the deformations obtained for the used elasto-plastic soil model for a rigid retaining structure are directly proportional to the square of the excavation, and inversely proportional to the deformation modulus E_{50} . The displacements of the retaining structure can be determined using (15).

$$u = u^* \gamma h^2 / E_{50} \quad (15)$$

where u is the displacement of the actual structure and u^* the displacement determined on a generalized system with normalized quantities $h^* = h/h = 1$, $d^* = d/h$, $t^* = t/h$, $\gamma^* = 1$, c^* , q^* and p^* , where t is the thickness of the retaining wall. The actual values of maximum bending moments and shear forces can be determined on the basis of their normalized values using (6).

Variation in the normalized values of the horizontal displacements at the top of the retaining structure u_o^* with arbitrary excavation depths h^* for $p^* = q^* = c^* = 0$ (see Fig. 4) are shown in Fig. 6a. Variation in the normalized values of displacements u_o^* with arbitrary excavation depths h^* for $p^* = q^* = 0$ and $c^* = 0.2$ are presented in Fig. 6b, and for $q^* = c^* = 0$ and $p^* = 0.2$ in Fig. 6c.

The results of numerical simulations have shown that at higher friction angles the bearing capacity limit state occurs at smaller excavation depths than those determined by classic methods (UK simplified, UK full and USA). King (1995) and Day (1999) drew similar conclusions. Only in the case where $p^* = q^* = c^* = 0$ are the results of FE analyses comparable with the results of King's and Day's solutions. The differences are considerable, especially for the required embedment depth (ultimate limit state of the ground), and for the maximum internal shear forces of the retaining structures (section strength limit state of the retaining structures). The deviations are observed for retaining structures in homogeneous and layered ground, as well as for surcharges.

In geotechnical practice, retaining structures are most frequently embedded in soils of relatively high shear strength. Therefore, the choice of method for geomechanical analysis is often decisive for safety, as well as for the economy of the designed retaining structure. For this reason, the next section presents a new method which yields more reliable results. It makes it possible to design retaining structures of comparable safety for the ultimate limit state of the ground, as well as for the section strength limit states of the retaining structures.

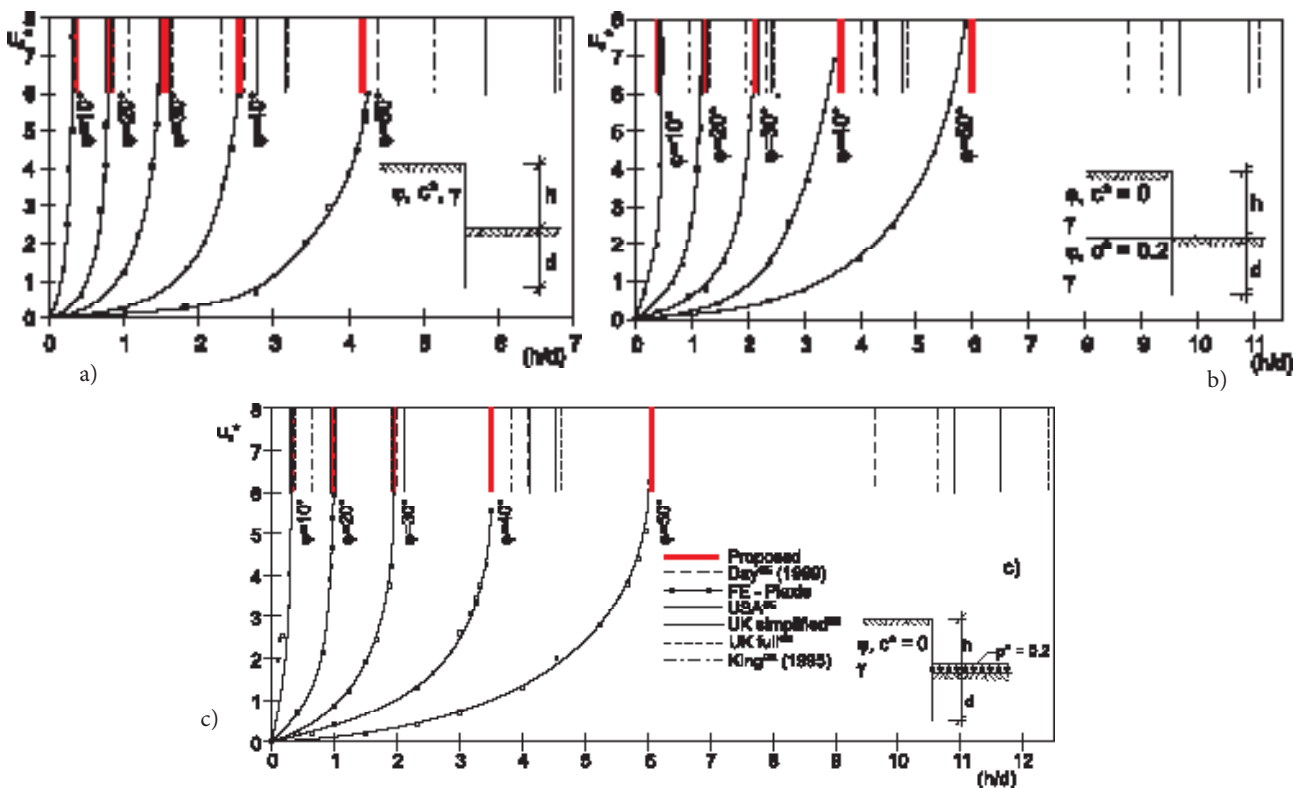


Figure 6. Normalized Values of Displacements u_o^* for: a) $p^* = q^* = c^* = 0$; b) $p^* = q^* = 0$, $c^* = 0.2$; c) $q^* = c^* = 0$, $p^* = 0.2$

4 PROPOSED METHOD

Classical methods of numerical analysis (UK simplified, UK full and USA) suppose that all available passive earth pressures are mobilized in the region of embedment in the limit state of the retaining structure. The results of more recent researches (King 1995 and Day 1999) show that these resistances could not actually be mobilized as ideally as was expected. Therefore, King (1995) and Day (1999) proposed some changes in net pressure diagram. However, their approaches only ensure good results for ideal cases of retaining structures in homogeneous cohesionless ground without surcharge loading.

The proposed method is based on the results of an experimental investigation into the resistance activation in the region of the embedded part of the retaining structure at forced displacements (Fang et al. 1994). It considers the results of numerical analyses according to FEM (Day 1999), and partly the results of centrifuge tests (King 1995). The data of experimental investigation from Fang et al. 1994 were used to choose the shapes of resistances, while the data from FE analyses were used to adjust assumed parameters p_0 , m and n with the results of FE analyses at the limit state.

The results of small scale laboratory experiments (Fang et al. 1994) show that resistances at the embedded part are activated in polygonal shape only at the translational displacements of the wall, and only in those cases where they approximately correspond to the passive resistance. If the wall rotates, the resistance is activated in the shape of exponential functions. The shape and the magnitude depend on the position of the rotation point and on the magnitude of the forced displacement. Fang et al. (1994) presented the experimentally determined the shapes of the activated resistances at the wall rotations around the upper and lower points.

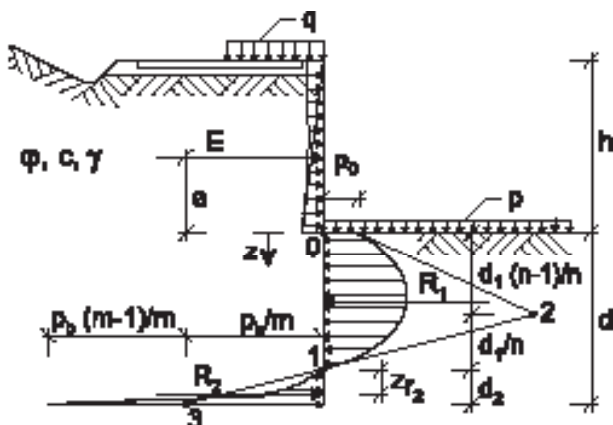


Figure 7. Influences and Activated Resistances at Limit State

The results of FE analyses show that at the limit state the rigid retaining structure rotates around the point at the depth d_1 . For all analyzed cases this point is located approximately at the depth where the pressures on the wall from left and right are equal. Therefore, it can be supposed that net pressure under dredge level is mobilized in the shape of two exponential functions as presented in Fig. 7.

From the experimental research results of Fang et al. (1994), it can be assumed that the total passive resistance (p_0) is mobilized at the excavation depth, and further up to the depth (d_1) it has the form of the following function:

$$p(x) = p_0 + C_1(x/d_1) + C_2(x/d_1)^n \quad (16)$$

where C_1 and C_2 are constants determined by boundary conditions (17) and (18).

$$p(x = d_1) = p_0 + C_1 + C_2 = 0 \quad (17)$$

$$\left. \frac{dp(x)}{dx} \right|_{x=0} = \frac{C_1}{d_1} = \gamma(K_{ps} - K_{ps'}) \quad (18)$$

After solving (17) and (18) we obtain:

$$C_1 = \gamma(K_{ps} - K_{ps'})d_1 \quad (19)$$

$$C_2 = -p_0 - \gamma(K_{ps} - K_{ps'})d_1 \quad (20)$$

The boundary values of (18) that can only appear at the embedment in cohesive ground or when surcharge loading is in front of the retaining structure are:

$$\left. \frac{dp(x)}{dx} \right|_{x=0} = \left(\frac{C_1}{d_1} + \frac{C_2 n x^{n-1}}{d_1^n} \right) \Big|_{x=0} = -\frac{p_0}{d_1} \quad (21)$$

$$\left. \frac{dp(x)}{dx} \right|_{x=d_1} = \left(\frac{C_1}{d_1} + \frac{C_2 n x^{n-1}}{d_1^n} \right) \Big|_{x=d_1} = -\infty \quad (22)$$

It has to be noted that the infinite slope boundary condition in (22) can only appear for higher cohesion or surcharge loading with a simultaneously high friction angle. The distribution of the mobilized earth pressures in the whole region of the embedment depth d_1 follows the exponential function given below:

$$p^*(x) = \frac{2p(x)}{\gamma n K_{ps}} = p_0^* + 2(K_{ps} - 1)d_1 \left(\frac{x}{d_1} \right) - (p_0^* + 2(K_{ps} - 1)d_1) \left(\frac{x}{d_1} \right)^n \quad (23)$$

The resulting horizontal force and moment around point O of the mobilized earth pressures are given in (24) and (25).

$$R_1^* = p_0^* a_1^* \left(\frac{n}{n+1}\right) + (K-1) a_1^{*2} \left(\frac{n-1}{n+1}\right) \quad (24)$$

$$M_{s1}^* = p_0^* a_1^{*2} \left(\frac{n}{2(n+2)}\right) + 2(K-1) a_1^* \left(\frac{n-1}{3(n+2)}\right) \quad (25)$$

In the region of embedment depth d_2 the following distribution of earth pressures is considered:

$$p(x) = p_b^* \left(\frac{x-d_1}{d_2}\right)^m \quad (26)$$

where p_b denotes the horizontal pressure on the wall at the toe of the retaining structure. The resulting horizontal force of the pressures in the region of depth d_2 is given in (27), and the distance of the resulting horizontal force from point I in (28).

$$R_2^* = p_b^* \left(\frac{d_2}{m+1}\right) \quad (27)$$

$$x_s^* = a_2^* \left(\frac{m+1}{m+2}\right) \quad (28)$$

Different values of parameters p_0^* , p_b^* , $(K-1)$, m and n define a family of exponential functions that agrees with the experimental distribution of pressures along the embedment depths of the rigid retaining structures.

The values of parameters m and p_b^* are determined from the results of numerical simulations of the limit states of retaining structures embedded in cohesionless and layered ground, as well as for the case of surcharge loading in front of the retaining structure. Parameter m is based on numerical interpolation using results of elasto plastic analyses using FEM and can be expressed as:

$$m = 2 + \ln(K)/4 \quad (29)$$

The comparative value of parameter p_b^* is determined experimentally for individual numerical solutions at the ultimate limit state:

$$p_b^* = \frac{|T_m^*|(m+1)}{a_2^*} \quad (30)$$

where T_m^* denotes the maximum normalized shear force acting on the retaining structure at limit state determined using FEM. The numerically (using FEM) and analytically (using Eq. 31) determined values of parameter p_b^* are presented in Fig. 8.

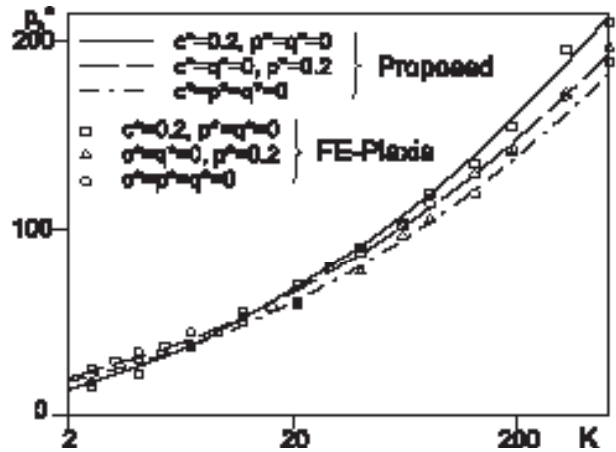


Figure 8. Numerical and Analytical Values of Parameter p_b^*

In the analysis of retaining structures we can consider the following normalized values of pressures at the toe of the pile wall in a wider region of the value K (Fig. 8):

$$p_b^* = (1 + a^* + c^*) (\ln K + 3.8 \ln^2 K) \quad (31)$$

Equation (31) is the approximation of the results using FEM determined by method of the least square. The mobilized pressures in front of and behind the retaining structure (defined by parameters n and m) are linked with (32). The relationship is determined by the slope of the tangent (line 2-3, see Fig. 7) to the net pressure function in front of the retaining structure through point I .

$$n = \frac{p_0^* a_1^* / m + 2(K-1) a_1^* a_2^*}{p_b^* a_2^* + 2(K-1) a_1^* a_2^*} \quad (32)$$

The embedment depths of the retaining structure d_1^* and d_2^* are determined considering the moment equilibrium around point I (33), and the horizontal forces' equilibrium condition (34).

$$E^* (a^* + a_1^*) - p_0^* a_1^{*2} \left(\frac{n}{n+1} - \frac{n}{2(n+2)}\right) - (K-1) a_1^* \left(\frac{n-1}{n+1} - \frac{2(n-1)}{3(n+2)}\right) - p_b^* \frac{a_2^{*2}}{m+2} = 0 \quad (33)$$

$$E^* - p_0^* a_1^* \left(\frac{n}{n+1}\right) - (K-1) a_1^{*2} \left(\frac{n-1}{n+1}\right) + p_b^* a_2^* / (m+1) = 0 \quad (34)$$

The required embedment depth d^* and the parameter n , representing the stage of pressure mobilization along the embedment depth d_1^* , are determined for each considered case separately by solving a system of three nonlinear equations (32), (33) and (34). The maximum bending moment and shear force acting on the embed-

ded retaining structure at limit state are determined using (35) and (36).

$$T_m^* = E^* - p_0^* a_1^* \left(\frac{n}{n+1} \right) - (K-1) a_1^* \left(\frac{n-1}{n+1} \right) \quad (35)$$

$$M_m^* = E^* (a^* + x_m^*) - p_0^* x_m^* \left(\frac{1}{2} - \frac{x_m^*}{a_1^* (n^2 + 3n + 2)} \right) - (K-1) x_m^* \left(\frac{1}{3} - \frac{2x_m^{*1}}{a_1^{*1} (n^2 + 3n + 2)} \right) \quad (36)$$

The distance of point x_m^* , where the maximum bending moment acts, from the toe of the excavation is determined using (37).

$$E^* - p_0^* x_m^* \left(1 - \frac{x_m^*}{a_1^* (n+1)} \right) - (K-1) x_m^* \left(1 - \frac{2x_m^{*1}}{a_1^{*1} (n+1)} \right) = 0 \quad (37)$$

Numerical procedure

- i) We determine $K = K_{py} / K_{ay}$; $E^* = 2E / (\gamma h^2 K_{ay})$; $a^* = a/h$, $p_0^* = 2p_0 / (\gamma h K_{ay})$, $m = 2 + \ln(K) / 4$
- ii) Using Microsoft Solver real minimum solution of $d_1^* + d_2^*$ of nonlinear equations (31) - (34) with constraints ($d_1^* > 0$ and $d_2^* > 0$).
- iii) For obtained values d_1^* and d_2^* the position of maximum bending moment x_m^* (Eq 37) and values of maximum shear force T_m^* (Eq 35) and maximum bending moment M_m^* (Eq 36) are determined. For case $c^* = q^* = p^* = 0$ of geomechanical analysis for shear angles $\varphi = 15^\circ, 20^\circ, 25^\circ, 30^\circ, 35^\circ, 40^\circ, 45^\circ$, and 50° are given in Table 1.

Table 1. The Results of Analyses for $\delta/\varphi = 1$, for $c^* = q^* = p^* = 0$

φ [°]	p_b^*	m	n	d_1^*	d_2^*	M_m^*	T_m^*
(1)	(2)	(3)	(4)	(5)	(6)	(7)	(8)
15	26.012	2.355	8.713	1.5630	0.2957	1.2892	2.293
20	36.708	2.488	8.252	1.0273	0.2060	0.8586	2.168
25	48.997	2.621	7.243	0.7302	0.1592	0.6594	2.155
30	63.926	2.762	5.996	0.5359	0.1297	0.5452	2.203
35	83.642	2.925	4.656	0.3942	0.1082	0.4703	2.306
40	108.645	3.102	3.472	0.2953	0.0927	0.4226	2.454
45	142.887	3.311	2.489	0.2224	0.0802	0.3905	2.657
50	191.143	3.559	1.774	0.1705	0.0697	0.3697	2.924

Table 2. The Results of Analyses for Different Combinations of h and p values

	(1)	(2)	(3)	Method						
				UK Simpl.	UK Full	USA	King	Day	FE	Proposal
	(1)	(2)	(3)	(4)	(5)	(6)	(7)	(8)	(9)	(10)
(a) $h=10.0$ m, $p=0$										
Total wall height		$h+d$	(m)	11.77	11.52	11.53	12.01	12.32	12.44	12.43
Max. shear force		T_m	(kN/m)	910.2	854.0	766.5	389.9	310.0	302.1	297.3
Max. bending moment		M_m	(kNm/m)	373.3	373.3	373.8	373.3	373.3	379.3	377.9
(b) $h=10.5$ m, $p=10$ kPa										
Total wall height		$h+d$	(m)	11.85	11.67	11.68	11.92	12.03	12.56	12.52
Max. shear force		T_m	(kN/m)	1011.7	945.5	860.5	559.2	491.3	366.0	317.3
Max. bending moment		M_m	(kNm/m)	404.7	404.7	404.7	404.7	404.7	410.6	406.2
(c) $h=11.0$ m, $p=20$ kPa										
Total wall height		$h+d$	(m)	12.14	12.01	12.02	12.17	12.24	12.92	12.89
Max. shear force		T_m	(kN/m)	1205.4	1115.7	958.1	735.9	664.3	382.2	351.3
Max. bending moment		M_m	(kNm/m)	455.7	455.7	455.7	455.7	455.7	460.1	456.5

Note: All methods in columns (4) to (8) are generalized and extended (GE)

5 VALIDATION OF THE METHOD

A comprehensive set of results has been calculated for comparisons in order to validate the performance of the proposed method. Four cases are presented. In the first case, a cantilever reinforced concrete retaining structure of a certain width, embedded in homogeneous cohesionless ground of certain properties at a certain soil-wall friction, was analyzed, where the height of the retaining structure and surcharge loading had been altered. The remaining three cases concerned a cantilever embedded retaining structure of certain height, where analyses were performed for different combinations of normalized c^* and p^* . The variation of (h/d) , M_m^* and T_m^* with K is given in the form of diagrams.

5.1 CASE 1

A cantilever embedded reinforced concrete retaining structure (1.0 m in width) for the protection of a construction pit in homogeneous cohesionless ground was considered. The following ground properties were considered: $\varphi = 49.5^\circ$, $c = 0$, $\delta = 20 \text{ kN/m}^3$, and friction between soil and wall $\delta = \varphi$. Three examples were analyzed:

- (a) $h = 10.0\text{m}$, $p = 0$,
- (b) $h = 10.5\text{m}$, $p = 10 \text{ kPa}$
- (c) $h = 11.0\text{m}$, $p = 20 \text{ kPa}$.

The results of analyses are presented in Table 2.

The results of analyses for example (a) show, that in ideal homogeneous cohesionless ground the classical analytical methods (UK simplified, UK full and USA) give similar results. They differ from the solutions of more recent methods (King, Day, FE and Proposal) in required embedment depths and maximum internal shear forces. The differences in embedment depths are up to 61%, for maximum internal shear forces up to 206%, and for bending moments up to 1.6% with regard to the smallest values.

In examples (b) and (c) the weight of the ground at the toe of excavation was substituted with the pertinent surcharge loading (soil without shear strength). The differences with the smallest values for embedment depths are up to 76% in example (b) and grow up to 90% in example (c), for maximum internal shear forces up to 219% and 243%, and for bending moments up to 1.5% and 1%. In these cases King's and Day's method exhibit unacceptable solutions, because the required embedment depth is smaller than that of a ground with very high pressure resistance at the dredge level. For such

cases, the results of analyses obtained by the two newer methods are comparable with the results obtained using classical methods. It can be concluded from the above examples, that all the presented methods give practically the same values of bending moments. This is due to the fact that bending moments depend mostly on wall height.

When the surcharge loading in the excavation pit at the dredge line level is considered, only the results of the proposed method are comparable with the results of FEM elasto-plastic analyses.

5.2 CASE 2

The limit states of a rigid cantilever reinforced concrete retaining structure embedded in homogeneous cohesionless ground were considered. The numerical analyses were done for ground with friction angles from $\varphi = 10^\circ$ to $\varphi = 50^\circ$ in steps of 2.5° , cohesion $c = 0$, and without surcharge loading. The analyses were performed for all considered methods. In all analyses the rigid retaining structure of total height $h + d = 10.0 \text{ m}$, friction between soil and wall $\delta = \varphi$, dilatation angle $\psi = \varphi/2$, and unit weight $\gamma = 20 \text{ kN/m}^3$ were considered. Fig. 9 shows the distribution of horizontal soil pressures acting on the retaining structure in homogeneous ground for $\varphi = 20$, 35 and 50° . The solution according to FEM is presented in the same way as the results published by Day (1999). The excavation depths for each individual method are presented in the same diagram.

It can be concluded from the net pressure distributions in Fig. 9, that the pressure distribution given by the proposed method agrees very well with the calculated net pressure points using FEM (Day 1999). Fig. 10a presents the variation of the required normalized values of embedment depth d^* ($d^* = d/h$), maximum bending moments M_m^* , and maximum shear forces T_m^* with parameter K .

It is evident from Fig. 10a that the results of the proposed method are in agreement with the results of FE analyses and the solutions of Day (1999). The latest solutions show larger deviations at higher values of K ratios, which do not appear in practice. However, these deviations arise in further analyses for layered ground and when surcharge loading is presented.

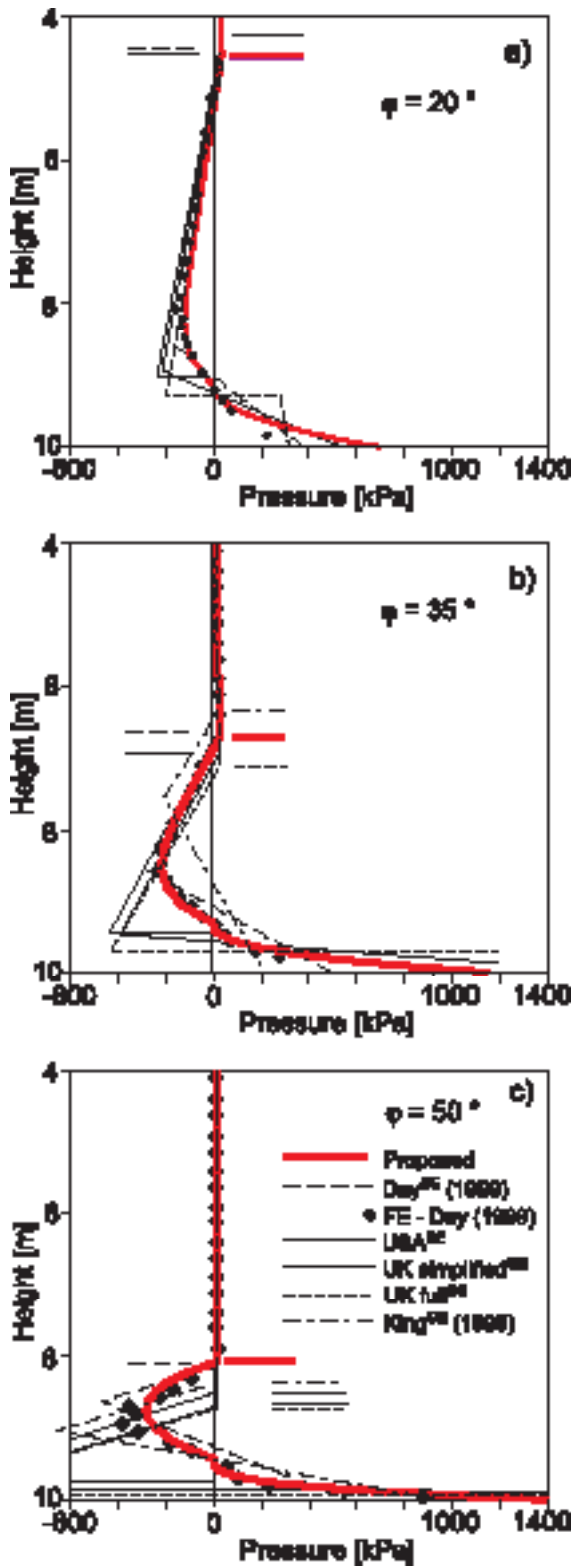


Figure 9. Net Pressure Distribution:
 (a) $\varphi = 20^\circ$
 (b) $\varphi = 35^\circ$
 (c) $\varphi = 50^\circ$

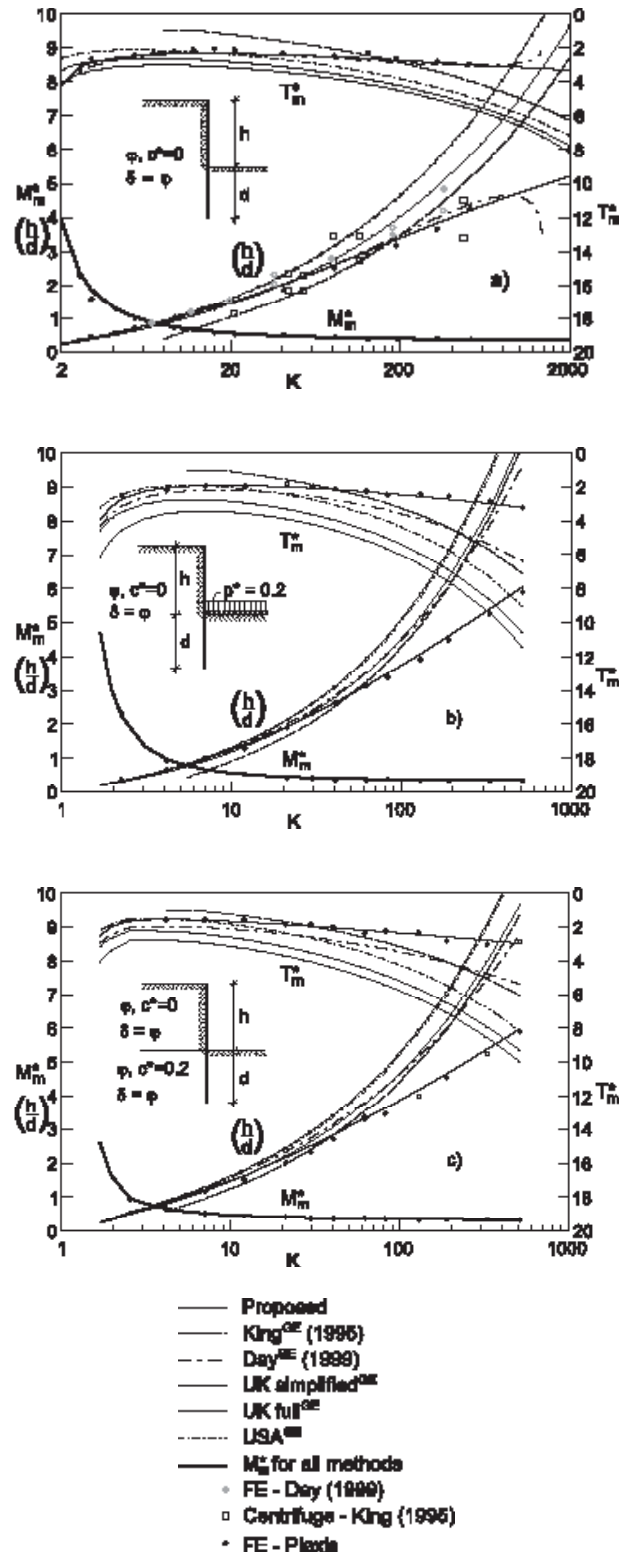


Figure 10. Variation of (h/d) , M_m^* and T_m^* with K for:
 a) $c^* = q^* = p^* = 0$
 b) $c^* = q^* = 0$ and $p^* = 0.2$
 c) $p^* = q^* = 0$ and $c^* = 0.2$

It is evident from Fig. 10a that the results of the proposed method are in agreement with the results of FE analyses and the solutions of Day (1999). The latest solutions show larger deviations at higher values of K ratios, which do not appear in practice. However, these deviations arise in further analyses for layered ground and when surcharge loading is presented.

5.3 CASE 3

The limit states of the rigid cantilever reinforced concrete retaining structure embedded in homogeneous cohesionless ground were considered again. The influence of surcharge loading in front of the retaining structure at the toe of the construction pit was considered, too. In geotechnical practice such loading represents the influences of soil layers with low pressure resistance, which are located above the foreseen embedment depth of the retaining structure. Fig. 10b presents the variation of the required normalized embedment values of the depth d' ($d' = d/h$), maximum bending moments M_m^* , and maximum shear forces T_m^* with parameter K . It is evident from Fig. 10b that only the results of the proposed method agree with the numerical results of FEM analyses.

5.4 CASE 4

The limit states of the rigid cantilever retaining structure in homogeneous ground were considered further, where soils under the dredge level have a part of the cohesion shear strength of the upper layer, $c^* = 0.2$. Fig. 10c presents the variation of the required embedment depth normalized values d' ($d' = d/h$), maximum bending moments M_m^* , and maximum shear forces T_m^* with parameter K . It is again evident from Fig. 10c that only the results of the proposed method agree with the numerical results of FE analyses.

6 CONCLUSIONS

The results of analyses show that, due to the interaction between rigid cantilever retaining structures and the ground, the entire passive resistance is not actually mobilized, as is considered in classical methods for retaining structure analyses (UK simplified, UK full and USA).

The greatest differences are exhibited for structures embedded in soils with high shear strength when higher friction between the structure and the ground is consid-

ered. Furthermore, the largest differences are obtained in the region of the wall's fictitious rotation point at embedment depth, and at the toe of the embedded retaining structure.

This paper presents the equations of the existing methods in generalized form, which enables analyses of retaining structures considering layered ground and surcharge loading.

Based on the performed analyses it can be established that the results of the proposed method agree very well with the results of finite element elastoplastic analysis and with the results of centrifuge tests. All the existing methods for cantilever pile wall analysis, as well as the proposed one, give nearly the same values for maximum bending moments. Furthermore, only the proposed method yields a reliable embedment depth and maximum internal shear force and does not underestimate embedment depths and overestimate internal shear forces, as do the existing methods.

The special benefit of this method is due to the realistic values for internal shear forces, which are, as a rule, strongly overestimated in the remaining methods. This benefit leads to a more economical design of pile walls, since larger pile spacing is possible. Consequently, the total bearing capacity of the reinforced concrete section can be exploited and a comparable safety of ground bearing capacity and strength of structure sections can be reached.

In practice, almost all retaining structures are erected in layered ground; the existing methods only give exact solutions for retaining structures in cohesionless ground. Therefore, this proposed method is more convenient and more applicable in the analysis and design of cantilever structures in geotechnical practice.

APPENDIX I.

REFERENCES

- Bica, A. V. D., and Clayton, C. I. R. (1989). Limit equilibrium design methods for free embedded cantilever walls in granular materials. *Proc. Instn Civ. Engrs Part 1*, 879-989.
- Bica, A. V. D. and Clayton, C. I. R. (1993). The preliminary design of free embedded cantilever walls in granular soil. *Retaining structures*, C. R. I. Clayton, ed., Thomas Telford, London, England, 731-740.

Bowles, J. E. (1988). *Foundation analysis and design*, 4th Ed., McGraw-Hill Book Co., New York, N.Y., 613-618.

Day, R. A. (1999). Net pressure analysis of cantilever sheet pile walls. *Geotechnique*, London, England, 49(2), 231-245.

Fang, Y. S., Chen, T. J., and Wu, B. F. (1994). Passive earth pressures with various wall movements. *J. Geotech. Engng Div.*, ASCE, 120(8), 1307-1323.

Kérisel, J., and Absi, E. (1990). *Tables for the calculation of passive pressure, active pressure and bearing capacity of foundations*. Gauthier-Villard, Paris, France.

King, G. J. W. (1995). Analysis of cantilever sheet-pile walls in cohesionless soil. *J. Geotech. Engng Div.*, ASCE, 121(9), 629-635.

Lyndon, A., and Pearson, R. A. (1985). Pressure distribution on a rigid retaining wall in cohesionless material. *Proc., Int. Symp. on Application of Centrifuge Modeling to Geotech. Design*, W. H. Craig, ed., A. A. Balkema, Rotterdam, The Netherlands, 271-280.

Padfield, C. J., and Mair, R. J. (1984). Design of retaining walls embedded in stiff clays. *CIRIA Report 104*, London, Constr. Industry Res. and Information Assoc. (CIRIA), London, England.

PLAXIS user's manual, version 7 (1998). R. B. J. Brinkgreve, and P. A. Vermeer, eds., A. A. Balkema, Rotterdam, The Netherlands

Rowe, P. W. (1951). Cantilever sheet piling in cohesionless soil. *Engrg.*, London, England, (Sept.), 316-319.

APPENDIX II.

NOTATION

The following symbols are used in this paper:

- a = distance of the resulting force of active pressures from the dredge line (see Figs. 2 and 3);
 a^* = normalized quantity defined as ratio a/h ;
 c^* = normalized quantity defined as ratio $2c/(\gamma h)$;
 C_1, C_2 = integration constants (see Eq. 16);

- d = total embedment depth (see Figs. 2 and 3);
 d_1, d_2 = partial embedment depths (see Figs. 2 and 3);
 d^*, d_1^*, d_2^* = normalized quantity defined as ratios $d/h, d_1/h$ and d_2/h ;
 E = resulting force of active pressures above dredge line (see Figs. 2 and 3);
 E^* = normalized quantity defined as ratio $2E/(\gamma h^2 K_{ay})$;
 E_{50}^{ref} = secant stiffness in standard drained triaxial test at the reference pressure;
 E_{oed}^{ref} = tangent stiffness for primary oedometer loading at the reference pressure;
 E_{ur}^{ref} = unloading / reloading stiffness in Hardening-Soil model (considered $E_{ur}^{ref} = 3 E_{50}^{ref}$);
 h = height of the retaining structure (see Figs. 2 and 3);
 h_c = critical (allowable) excavation depth;
 K = ratio between K_{py} and K_{ay} ;
 K_{pc}, K_{ac} = coefficient of passive and active earth pressure for influence of cohesion;
 K_{py}, K_{ay} = coefficients of passive and active earth pressure for influence of soil weight;
 K_{pq} = coefficient of passive earth pressure for influence of surcharge;
 m = parameter in elasto-plastic Hardening-Soil model (it is the input parameter in the relationship for stress dependent stiffness according to a power law) and parameter that defines family of exponential functions in proposed method;
 n = parameter that defines family of exponential functions in proposed method;
 M_m = maximum value of bending moment;
 M_m^* = normalized value of maximum bending moment;
 p_0 = pressure on the pile wall at the dredge line (see Figs. 2 and 3);
 p_0^* = normalized quantity defined as ratio $2p_0/(\gamma h K_{ay})$;
 p_b = net pressure at the toe of the pile wall (see Figs. 2 and 3);
 p_b^* = normalized quantity defined as ratio $2p_b/(\gamma h K_{ay})$;
 p^{ref} = reference pressure in elasto-plastic Hardening-Soil model;

- R_f = parameter in elasto-plastic Hardening-Soil model that defines failure ratio q_f/q_a (ultimate deviatoric stress / asymptotic value of the shear strength), is derived from the Mohr-Coulomb failure criterion;
- R_1^* = normalized resulted horizontal force in region of depth d_1 ;
- R_2^* = normalized resulted horizontal force in region of depth d_2 ;
- $M_{R_1^*}^0$ = normalized resulted moment of activated resistances in region of depth d_1 ;
- q^* = normalized quantity defined as ratio $2q/(\gamma h)$;
- T_m = maximum value of shear force;
- T_m^* = normalized value of maximum shear force;
- t = thickness of the retaining structure;
- t^* = normalized quantity defined as ratio t/h ;
- u = horizontal displacement;
- u^* = normalized horizontal displacement;
- u_0^* = normalized horizontal displacement at the top of the retaining structure;
- x_m^* = distance of the point where maximum bending moment acts measured from the bottom of excavation;
- z = independent variable that denotes depth;
- $z_{R_2^*}^*$ = distance of the resulted horizontal force;
- γ = unit weight of the soil;
- γ^* = ratio between average unit weight of the backfill ground above dredge line and the unit weight of the ground under dredge line;
- δ = friction angle at the soil-structure interface;
- ε = experimentally determined parameter that defines depth at which activated contact stresses in front of and behind embedded pile are balanced wall (see Fig. 3);
- ν_{ur} = Poisson's ratio for unloading-reloading in Hardening-Soil model (considered $\nu_{ur} = 0.2$);
- φ = angle of internal friction of the soil; and
- ψ = angle of dilatation of the soil.

NAVODILA AVTORJEM

Članki so objavljeni v angleškem jeziku s prevodom izvlečka v slovenski jezik.

VSEBINA ČLANKA

Članek naj bo napisan v naslednji obliki:

- Naslov, ki primerno opisuje vsebino članka in ne presega 80 znakov.
- Izvleček, ki naj bo skrajšana oblika članka in naj ne presega 250 besed. Izvleček mora vsebovati osnove, jedro in cilje raziskave, uporabljeno metodologijo dela, povzetek izidov in osnovne sklepe.
- Uvod, v katerem naj bo pregled novejšega stanja in zadostne informacije za razumevanje ter pregled izidov dela, predstavljenih v članku.
- Teorija.
- Eksperimentalni del, ki naj vsebuje podatke o postavitvi preiskusa in metode, uporabljene pri pridobitvi izidov.
- Izidi, ki naj bodo jasno prikazani, po potrebi v obliki slik in preglednic.
- Razprava, v kateri naj bodo prikazane povezave in posplošitve, uporabljene za pridobitev izidov. Prikazana naj bo tudi pomembnost izidov in primerjava s poprej objavljenimi deli.
- Sklepi, v katerih naj bo prikazan en ali več sklepov, ki izhajajo iz izidov in razprave.
- Literatura, ki mora biti v besedilu oštevilčena zaporedno in označena z oglatimi oklepaji [1] ter na koncu članka zbrana v seznamu literature.

OBLIKA ČLANKA

Besedilo naj bo pisano na listih formata A4, z dvojnimi presledki med vrstami in s 3.0 cm širokim robom, da je dovolj prostora za popravke lektorjev. Najbolje je, da pripravite besedilo v urejevalniku Microsoft Word. Hkrati dostavite odtis članka na papirju, vključno z vsemi slikami in preglednicami ter identično kopijo v elektronski obliki.

Enačbe naj bodo v besedilu postavljene v ločene vrstice in na desnem robu označene s tekočo številko v okroglih oklepajih.

ENOTE IN OKRAJŠAVE

V besedilu, preglednicah in slikah uporabljajte le standardne označbe in okrajšave SI. Simbole fizikalnih

veličin v besedilu pišite poševno (npr. v , T itn.). Simbole enot, ki sestojijo iz črk, pa pokončno (npr. Pa, m itn.).

Vse okrajšave naj bodo, ko se prvič pojavijo, izpisane v celoti.

SLIKE

Slike morajo biti zaporedno oštevilčene in označene, v besedilu in podnaslovu, kot sl. 1, sl. 2 itn. Posnete naj bodo v kateremkoli od razširjenih formatov, npr. BMP, JPG, GIF. Za pripravo diagramov in risb priporočamo CDR format (CorelDraw), saj so slike v njem vektorske in jih lahko pri končni obdelavi preprosto povečujemo ali pomanjšujemo.

Pri označevanju osi v diagramih, kadar je le mogoče, uporabite označbe veličin (npr. v , T). V diagramih z več krivuljami mora biti vsaka krivulja označena. Pomen oznake mora biti razložen v podnapisu slike.

Za vse slike po fotografskih posnetkih je treba priložiti izvorne fotografije ali kakovostno narejen posnetek.

PREGLEDNICE

Preglednice morajo biti zaporedno oštevilčene in označene, v besedilu in podnaslovu, kot preglednica 1, preglednica 2 itn. V preglednicah ne uporabljajte izpisanih imen veličin, ampak samo ustrezne simbole. K fizikalnim količinam, npr. t (pisano poševno), pripišite enote (pisano pokončno) v novo vrsto brez oklepajev.

Vse opombe naj bodo označene z uporabo dvignjene številke¹.

SEZNAM LITERATURE

Vsa literatura mora biti navedena v seznamu na koncu članka v prikazani obliki po vrsti za revije, zbornike in knjige:

- [1] Feng, T. W. (2000). Fall-cone penetration and water content relationship of clays. *Geotechnique* 50, No. 2, 181-187.
- [2] Ortolan, Ž. and Mihalinec, Z. (1998). Plasticity index-Indicator of shear strength and a major axis of geotechnical modelling. *Proceedings of the Elev-*

enth Danube-European conference on soil mechanics and geotechnical engineering, Poreč, 25 –29 May 1998.

- [3] Toporišič, J. (1994). *Slovenski pravopis*. 2nd.ed., DZS, Ljubljana.

PODATKI O AVTORJIH

Članku priložite tudi podatke o avtorjih: imena, nazive, popolne poštno naslove, številke telefona in faksa, naslove elektronske pošte. Navedite kontaktno osebo.

SPREJEM ČLANKOV IN AVTORSKE PRAVICE

Uredništvo si pridržuje pravico do odločanja o sprejemu članka za objavo, strokovno oceno mednarodnih recenzentov in morebitnem predlogu za krajšanje ali izpopolnitev ter terminološke in jezikovne korekture.

Avtor mora predložiti pisno izjavo, da je besedilo njegovo izvirno delo in ni bilo v dani obliki še nikjer objavljeno. Z objavo preidejo avtorske pravice na revijo ACTA GEOTECHNICA SLOVENICA. Pri morebitnih kasnejših objavah mora biti AGS navedena kot vir.

Rokopisi člankov ostanejo v arhivu AGS.

Vsa nadaljnja pojasnila daje:

Uredništvo
ACTA GEOTECHNICA SLOVENICA
Univerza v Mariboru
Fakulteta za gradbeništvo
Smetanova ulica 17
2000 Maribor
Slovenija
E-pošta: ags@uni-mb.si

INSTRUCTIONS FOR AUTHORS

The papers are published in English with a translation of the abstract into Slovene.

FORMAT OF THE PAPER

The paper should have the following structure:

- A Title that adequately describes the content of the paper and should not exceed 80 characters;
- An Abstract, which should be viewed as a mini version of the paper and should not exceed 250 words. The Abstract should state the principal objectives and the scope of the investigation and the methodology employed, it should also summarise the results and state the principal conclusions;
- An Introduction, which should provide a review of recent literature and sufficient background information to allow the results of the paper to be understood and evaluated;
- A Theoretical section;
- An Experimental section, which should provide details of the experimental set-up and the methods used for obtaining the results;
- A Results section, which should clearly and concisely present the data using figures and tables where appropriate;
- A Discussion section, which should describe the relationships shown and the generalisations made

possible by the results and discuss the significance of the results, making comparisons with previously published work;

- Conclusions, which should present one or more conclusions that have been drawn from the results and subsequent discussion;
- References, which must be numbered consecutively in the text using square brackets [1] and collected together in a reference list at the end of the paper.

LAYOUT OF THE TEXT

The text should be written in A4 format, with double spacing and margins of 3 cm, to provide editors with space to write in their corrections. Microsoft Word for Windows is the preferred format for submission. One hard copy, including all figures, tables and illustrations and an identical electronic version of the manuscript must be submitted simultaneously.

Equations should be on a separate line in the main body of the text and marked on the right-hand side of the page with numbers in round brackets.

UNITS AND ABBREVIATIONS

Only standard SI symbols and abbreviations should be used in the text, tables and figures. Symbols for physical

quantities in the text should be written in *Italics* (e.g. v , T , etc.). Symbols for units that consist of letters should be in plain text (e.g. Pa, m, etc.).

All abbreviations should be spelt out in full on first appearance.

FIGURES

Figures must be cited in consecutive numerical order in the text and referred to in both the text and the caption as Fig. 1, Fig. 2, etc. Figures may be saved in any common format, e.g. BMP, JPG, GIF. However, the use of CDR format (CorelDraw) is recommended for graphs and line drawings, since vector images can be easily reduced or enlarged during final processing of the paper.

When labelling axes, physical quantities (e.g. v , T) should be used whenever possible. Multi-curve graphs should have individual curves marked with a symbol; the meaning of the symbol should be explained in the figure caption.

Good quality black-and-white photographs or scanned images should be supplied for illustrations.

TABLES

Tables must be cited in consecutive numerical order in the text and referred to in both the text and the caption as Table 1, Table 2, etc. The use of names for quantities in tables should be avoided if possible: corresponding symbols are preferred. In addition to the physical quantity, e.g. t (in *Italics*), units (normal text), should be added on a new line without brackets.

Any footnotes should be indicated by the use of the superscript¹.

LIST OF REFERENCES

References should be collected at the end of the paper in the following styles for journals, proceedings and books, respectively:

- [1] Feng, T. W. (2000). Fall-cone penetration and water content relationship of clays. *Geotechnique* 50, No. 2, 181-187.
- [2] Ortolan, Ž. and Mihalinec, Z. (1998). Plasticity index-Indicator of shear strength and a major axis of geotechnical modelling. *Proceedings of the Eleventh Danube-European conference on soil mechanics and geotechnical engineering*, Poreč, 25 –29 May 1998.

- [3] Toporišič, J. (1994). *Slovenski pravopis*. 2nd.ed., DZS, Ljubljana.

AUTHOR INFORMATION

The following information about the authors should be enclosed with the paper: names, complete postal addresses, telephone and fax numbers and E-mail addresses. Indicate the corresponding person.

ACCEPTANCE OF PAPERS AND COPYRIGHT

The Editorial Committee of the Slovenian Geotechnical Review reserves the right to decide whether a paper is acceptable for publication, to obtain peer reviews for submitted papers, and if necessary, to require changes in the content, length or language.

Authors must also enclose a written statement that the paper is original unpublished work, and not under consideration for publication elsewhere. On publication, copyright for the paper shall pass to the ACTA GEOTECHNICA SLOVENICA. The AGS must be stated as a source in all later publication.

Papers will be kept in the archives of the AGS.

For further information contact:

Editorial Board
ACTA GEOTECHNICA SLOVENICA
University of Maribor
Faculty of Civil Engineering
Smetanova ulica 17
2000 Maribor
Slovenia
E-mail: ags@uni-mb.si

NAMEN REVIJE

Namen revije ACTA GEOTECHNICA SLOVENICA je objavljavanje kakovostnih teoretičnih člankov z novih pomembnih področij geomehanike in geotehnike, ki bodo dolgoročno vplivali na temeljne in praktične vidike teh področij.

ACTA GEOTECHNICA SLOVENICA objavlja članke s področij: mehanika zemljin in kamnin, inženirska geologija, okoljska geotehnika, geosintetika, geotehnične konstrukcije, numerične in analitične metode, računalniško modeliranje, optimizacija geotehničnih konstrukcij, terenske in laboratorijske preiskave.

Revija redno izhaja dvakrat letno.

AVTORSKE PRAVICE

Ko uredništvo prejme članek v objavo, prosi avtorja(je), da prenese(jo) avtorske pravice za članek na izdajatelja, da bi zagotovili kar se da obsežno razširjanje informacij. Naša revija in posamezni prispevki so zaščiteni z avtorskimi pravicami izdajatelja in zanje veljajo naslednji pogoji:

fotokopiranje

V skladu z našimi zakoni o zaščiti avtorskih pravic je dovoljeno narediti eno kopijo posameznega članka za osebno uporabo. Za naslednje fotokopije, vključno z večkratnim fotokopiranjem, sistematičnim fotokopiranjem, kopiranjem za reklamne ali predstavitvene namene, nadaljnjo prodajo in vsemi oblikami nedobičkonosne uporabe je treba pridobiti dovoljenje izdajatelja in plačati določen znesek.

Naročniki revije smejo kopirati kazalo z vsebino revije ali pripraviti seznam člankov z izvlečki za rabo v svojih ustanovah.

elektronsko shranjevanje

Za elektronsko shranjevanje vsakršnega gradiva iz revije, vključno z vsemi članki ali deli članka, je potrebno dovoljenje izdajatelja.

ODGOVORNOST

Revija ne prevzame nobene odgovornosti za poškodbe in/ali škodo na osebah in na lastnini na podlagi odgovornosti za izdelke, zaradi malomarnosti ali drugače, ali zaradi uporabe kakršnekoli metode, izdelka, navodil ali zamisli, ki so opisani v njej.

AIMS AND SCOPE

ACTA GEOTECHNICA SLOVENICA aims to play an important role in publishing high-quality, theoretical papers from important and emerging areas that will have a lasting impact on fundamental and practical aspects of geomechanics and geotechnical engineering.

ACTA GEOTECHNICA SLOVENICA publishes papers from the following areas: soil and rock mechanics, engineering geology, environmental geotechnics, geosynthetic, geotechnical structures, numerical and analytical methods, computer modelling, optimization of geotechnical structures, field and laboratory testing.

The journal is published twice a year.

COPYRIGHT

Upon acceptance of an article by the Editorial Board, the author(s) will be asked to transfer copyright for the article to the publisher. This transfer will ensure the widest possible dissemination of information. This review and the individual contributions contained in it are protected by publisher's copyright, and the following terms and conditions apply to their use:

photocopying

Single photocopies of single articles may be made for personal use, as allowed by national copyright laws. Permission of the publisher and payment of a fee are required for all other photocopying, including multiple or systematic copying, copying for advertising or promotional purposes, resale, and all forms of document delivery.

Subscribers may reproduce tables of contents or prepare lists of papers, including abstracts for internal circulation, within their institutions.

electronic storage

Permission of the publisher is required to store electronically any material contained in this review, including any paper or part of the paper.

RESPONSIBILITY

No responsibility is assumed by the publisher for any injury and/or damage to persons or property as a matter of product liability, negligence or otherwise, or from any use or operation of any methods, products, instructions or ideas contained in the material herein.